

POLITECNICO DI TORINO



Master of Science in Mechanical Engineering

Turbulent Round Jet CFD Analysis
with SU2 Code: from Validation to
Aircraft's Exhaust

A.Y. 2018/2019

Supervisors

Prof.ssa Daniela Anna Misul

Candidate

Francesco D'Amico

ACKNOWLEDGMENTS

Ringrazio in primis la commissione per essere qui oggi e un grazie particolare va necessariamente a chi in prima persona mi ha aiutato nelle difficoltà di questo progetto. Grazie davvero per tutto il sostegno di questi mesi, Professoressa Misul. Dal punto di vista professionale, vorrei poi esprimere la gratitudine ad ogni docente o assistente che ho trovato sul mio percorso, per il contributo che ognuno di voi ha avuto alla mia formazione, nel bene e nel male.

Passando poi alla sfera personale, il problema è sempre da dove iniziare. Per questo ho deciso di farlo con una persona che mi ha sempre anche involontariamente alleggerito la vita con una risata neanche troppo motivata. Per questo e tanto altro, grazie, Raffaele.

Grazie a Sasà, Fabio, Paolo, Ciccio e Michele, perché potrò anche arrivare su Marte ma non potrò mai scordarmi da dove e con chi sono partito, e non potrò mai smettere di voler bene a quelle persone che ci sono da sempre. Letteralmente, da quando ho memoria.

Grazie a Matteo e Alfro semplicemente perché siete magici e non c'è parola che vi possa descrivere meglio. Spa, lo sappiamo entrambi che se le nostre vite si sono intrecciate con questa trama incredibile non può essere successo per caso, e l'aver conosciuto una persona che per me ha un'importanza difficile da descrivere a parole come Alfredo lo può solo confermare. E grazie anche a Martina, Sara, Eleonora, Alessia e Claudia, le magiche di "Chieri"!

Grazie a quel che mi resta di un gruppo che una volta si chiamava family, perché a volte anche ciò che ti spezza il cuore ti fa crescere, capire. Grazie però soprattutto a Francesco ed Eleonora per esservi distinti da questo. E grazie anche ad Ilenia, nonostante tutto.

Grazie ai compagni del liceo e ai compagni di squadra, con cui sono cresciuto tanto e grazie a cui sono riuscito a capire tante cose, di me e non solo. E grazie alla prof Chiaravalloti

e a mister Chirumbolo per aver tirato fuori il caratter e la grinta da un ragazzino timido e impaurito.

Grazie al gruppo incredibile della classe di Torino. Il feeling che si è creato con voi è qualcosa di stupendo, la capacità di tutti di coordinare la voglia di spaccare il mondo con quella di divertirsi e svagarsi è qualcosa che porterò con me per la vita. Così come porterò ognuno di voi e ogni momento insieme con me ovunque sarò. Grazie Davide, Daniele, Nicola, Dmak, Zecco, Pres, Ale, Antonino. And a specific thanks to my bro Nader, it was a blessing for me to meet someone like you and I mean it.

Grazie a Daniele per essere quella persona che c'è da sempre anche se non la vedo mai. Per aver sempre avuto il giusto consiglio da darmi nel momento giusto, per aver rappresentato sempre la persona migliore a cui rivolgermi quando qualcosa non andava o quando non sapevo bene cosa fare. E grazie a Sisa per essere semplicemente una persona fantastica. Siamo arrivati a te, e con te un grazie non basta, non rende. Dirti solo grazie non farebbe capire cosa veramente tu sei per me. Il mio modo di dirti grazie è ricordarti ancora una volta che per me in quegli anni insieme sei diventato il fratello che non ho mai avuto e che da allora non ho mai più rimpianto di non avere. Perché ora ce l'ho e non ne avrei potuto scegliere uno migliore, e sei chiaramente tu, Vitaliano.

Ho voluto lasciare appositamente per ultime le due persone in assoluto più importanti. Grazie mamma per tutto quello che hai sempre fatto per me, incessantemente e senza minimamente chiedere nulla in cambio. Solo crescendo ho capito veramente l'amore che ci metti in tutto quello che fai per me, ho realizzato che nei tuoi occhi sono sempre stato la cosa più bella che tu abbia avuto. L'hai sempre dimostrato ogni giorno e non sai quanto mi faccia bene al cuore, tutto. E' difficile aggiungere parole ad un qualcosa che si è sempre esplicito più nei sentimenti che in qualcosa di descrivibile. Sappi solo che ti sono grato di

tutto, e che ti voglio un bene inquantificabile. Grazie papà per essere sempre stato un faro sul mio cammino, sempre lì ad illuminare la via migliore senza mai forzarmi a prenderla. Da quando sono nato sei sempre la stato il mio idolo, il mio punto di riferimento, quella persona che mi ha sempre fatto pensare: un giorno voglio essere come lui. E grazie anche per tutte le volte che sei stato duro con me nonostante io ci rimanessi male, perché non è mai stato fuori luogo ma mi ha sempre fatto crescere tantissimo. Grazie a voi due perché quello che avete sempre fatto e rappresentato per me è diverso, ma ugualmente importante e di cui avevo ugualmente bisogno. Ognuno ha sempre fatto la sua parte ma le due insieme si sono completate perfettamente rendendovi semplicemente impeccabili sotto tutti i punti di vista. Per me questo vuol dire famiglia, perché da soli possiamo andare dove vogliamo, ma insieme è più bello. Non so chi devo ringraziare per avermi regalato due genitori come voi, ma so che devo ringraziare voi all'infinito per ogni cosa che avete fatto e ogni parola che avete detto da quando sono nato.

Ho finito. Ho voluto spendere un po' di tempo per farvi sapere che se oggi sono quello che sono, è principalmente grazie a tutti voi. Per cui ancora, un'ultimissima volta, grazie, di cuore.

TABLE OF CONTENTS

<u>CHAPTER</u>		<u>PAGE</u>
1	INTRODUCTION	1
1.1	Computational Fluid Dynamics	1
1.2	SU2: a new open source CFD tool	1
1.3	Turbulent flows: characteristics and modelling	2
1.3.1	RANS approach	4
1.3.2	Spalart-Allmaras (SA) model	4
1.3.3	Menter Shear Stress Transport (SST) model	7
1.4	Turbulent round jet	12
2	TEST CASES	15
2.1	NASA validation test cases	15
2.1.1	ARN2 Hot Subsonic Jet	15
2.1.2	ARN2 Near-sonic Jet	18
2.2	SU2 simulations	20
2.2.1	CASE 01 - Validation and verification: Hot Subsonic Jet	21
2.2.2	CASE 02 - Validation and verification: Near-sonic Jet	23
2.2.3	CASE 03 - Hot Near-sonic Jet	25
2.2.4	CASE 04 - Flight free-stream conditions	27
2.2.5	CASE 05 - Aircraft's exhaust simulation	29
3	CURRENT STATUS AND BEST PRACTICE	32
3.1	3D one-degree mesh	33
3.2	2D mesh	36
3.3	3D mesh - Dimensional form of the Navier-Stokes equation	40
3.4	Best practice overview	45
3.5	Mesh generation	45
3.5.1	Boundary domains	52
4	VALIDATION RESULTS	56
4.0.1	CASE 01 - Hot-Subsonic turbulent round jet results	57
4.0.1.1	CASE 01 - Spalart-Almaras turbulence model results	57
4.0.1.2	CASE 01 -Menter Shear Stress Transport (SST) model results	63
4.0.2	CASE 02 - Near-sonic turbulent round jet results	66
4.0.2.1	CASE 02 - Spalart-Almaras turbulence model results	66
4.0.2.2	CASE 02 - Menter Shear Stress Transport (SST) model results	71

TABLE OF CONTENTS (continued)

<u>CHAPTER</u>		<u>PAGE</u>
5	ANALYSIS OF OTHER TURBULENT ROUND JETS CONFIGURATIONS	74
5.1	CASE 03 - Hot near-sonic turbulent round jet results	74
5.1.1	CASE 03 - Spalart-Almaras turbulence model results	75
5.1.2	CASE 03 - Menter Shear Stress Transport (SST) model results	80
5.2	CASE 04 - Flight free-stream conditions results	82
5.2.1	CASE 04 - Spalart-Almaras turbulence model results	83
5.2.2	CASE 04 - Menter Shear Stress Transport (SST) model results	88
5.3	CASE 05 - Aircraft's Exhaust	90
6	CONCLUSIONS	96
6.1	Future work	97
	APPENDICES	98
	Appendix A	99
	CITED LITERATURE	121

LIST OF TABLES

<u>TABLE</u>		<u>PAGE</u>
I	SA model constants values and expressions	8
II	Menter SST model constants values and expressions	10
III	ARN2 Hot Subsonic Jet: boundary conditions	17
IV	ARN2 Hot Subsonic Jet: relevant quantities at the nozzle exit . .	17
V	ARN2 Near-sonic Jet: boundary conditions	19
VI	ARN2 Near-sonic Jet: relevant quantities at the nozzle exit	20
VII	Boundary conditions comparison between all simulations	31
VIII	Nozzle's exit quantities comparison between all simulations	31
IX	Pressure non-dimensional equations: reference quantities calculation	44
X	Velocity non-dimensional equations: reference quantities calculation	44
XI	Number of total elements for the different adopted grids	53

LIST OF FIGURES

<u>FIGURE</u>		<u>PAGE</u>
1	Schematic representation of a turbulent round jet flow	12
2	Schematic case set up for the Hot Subsonic Jet CFD simulations performed by NASA.	16
3	Flow field resulting from NASA CFD simulations of the Hot Subsonic Jet	18
4	Schematic case set up for the Near-sonic Jet CFD simulations performed by NASA.	19
5	Flow field resulting from NASA CFD simulations of the Near-sonic Jet	20
6	Free-stream conditions' values imposed for the Hot Subsonic Jet simulations	22
7	Boundary conditions' values imposed for the Hot Subsonic Jet simulations	23
8	Boundary conditions' values imposed for the Near-sonic Jet simulations	24
9	Free-stream conditions' values imposed for the Near-sonic Jet simulations	25
10	Boundary conditions' values imposed for the Hot Near-sonic Jet simulations	26
11	Flight free-stream conditions imposed to the Hot Near-sonic jet simulations	28
12	Boundary conditions for the Hot Near-sonic jet simulations in flight free-stream conditions.	29
13	Flight free-stream conditions including the imposition of the aircraft's speed.	30
14	One-degree 3D domain configuration.	34
15	Non-dimensional velocity flow field result obtained with the one-degree domain configuration.	35
16	Centerline zoom of the non-dimensional velocity flow field result obtained with the one-degree domain configuration.	36
17	Two dimensional grid.	37
18	Non-dimensional velocity flow field result obtained with the 2D domain configuration.	38
19	Centerline zoom of the non-dimensional velocity flow field result obtained with the 2D domain configuration.	39
20	Centerline axial velocity profile for the 2D configuration.	40
21	Non-dimensional velocity flow field result obtained with the 3D domain configuration in the dimensional form of the equations.	41
22	Centerline axial velocity profile for the 3D configuration in dimensional form of the equations.	42

LIST OF FIGURES (continued)

<u>FIGURE</u>		<u>PAGE</u>
23	2D mesh domain.	46
24	Mesh rotation process.	47
25	Complete mesh rotation.	48
26	Mesh blocks splitting.	49
27	Mesh surface at the empty region boundary.	50
28	Solve operation on axial boundary domains.	51
29	Axial boundary domain after performing solve operation.	52
30	Nozzle's inlet boundary.	53
31	Domain's outflow boundary.	54
32	Far-field boundaries.	54
33	Nozzle's walls.	55
34	SA results: axial velocity profile along centerline for the Hot Subsonic jet.	58
35	$X = 2D$ line representation on the fluid flow of the Hot Subsonic jet.	59
36	SA results: axial (left) and radial (right) velocity radial profiles at $x = 2D$ for the Hot Subsonic jet.	59
37	$X = 5D$ line representation on the fluid flow of the Hot Subsonic jet.	60
38	SA results: axial (left) and radial (right) velocity radial profiles at $x = 5D$ for the Hot Subsonic jet.	60
39	$X = 10D$ line representation on the fluid flow of the Hot Subsonic jet.	61
40	SA results: axial (left) and radial (right) velocity radial profiles at $x = 10D$ for the Hot Subsonic jet.	61
41	$X = 15D$ line representation on the fluid flow of the Hot Subsonic jet.	62
42	SA results: axial (left) and radial (right) velocity radial profiles at $x = 15D$ for the Hot Subsonic jet.	62
43	SST results: axial velocity profile along centerline for the Hot Subsonic jet.	63
44	SST results: axial (left) and radial (right) velocity radial profiles at $x = 2D$ for the Hot Subsonic jet.	64
45	SST results: axial (left) and radial (right) velocity radial profiles at $x = 5D$ for the Hot Subsonic jet.	64
46	SST results: axial (left) and radial (right) velocity radial profiles at $x = 10D$ for the Hot Subsonic jet.	65
47	SST results: axial (left) and radial (right) velocity radial profiles at $x = 15D$ for the Hot Subsonic jet.	65
48	SA results: axial velocity profile along centerline for the Near-sonic jet.	66
49	$X = 2D$ line representation on the fluid flow of the Near-sonic jet.	67
50	SA results: axial (left) and radial (right) velocity radial profiles at $x = 2D$ for the Near-sonic jet.	67
51	$X = 5D$ line representation on the fluid flow of the Near-sonic jet.	68
52	SA results: axial (left) and radial (right) velocity radial profiles at $x = 5D$ for the Near-sonic jet.	68

LIST OF FIGURES (continued)

<u>FIGURE</u>		<u>PAGE</u>
53	$X = 10D$ line representation on the fluid flow of the Near-sonic jet.	69
54	SA results: axial (left) and radial (right) velocity radial profiles at $x = 10D$ for the Near-sonic jet.	69
55	$X = 15D$ line representation on the fluid flow of the Near-sonic jet.	70
56	SA results: axial (left) and radial (right) velocity radial profiles at $x = 15D$ for the Near-sonic jet.	70
57	SST results: axial velocity profile along centerline for the Near-sonic jet.	71
58	SST results: axial (left) and radial (right) velocity radial profiles at $x = 2D$ for the Near-sonic jet.	72
59	SST results: axial (left) and radial (right) velocity radial profiles at $x = 5D$ for the Near-sonic jet.	72
60	SST results: axial (left) and radial (right) velocity radial profiles at $x = 10D$ for the Near-sonic jet.	73
61	SST results: axial (left) and radial (right) velocity radial profiles at $x = 15D$ for the Near-sonic jet.	73
62	SA results: axial velocity profile along centerline for the Hot Near-sonic jet.	75
63	$X = 2D$ line representation on the fluid flow of the Hot Near-sonic jet.	76
64	SA results: axial (left) and radial (right) velocity radial profiles at $x = 2D$ for the Hot Near-sonic jet.	76
65	$X = 5D$ line representation on the fluid flow of the Hot Near-sonic jet.	77
66	SA results: axial (left) and radial (right) velocity radial profiles at $x = 5D$ for the Hot Near-sonic jet.	77
67	$X = 10D$ line representation on the fluid flow of the Hot Near-sonic jet.	78
68	SA results: axial (left) and radial (right) velocity radial profiles at $x = 10D$ for the Hot Near-sonic jet.	78
69	$X = 15D$ line representation on the fluid flow of the Hot Near-sonic jet.	79
70	SA results: axial (left) and radial (right) velocity radial profiles at $x = 15D$ for the Hot Near-sonic jet.	79
71	SST results: axial velocity profile along centerline for the Hot Near-sonic jet.	80
72	SST results: axial (left) and radial (right) velocity radial profiles at $x = 2D$ for the Hot Near-sonic jet.	80
73	SST results: axial (left) and radial (right) velocity radial profiles at $x = 5D$ for the Hot Near-sonic jet.	81
74	SST results: axial (left) and radial (right) velocity radial profiles at $x = 10D$ for the Hot Near-sonic jet.	81
75	SST results: axial (left) and radial (right) velocity radial profiles at $x = 15D$ for the Hot Near-sonic jet.	82

LIST OF FIGURES (continued)

<u>FIGURE</u>		<u>PAGE</u>
76	SA results: axial velocity profile along centerline for the Hot Near-sonic jet in flight free-stream conditions.	83
77	$X = 2D$ line representation on the fluid flow of the Hot Near-sonic jet in flight free-stream conditions.	84
78	SA results: axial (left) and radial (right) velocity radial profiles at $x = 2D$ for the Hot Near-sonic jet in flight free-stream conditions.	84
79	$X = 5D$ line representation on the fluid flow of the Hot Near-sonic jet in flight free-stream conditions.	85
80	SA results: axial (left) and radial (right) velocity radial profiles at $x = 5D$ for the Hot Near-sonic jet in flight free-stream conditions.	85
81	$X = 10D$ line representation on the fluid flow of the Hot Near-sonic jet in flight free-stream conditions.	86
82	SA results: axial (left) and radial (right) velocity radial profiles at $x = 10D$ for the Hot Near-sonic jet in flight free-stream conditions.	86
83	$X = 15D$ line representation on the fluid flow of the Hot Near-sonic jet in flight free-stream conditions.	87
84	SA results: axial (left) and radial (right) velocity radial profiles at $x = 15D$ for the Hot Near-sonic jet in flight free-stream conditions.	87
85	SST results: axial velocity profile along centerline for the Hot Near-sonic jet in flight free-stream conditions.	88
86	SST results: axial (left) and radial (right) velocity radial profiles at $x = 2D$ for the Hot Near-sonic jet in flight free-stream conditions.	88
87	SST results: axial (left) and radial (right) velocity radial profiles at $x = 5D$ for the Hot Near-sonic jet in flight free-stream conditions.	89
88	SST results: axial (left) and radial (right) velocity radial profiles at $x = 10D$ for the Hot Near-sonic jet in flight free-stream conditions.	89
89	SST results: axial (left) and radial in flight free-stream conditions(right) velocity radial profiles at $x = 15D$ for the Hot Near-sonic jet.	90
90	Mach number flow field for the aircraft's exhaust simulation.	92
91	Pressure field for the aircraft's exhaust simulation.	93
92	SA results: Mach (left) and pressure (right) centerline profiles for the aircraft's exhaust simulation.	94
93	SST results: Mach (left) and pressure (right) centerline profiles for the aircraft's exhaust simulation.	95
94	SA - SST results comparison: Mach (left) and pressure (right) centerline profiles for the aircraft's exhaust simulation on the finest grid level.	95

LIST OF ABBREVIATIONS

CFD	Computational Fluid Dynamics
ARN2	Acoustic Research Nozzle 2
SA	Spalart-Allmaras
SST	Menter Shear Stress Transport
D	Nozzle's outlet section diameter
JST	Jameson-Schmidt-Turkel numerical scheme

SUMMARY

Computational Fluid Dynamics is getting more and more an established reality in nowadays engineering applications involving fluids. Being able to simulate fluids' behavior in different configurations is an incredibly strong tool for many engineering fields varying from components' design to climatic effects' estimations. A lot of research is currently based on using CFD software to obtain results in a faster, easier and less expensive way, compared to reproducing the fluids behavior in experiments. This is why it becomes very interesting understanding what tools are available, what is their current status, how to better exploit them. There are already some well-established CFD codes that are widely adopted and that have been intensively developed during the years, but most of them are really expensive. The first aim of this work is to evaluate SU2, a new open-source (free) CFD code developed by Stanford University, in the specific configuration of turbulent round jets. This tool already shows incredible capability and it has been used with success in a wide range of other cases. My intent was to give my contribution by testing the software in such configuration. The idea is to show potential new users how to better adjust the settings to obtain reliable results, but also to give a feedback to the software developers on possible improvements to be performed on the code. Second aim is to provide a wide range of results when dealing with turbulent round jets with the ultimate goal to get as close as possible to precisely simulate a general aircraft's exhaust fluid flow.

CHAPTER 1

INTRODUCTION

1.1 Computational Fluid Dynamics

The practice of simulating fluid behavior on software is called Computational Fluid Dynamics. It is an incredibly powerful discipline as it allows to obtain fast predictions of fluid flows with relatively low costs compared to experiments. This is the reason why in the last years a lot of development has been pushed in this direction. However, finding feasible and reliable ways to numerically solve the Navier-Stokes equations has always been a very challenging task. This complexity is further increased when dealing with turbulent flows. In the last years though the great improvements in computers' calculation capability, together with the optimization of numerical methods, has made feasible and fast solving such problems. So, nowadays Computational Fluid Dynamics is a well-established practice for a wide range of applications.

1.2 SU2: a new open source CFD tool

SU2 is a new, open-source C++ based software capable of solving partial differential equations (PDE) and mainly suitable for Computational Fluid Dynamics applications. It has been developed in the last years by Stanford University. Being a very recent tool (first release was in 2012), any contribution could be very important for the growth of this tool. Several validation cases are already available, covering different areas including both compressible and incom-

compressible, turbulent and laminar flows. However, literature is poor of simulations performed on Turbulent Round Jets. This project's goal is indeed to test the software in this specific configuration, giving feedback on the current status of many solver's features, best practice in terms of case set-up and a wide range of results.

When working with SU2, the workflow's first step is to create the mesh file on some other software. For this thesis Pointwise has been adopted, which allows extracting the mesh file in the specific ".su2" format. This is an ASCII mesh file reporting points' coordinates associated with cells' enumeration and physical quantities' values. Being an ASCII format file, it is pretty heavy in terms of memory occupied compared to other formats. However, it is not the only mesh file format that is supported by SU2 as it is also possible to use ".cgns" mesh files. The second element that needs to be provided in the simulation folder together with the mesh file is the so called configuration file ".cfg" where all the simulation's specifications are given by the user. It is easy to find and download the complete template of the configuration file. Then, one can choose the specifications they need, set the desired features and values and delete what is unnecessary to set up the whole simulation. Finally, all post-process actions were performed on ParaView, after importing the ".vtk" result file.

1.3 Turbulent flows: characteristics and modelling

A turbulent flow is easy to recognize by its characteristics, being clearly irregular, unsteady and random. As a consequence, its velocity field, denoted as $U(x, t)$, shows a really complex behavior. What defines a turbulent flow is the Reynolds number, namely $Re = U \cdot D/\nu$ where D is the characteristic length of the flow and ν the fluid's kinematic viscosity. A flow can be

considered turbulent if this non-dimensional number is higher than 4000. Above this threshold, the higher the value of the Reynolds number the more the turbulent behavior of the flow will be dominant. Turbulence occurs and appears on different scales. What happens on large-scale depends on the flows' geometric characteristics, small-scale phenomena are instead driven by the energy they receive by the large scales and by the fluid's viscosity. The size of the smallest scale decreases as the Reynolds number increases and the smaller it is the more information will be contained in the flow field. That means, an incredible amount of information will be contained in a high Reynolds number flow. No matter if a fluid flow is laminar or turbulent, the fluid dynamics is described in full details and with maximum precision by the Navier-Stokes equations. For very high Reynolds number fluid flows, the amount of information the Navier-Stokes equations retain is incredibly high, so that their direct solution is not feasible. Therefore, common practice when dealing with modelling turbulence is to solve some relevant flow's statistics. The main one is the mean velocity field, denoted as $\langle U(x, t) \rangle$. Any turbulent flow's velocity field can be split in two contributions: the mean velocity field $\langle U(x, t) \rangle$ and the fluctuating velocity field, defined as $u(x, t) = U(x, t) - \langle U(x, t) \rangle$. The mean velocity field is what defines the overall behavior of the flow in time. It smoothly changes in time, so that solving the Navier-Stokes equations requires much less effort. On the other hand with this approach only an averaged solution is obtained, so that any other information about the turbulent flow is lost.

1.3.1 RANS approach

This simplified approach reduces to solving the so called Reynolds-Averaged Navier-Stokes (RANS) equations. They basically consist in the compressible Navier-Stokes equations solved for the mean velocity field $\langle U(x, t) \rangle$. The turbulent behavior of the flow is described in the equations by the so called Reynolds stresses $\langle u_i u_j \rangle$. The key idea in modeling turbulence is provided by the turbulent-viscosity hypothesis [1], which states that the effect of turbulence can be considered as an increase in the viscosity. According to thi hypothesis, the Reynolds stresses are defined as:

$$\langle u_i u_j \rangle = \frac{2}{3} k \delta_{ij} - \nu_t \left(\frac{\partial \langle U_i \rangle}{\partial x_j} + \frac{\partial \langle U_j \rangle}{\partial x_i} \right) \quad (1.1)$$

where ν_t is the term representing the turbulent viscosity, while k is the turbulent kinetic energy and δ_{ij} the Kronecker delta ($\delta_{ij} = 1$ if $i = j$, $\delta_{ij} = 0$ if $i \neq j$). A closure problem arises then for the system of equations as ν_t represents a new unknown. Therefore, a suitable model for the turbulent viscosity is needed. There are different models available. The two most common ones are the ‘‘Spalart-Allmaras (SA)’’ model and the ‘‘Menter Shear Stress Transport (SST)’’ model. Both of them are implemented in SU2 and both of them have been adopted in the simulations reported in the following sections.

1.3.2 Spalart-Allmaras (SA) model

The Spalart-Allmaras model is the simplest one, as it only consists in solving a single transport equation for the turbulent viscosity ν_t . Therefore, it is commonly referred to as a

one-equation model. It is mainly designed for aerodynamic flows, so where a fluid flow over walls is involved. For these applications it shows successful results. On the other hand though, it is not the best option for many other cases. The equation to be solved retains the following general formulation [1]:

$$\frac{\overline{D}\nu_t}{\overline{D}t} = \nabla \cdot \left(\frac{\nu_t}{\sigma_\nu} \nabla \nu_t \right) + S_\nu \quad (1.2)$$

where σ_ν is a constant and S_ν is a source term depending on several factors, including the viscosities ν and ν_t , the vorticity magnitude Ω , the turbulent viscosity gradient $\nabla \nu_t$ and the distance from the closest wall l_w . The details of the models are extracted from [2] while the farfield boundary conditions from [3] and [4]. NASA has dedicated webpages about turbulence models implementation, so [5] is another important reference. The full equation constituting this one-equation model is:

$$\begin{aligned} \frac{\partial \hat{\nu}}{\partial t} + u_j \frac{\partial \hat{\nu}}{\partial x_j} = c_{b1} (1 - f_{t2}) \hat{S} \hat{\nu} - \left[c_{w1} f_w - \frac{c_{b1}}{\kappa^2} f_{t2} \right] \left(\frac{\hat{\nu}}{l_w} \right)^2 + \\ + \frac{1}{\sigma} \left[\frac{\partial}{\partial x_j} \left((\nu + \hat{\nu}) \frac{\partial \hat{\nu}}{\partial x_j} \right) + c_{b2} \frac{\partial \hat{\nu}}{\partial x_i} \frac{\partial \hat{\nu}}{\partial x_i} \right] \end{aligned} \quad (1.3)$$

Then, the turbulent viscosity ν_t is calculated as:

$$\nu_t = \hat{\nu} f_{v1} \quad (1.4)$$

The constant f_{v1} is defined as follows:

$$f_{v1} = \frac{\chi^3}{\chi^3 + c_{v1}^3} \quad (1.5)$$

where c_{v1} is a constant whose value is reported in Table I and χ represents the following viscosities ratio:

$$\chi = \frac{\hat{\nu}}{\nu} \quad (1.6)$$

The parameter \hat{S} in Equation 1.3 is defined by:

$$\hat{S} = \Omega + \frac{\hat{\nu}}{\kappa^2 l_w^2} f_{v2} \quad (1.7)$$

It is still necessary to define the vorticity magnitude $\Omega = \sqrt{2W_{ij}W_{ji}}$ and:

$$W_{ij} = \frac{1}{2} \left(\frac{\partial u_i}{\partial x_j} - \frac{\partial u_j}{\partial x_i} \right) \quad (1.8)$$

Table I reports all the model constants' values. To complete the model's description, the following definitions must be added:

$$f_{v2} = 1 - \frac{\chi}{1 + \chi f_{v1}} \quad (1.9)$$

$$f_w = g \left[\frac{1 + c_{w3}^6}{g^6 + c_{w3}^6} \right]^{\frac{1}{6}} \quad (1.10)$$

$$g = r + c_{w2}(r^6 - r) \quad (1.11)$$

$$r = \min \left[\frac{\hat{\nu}}{\hat{S}\kappa^2 l_w^2}, 10 \right] \quad (1.12)$$

$$f_{t2} = c_{t3} \exp(-c_{t4}\chi^2) \quad (1.13)$$

Finally, the equation needs proper boundary conditions to be solved. Wall and farfield boundary conditions are defined as follows:

$$\hat{\nu}_{wall} = 0 \quad (1.14)$$

$$3\nu_\infty \leq \hat{\nu}_{farfield} \leq 5\nu_\infty \quad (1.15)$$

1.3.3 Menter Shear Stress Transport (SST) model

The SST model is a two-equations model. It is a variant proposed by Menter [6] of the standard so called κ - ω model. The turbulent viscosity approximation is supported by a transport equation for the turbulent kinetic energy κ and a model transport equation for the turbulence

TABLE I: SA model constants values and expressions

SA model constants	
c_{b1}	0.1355
c_{b2}	0.622
σ	2/3
κ	0.41
c_{w2}	0.3
c_{w3}	2
c_{v1}	7.1
c_{t3}	1.2
c_{t4}	0.5
c_{w1}	3.3291

frequency ω . The latter is defined as the ratio between the turbulent dissipation ϵ and the turbulent kinetic energy κ , namely $\omega = \epsilon/\kappa$. This is the most interesting model for applications such turbulent round jets. All the details about the model are extracted from [6] always keeping a NASA webpage as reference [7]. The two transport equations are formulated as follows:

$$\frac{\partial(\rho k)}{\partial t} + \frac{\partial(\rho u_j k)}{\partial x_j} = P - \beta^* \rho \omega k + \frac{\partial}{\partial x_j} \left[\left(\frac{\nu}{\rho} + \sigma_k \frac{\nu_t}{\rho} \right) \frac{\partial k}{\partial x_j} \right] \quad (1.16)$$

$$\frac{\partial(\rho \omega)}{\partial t} + \frac{\partial(\rho u_j \omega)}{\partial x_j} = \frac{\gamma}{\nu_t} P - \beta \rho \omega^2 + \frac{\partial}{\partial x_j} \left[\left(\frac{\nu}{\rho} + \sigma_\omega \frac{\nu_t}{\rho} \right) \frac{\partial \omega}{\partial x_j} \right] + 2(1 - F1) \frac{\rho \sigma_{\omega 2}}{\omega} \frac{\partial k}{\partial x_j} \frac{\partial \omega}{\partial x_j} \quad (1.17)$$

To better understand these equations, it is important to point out that β , γ , σ_k and σ_ω are constants and to give a definition to the following terms:

$$P = \tau_{ij} \frac{\partial u_j}{\partial x_j} \quad (1.18)$$

$$\tau_{ij} = \frac{\nu_t}{\rho} \left(2S_{ij} - \frac{2}{3} \frac{\partial u_k}{\partial x_k} \delta_{ij} \right) - \frac{2}{3} \rho k \delta_{ij} \quad (1.19)$$

$$S_{ij} = \frac{1}{2} \left(\frac{\partial u_i}{\partial x_j} + \frac{\partial u_j}{\partial x_i} \right) \quad (1.20)$$

The turbulent viscosity is given by:

$$\mu_t = \frac{\nu_t}{\rho} = \frac{\rho a_1 \kappa}{\max(a_1 \omega, \Omega F_2)} \quad (1.21)$$

There is a relation that holds for each of the previously mentioned constants and it is important to keep it in mind for defining the constants' values. Each of them can be split into an inner and outer constant. Defining as ϕ a general constant, ϕ_1 its inner component and ϕ_2 its outer component, the relation has the form:

$$\phi = F_1 \phi_1 + (1 - F_1) \phi_2 \quad (1.22)$$

Then, the following definitions must be provided:

$$F_1 = \tanh(\arg_1^4) \quad (1.23)$$

TABLE II: Menter SST model constants values and expressions

Menter SST model constants	
γ_1	0.5532
γ_2	0.4404
σ_{k1}	0.85
σ_{k2}	1
$\sigma_{\omega 1}$	0.5
$\sigma_{\omega 2}$	0.856
β_1	0.075
β_2	0.0828
β^*	0.09
κ	0.41
a_1	0.31

$$arg_1 = \min \left[\max \left(\frac{\sqrt{k}}{\beta^* \omega l_w}, \frac{500\nu}{l_w^2 \omega} \right), CD_{k\omega} \frac{k}{l_w^2} \right] \quad (1.24)$$

$$CD_{k\omega} = \max \left(2\rho\sigma_{\omega 2} \frac{1}{\omega} \frac{\partial k}{\partial x_j} \frac{\partial \omega}{\partial x_j}, 10^{-20} \right) \quad (1.25)$$

$$F_2 = \tanh (arg_2^2) \quad (1.26)$$

$$arg_2 = \max \left(2 \frac{\sqrt{k}}{\beta^* \omega l_w}, \frac{500\nu}{l_w^2 \omega} \right) \quad (1.27)$$

The values of the different constants are reported in Table II.

It is also useful to have a better understanding on how the boundary conditions for the turbulent variables k and ω work and are implemented in the software, to be aware of the kind of imposition we are dealing with when setting up a simulation. The definitions for the far-field boundary conditions are reported by Equation 1.28 and Equation 1.29, while for the no-slip wall boundary condition by Equation 1.30 and Equation 1.31. It is possible to notice how the far-field ones yield an open definition: the idea is that the turbulent viscosity must have a value between 10^{-2} and 10^{-5} the one of the freestream laminar viscosity. For the inlet boundary condition, the values are prescribed by some parameters in the simulation settings, namely "FREESTREAM_TURBULENCEINTENSITY" and "FREESTREAM_TURB2LAMVISCRATIO", whose default values of 0.05 and 10 have been adopted.

$$\frac{10^{-5}U_{\infty}^2}{Re_L} < k_{farfield} < \frac{0.1U_{\infty}^2}{Re_L} \quad (1.28)$$

$$\frac{U_{\infty}}{L} < \omega_{farfield} < \frac{10U_{\infty}}{L} \quad (1.29)$$

$$k_{wall} = 0 \quad (1.30)$$

$$\omega_{wall} = 10 \frac{6\nu}{\beta_1(\Delta l_w)^2} \quad (1.31)$$

1.4 Turbulent round jet

A turbulent round jet is a statistically steady and axisymmetric flow that forms at a nozzle's exit, as shown in Figure 1. During the years a lot of research aimed to obtain an analytical treatment of such flow configuration, mainly through experimental evidences. A solution was indeed found, but it is only able to describe the flow far enough from the nozzle's outlet, beyond the so called development region of the jet. Usually a minimum distance of $x/D = 30$ is considered as reference value, where D is the nozzle's outlet section diameter and x the axial coordinate, whose origin is placed at the nozzle's exit. The whole theory is reported in [1].

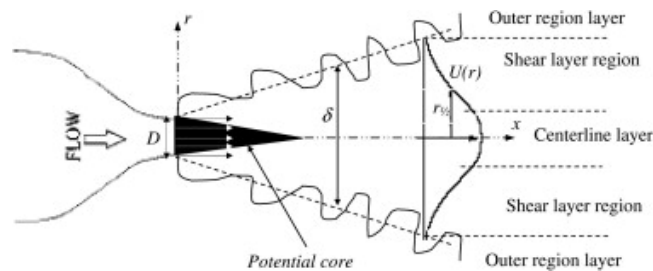


Figure 1: Schematic representation of a turbulent round jet flow

The main idea behind this analytical description is the self-similarity property of the flow. It has been proved empirically and it is only valid beyond the development region of the jet. Self-similarity means the radial profile of both axial mean velocity $\langle U \rangle$ and Reynolds stresses $\langle uv \rangle$ collapses into a single curve for any value of the axial coordinate, if properly scaled values

of the radial coordinate and of the two quantities of interest are considered. To clarify, let's first define the centerline mean axial velocity $U_0(x)$ of the flow as:

$$U_0(x) = \langle U(x, r = 0) \rangle \quad (1.32)$$

and the jet half-width $r_{1/2}$ as :

$$\langle U(x, r_{1/2}) \rangle = \frac{1}{2}U_0(x) \quad (1.33)$$

so as the radial coordinate at which the value of the mean axial velocity $\langle U \rangle$ is half the one on the jet's centerline $U_0(x)$. If one scales the velocity $\langle U \rangle$ by the centerline velocity $U_0(x)$ and the radial coordinate r by the jet half-width $r_{1/2}(x)$ and then plots $\langle U \rangle / U_0(x)$ against $r / r_{1/2}(x)$, for any $x/D > 30$ all the curves will be exactly the same. Same happens if one plots $\langle uv \rangle / U_0^2(x)$ against $r / r_{1/2}(x)$. Therefore, the two variables are defined self-similar and the region of interest ($x/D > 30$) is called self-similar region. An empirical law has been found for the jet half-width:

$$r_{1/2}(x) = S(x - x_0) \quad (1.34)$$

where $S \simeq 0.1$ is an important parameter called spreading rate independent also from the Reynolds number. The turbulent viscosity approximation for this flow reduces to the following formulation:

$$\langle uv \rangle = -\nu_T \frac{\partial \langle U \rangle}{\partial r} \quad (1.35)$$

From this formulation, it is easy to understand that if both $\langle U \rangle$ and $\langle uv \rangle$ are self-similar, also the turbulent viscosity will be so. Applying all this information to the boundary layer equations, which are a simplification of the Navier Stokes equations whose hypothesis are realistic in case of a turbulent round jet, it is possible to derive the following profiles for the mean axial velocity:

$$\langle U \rangle = \frac{8a\nu_T}{x} \frac{1}{(1 + a\eta^2)^2} \quad (1.36)$$

where:

$$a = \frac{(\sqrt{2} - 1)}{S^2} \quad (1.37)$$

$$\eta = \frac{r}{(x - x_0)} \quad (1.38)$$

However, there is no description for what happens in a round jet in the turbulence development region, especially in the close proximity of the nozzle exit. So, the idea is to characterize this flow configuration through a Computational Fluid Dynamic approach. This thesis will present several different cases of round jets, trying to provide a numerical prediction for a phenomenon that does not have any analytical solution known so far.

CHAPTER 2

TEST CASES

This chapter is dedicated to describe all the test cases covered in this thesis. First, two validation test cases provided by NASA will be shown, where both experimental and simulations' data are available. This will be the starting point for all the other simulations run for this project. First steps were coherently moved to understand how to set up SU2 to obtain proper results in this configuration, evaluated on a comparison base with the data provided by NASA. Then, more simulations were run to provide a wider description of the phenomenon. The different cases have been chosen following two main ideas. The first is to try to get as close as possible to simulate a real aircraft's engine exhaust jet. The second is to proceed in a way such that results can be somehow considered reliable even if no validation data are available.

2.1 NASA validation test cases

As a reference for the simulations of turbulent round jets, some validation cases carried out by NASA and whose results and data are freely available online have been considered. All these cases involve experiments conducted on the flow at the exit of the Acoustic Reference Research 2 (ARN2) nozzle.

2.1.1 ARN2 Hot Subsonic Jet

The first case is a high temperature and low Mach number jet flowing into quiescent air. All the relative documentation can be found on the website [8].

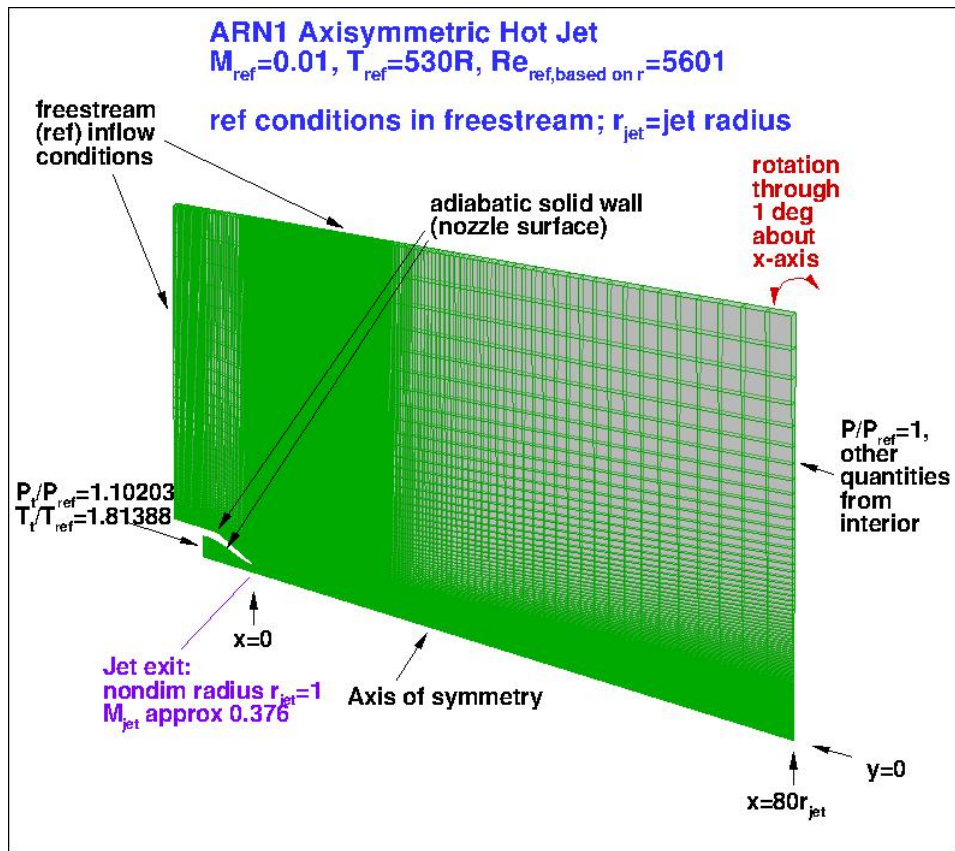


Figure 2: Schematic case set up for the Hot Subsonic Jet CFD simulations performed by NASA.

The free-stream conditions are imposed with a small approximation in the simulations. The Mach number, which should technically be 0 as the air around the jet is considered to be non-moving, is indeed set as $Ma_{ref} = 0.01$. This is because every CFD software gets really unstable when trying to solve such a flow if the Mach number is imposed to be identically 0. However, it has been proven that the influence of this approximation is very small and so such a set up is acceptable. Figure 2 shows a very useful schematic view where one can see the kind of

TABLE III: ARN2 Hot Subsonic Jet: boundary conditions

Boundary conditions		
Freestream	Ma_{free}	0.01
	T_{free}	294.44K
	Re_{free}	5601
Inlet	p_t	$p_{free} \cdot 1.81388$
	T_t	$T_{free} \cdot 1.10203$
Outlet	p	p_{free}

TABLE IV: ARN2 Hot Subsonic Jet: relevant quantities at the nozzle exit

Nozzle exit	
$Ma_{x=0}$	0.376
$T_{x=0}$	519.32K

domain NASA adopted, the boundary conditions used for the different areas of the domain, the reference coordinate system that has been chosen and other relevant quantities for the flow. All the important variables' values are also reported in Table III and Table IV to have an even clearer overview of the whole case. NASA provides on their website experimental data and simulations' results obtained with both SA and SST turbulence models, using two different CFD tools: CFL3D and WIND. Moreover, the adopted grids are also available. Let's clarify the variables' nomenclature used in this thesis to avoid confusion. "Free" quantities are referred to free-stream conditions, the suffix "t" stands for total properties. Quantities described by " $x = 0$ " are evaluated at the nozzle exit.

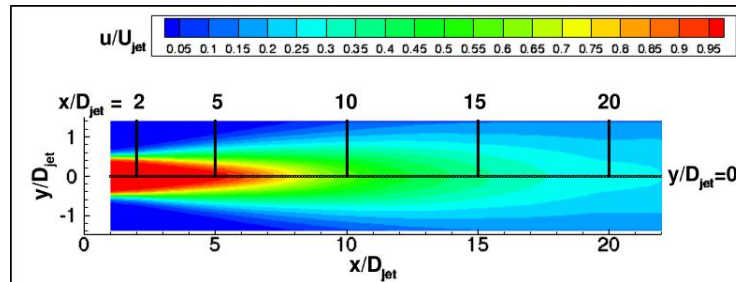


Figure 3: Flow field resulting from NASA CFD simulations of the Hot Subsonic Jet

2.1.2 ARN2 Near-sonic Jet

The second test case is always based on the same ARN2 nozzle and the same geometric configuration. What changes are the boundary conditions as the aim is now to simulate a low temperature flow whose Mach number at the nozzle exit is close to 1 ($Ma_{x=0} = 0.985$). The environment is again quiescent air. The same grids used for the Hot Subsonic case have been adopted for this simulation: this is an important point to keep in mind, further considerations on this will be deployed in the next sections to better understand the idea behind this thesis. Also in this case, NASA provides the same data set as for the Hot Subsonic case: experimental data and simulations results obtained with SA and SST turbulence models, using CFL3D and WIND codes. Documentation is available at the web-page [9].

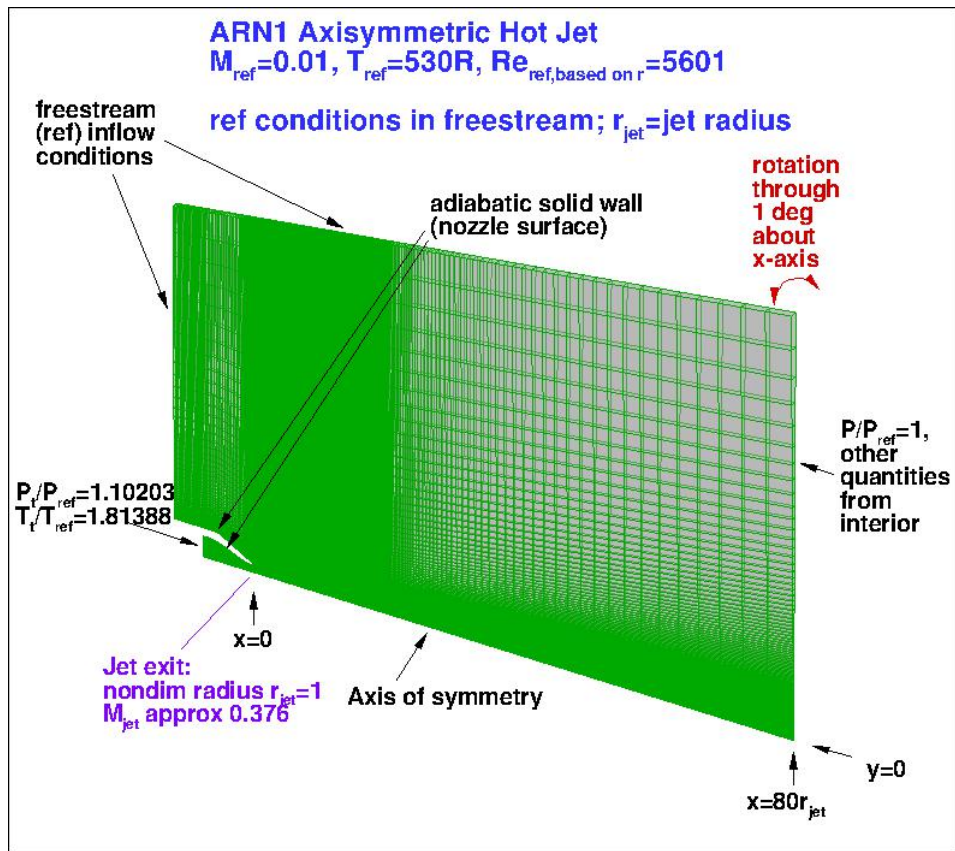


Figure 4: Schematic case set up for the Near-sonic Jet CFD simulations performed by NASA.

TABLE V: ARN2 Near-sonic Jet: boundary conditions

Boundary conditions		
Freestream	Ma_{free}	0.01
	T_{free}	294.44K
	Re_{free}	5601
Inlet	p_t	$p_{free} \cdot 1.861$
	T_t	$T_{free} \cdot 1.0$
Outlet	p	p_{free}

TABLE VI: ARN2 Near-sonic Jet: relevant quantities at the nozzle exit

Nozzle exit	
$Ma_{x=0}$	0.985
$T_{x=0}$	246.59K

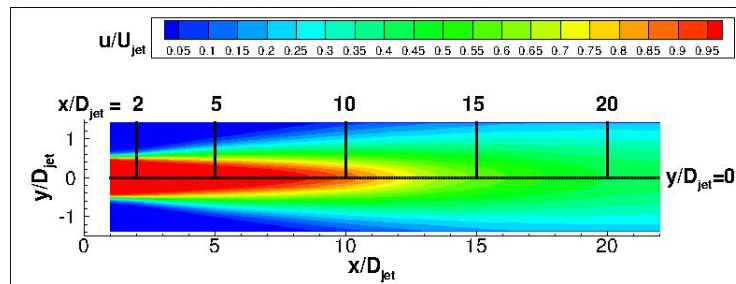


Figure 5: Flow field resulting from NASA CFD simulations of the Near-sonic Jet

2.2 SU2 simulations

A wide range of simulations have been run to in fact constitute the core of this project. The delicate task to test a new software, whose available documentation is still poor and most of the times non-official, has been faced moving progressive steps. The next sections are dedicated to the explanation of the different test cases. Each configuration was simulated with both SA and SST turbulence models and on grids with three different levels of resolution, to have a better idea of the mesh convergence.

2.2.1 CASE 01 - Validation and verification: Hot Subsonic Jet

The very first idea that comes to mind when dealing with a new configuration is to make sure to test the code in a case whose results are already well known. That is the reason why the first test case simulation that has been performed is a replication of the NASA test case of the Hot Subsonic Jet. The aim is to carry out both validation and verification of the SU2 turbulence models. Validation implies proving how close the simulations results are to reproduce real data and therefore the practice involves comparing them to the experimental data. Verification is instead carried out through a comparison between results on different software, so that one is able to distinguish where errors are intrinsic of the model and where the problems are instead related to the specific implementation of the code. So, verification has been performed comparing the SU2 results with the CFL3D and WIND ones that are also available for free download. To replicate the test case, the same specifications have been adopted, including the meshes resolution. This does not mean the same exact mesh file available on line have been adopted, as the software showed really high sensibility in this sense. In Section 3.5 the meshing procedure will be explained in details. However it was important to replicate simulations as close as possible to the ones carried out by NASA, so as to be able to have a fair comparison between the software that does not depend on simulations' parameters, mainly the mesh resolution, quality and structure. What will be presented in this and the following sections are screenshots of the configurations file used. The idea behind this approach is to give to the project also the function of a small user-tutorial guide for whoever could be interested in using the software for such configurations. Only the different free-stream and boundary

conditions values are reported in this section respectively in Figure 6 and Figure 7, whereas a complete configuration file will be attached in the appendix A.

```

% ----- COMPRESSIBLE FREE-STREAM DEFINITION -----%
%
% Mach number (non-dimensional, based on the free-stream values)
MACH_NUMBER= 0.01
%
% Angle of attack (degrees, only for compressible flows)
AOA= 0
%
% Side-slip angle (degrees, only for compressible flows)
SIDESLIP_ANGLE= 0.0
%
% Init option to choose between Reynolds (default) or thermodynamics quantities
% for initializing the solution (REYNOLDS, TD_CONDITIONS)
INIT_OPTION= TD_CONDITIONS
%
% Free-stream option to choose between density and temperature (default) for
% initializing the solution (TEMPERATURE_FS, DENSITY_FS)
FREESTREAM_OPTION= TEMPERATURE_FS
%
% Free-stream pressure (101325.0 N/m^2, 2116.216 psf by default)
FREESTREAM_PRESSURE= 98595
%
% Free-stream temperature (288.15 K, 518.67 R by default)
FREESTREAM_TEMPERATURE= 294.45
%
FREESTREAM_VISCOSITY=1.853E-5
%
% Reynolds length (1 m, 1 inch by default)
REYNOLDS_LENGTH= 1.0
%
% Compressible flow non-dimensionalization (DIMENSIONAL, FREESTREAM_PRESS_EQ_ONE,
% FREESTREAM_VEL_EQ_MACH, FREESTREAM_VEL_EQ_ONE)
REF_DIMENSIONALIZATION= FREESTREAM_PRESS_EQ_ONE

```

Figure 6: Free-stream conditions' values imposed for the Hot Subsonic Jet simulations

```

% ----- BOUNDARY CONDITION DEFINITION -----%
%
% Navier-Stokes (no-slip), constant heat flux wall marker(s) (NONE = no marker)
% Format: ( marker name, constant heat flux (J/m^2), ... )
MARKER_HEATFLUX= ( wall,0 )
%
% Far-field boundary marker(s) (NONE = no marker)
MARKER_FAR= ( farfield, lat_inlet )
%
% Inlet boundary type (TOTAL_CONDITIONS, MASS_FLOW)
INLET_TYPE= TOTAL_CONDITIONS
%
% Read inlet profile from a file (YES, NO) default: NO
SPECIFIED_INLET_PROFILE= NO
%
% File specifying inlet profile
INLET_FILENAME= inlet.dat
%
% Inlet boundary marker(s) with the following formats (NONE = no marker)
% Total Conditions: (inlet marker, total temp, total pressure, flow_direction_x,
%                   flow_direction_y, flow_direction_z, ... ) where flow_direction is
%                   a unit vector.
% Mass Flow: (inlet marker, density, velocity magnitude, flow_direction_x,
%             flow_direction_y, flow_direction_z, ... ) where flow_direction is
%             a unit vector.
% Incompressible: (inlet marker, temperature, velocity magnitude, flow_direction_x,
%                 flow_direction_y, flow_direction_z, ... ) where flow_direction is
%                 a unit vector.
MARKER_INLET= ( inflow, 534, 108654.4, 1, 0, 0 )
%
% Outlet boundary marker(s) (NONE = no marker)
% Format: ( outlet marker, back pressure (static), ... )
MARKER_OUTLET= ( outflow, 98595 )

```

Figure 7: Boundary conditions' values imposed for the Hot Subsonic Jet simulations

2.2.2 CASE 02 - Validation and verification: Near-sonic Jet

Also the second NASA test case described in Section 2.1.2 has been reproduced for further validation and verification. There is a reason why these two test cases were considered particularly interesting. The idea behind this project, as mentioned before, was to get as close as possible to simulate an aircraft engine exhaust gas flow. It is a sonic flow at high temperature, so that the two validation cases fill both tasks. Indeed, there is another similar test case that

```

% ----- BOUNDARY CONDITION DEFINITION -----%
%
% Navier-Stokes (no-slip), constant heat flux wall marker(s) (NONE = no marker)
% Format: ( marker name, constant heat flux (J/m^2), ... )
MARKER_HEATFLUX= ( wall,0 )
%
% Far-field boundary marker(s) (NONE = no marker)
MARKER_FAR= ( farfield, lat_inlet )
%
% Inlet boundary type (TOTAL_CONDITIONS, MASS_FLOW)
INLET_TYPE= TOTAL_CONDITIONS
%
% Read inlet profile from a file (YES, NO) default: NO
SPECIFIED_INLET_PROFILE= NO
%
% File specifying inlet profile
INLET_FILENAME= inlet.dat
%
% Inlet boundary marker(s) with the following formats (NONE = no marker)
% Total Conditions: (inlet marker, total temp, total pressure, flow_direction_x,
%                   flow_direction_y, flow_direction_z, ... ) where flow_direction is
%                   a unit vector.
% Mass Flow: (inlet marker, density, velocity magnitude, flow_direction_x,
%            flow_direction_y, flow_direction_z, ... ) where flow_direction is
%            a unit vector.
% Incompressible: (inlet marker, temperature, velocity magnitude, flow_direction_x,
%                flow_direction_y, flow_direction_z, ... ) where flow_direction is
%                a unit vector.
MARKER_INLET= ( inflow, 294.45, 183485.295, 1, 0, 0 )
%
% Outlet boundary marker(s) (NONE = no marker)
% Format: ( outlet marker, back pressure (static), ... )
MARKER_OUTLET= ( outflow, 98595 )

```

Figure 8: Boundary conditions' values imposed for the Near-sonic Jet simulations

NASA performed on a cold subsonic jet, but it was not really in the interest of the project and so it was not taken into consideration. The idea will be repeated and clarified when describing the next simulations. Figure 8 and Figure 9 report all the boundary conditions imposed for these simulations.

```

% ----- COMPRESSIBLE FREE-STREAM DEFINITION -----%
%
% Mach number (non-dimensional, based on the free-stream values)
MACH_NUMBER= 0.01
%
% Angle of attack (degrees, only for compressible flows)
AOA= 0
%
% Side-slip angle (degrees, only for compressible flows)
SIDESLIP_ANGLE= 0.0
%
% Init option to choose between Reynolds (default) or thermodynamics quantities
% for initializing the solution (REYNOLDS, TD_CONDITIONS)
INIT_OPTION= TD_CONDITIONS
%
% Free-stream option to choose between density and temperature (default) for
% initializing the solution (TEMPERATURE_FS, DENSITY_FS)
FREESTREAM_OPTION= TEMPERATURE_FS
%
% Free-stream pressure (101325.0 N/m^2, 2116.216 psf by default)
FREESTREAM_PRESSURE= 98595
%
% Free-stream temperature (288.15 K, 518.67 R by default)
FREESTREAM_TEMPERATURE= 294.45
%
FREESTREAM_VISCOSITY=1.853E-5
%
% Reynolds length (1 m, 1 inch by default)
REYNOLDS_LENGTH= 1.0
%
% Compressible flow non-dimensionalization (DIMENSIONAL, FREESTREAM_PRESS_EQ_ONE,
%                                     FREESTREAM_VEL_EQ_MACH, FREESTREAM_VEL_EQ_ONE)
REF_DIMENSIONALIZATION= FREESTREAM_PRESS_EQ_ONE

```

Figure 9: Free-stream conditions' values imposed for the Near-sonic Jet simulations

2.2.3 CASE 03 - Hot Near-sonic Jet

After the whole process of finding the correct settings for proper results and consequent validation and verification of the code, some other similar configurations have been simulated. An aircraft engine's emission is normally a high temperature sonic flow coming out of a nozzle, so something really close to the geometry and flow considered so far. Therefore, in order to

```

% ----- BOUNDARY CONDITION DEFINITION -----%
%
% Navier-Stokes (no-slip), constant heat flux wall marker(s) (NONE = no marker)
% Format: ( marker name, constant heat flux (J/m^2), ... )
MARKER_HEATFLUX= ( wall,0 )
%
% Far-field boundary marker(s) (NONE = no marker)
MARKER_FAR= ( farfield, lat_inlet )
%
% Inlet boundary type (TOTAL_CONDITIONS, MASS_FLOW)
INLET_TYPE= TOTAL_CONDITIONS
%
% Read inlet profile from a file (YES, NO) default: NO
SPECIFIED_INLET_PROFILE= NO
%
% File specifying inlet profile
INLET_FILENAME= inlet.dat
%
% Inlet boundary marker(s) with the following formats (NONE = no marker)
% Total Conditions: (inlet marker, total temp, total pressure, flow_direction_x,
%                   flow_direction_y, flow_direction_z, ... ) where flow_direction is
%                   a unit vector.
% Mass Flow: (inlet marker, density, velocity magnitude, flow_direction_x,
%            flow_direction_y, flow_direction_z, ... ) where flow_direction is
%            a unit vector.
% Incompressible: (inlet marker, temperature, velocity magnitude, flow_direction_x,
%                flow_direction_y, flow_direction_z, ... ) where flow_direction is
%                a unit vector.
MARKER_INLET= ( inflow, 692.6253552, 183485.295, 1, 0, 0 )
%
% Outlet boundary marker(s) (NONE = no marker)
% Format: ( outlet marker, back pressure (static), ... )
MARKER_OUTLET= ( outflow, 98595 )

```

Figure 10: Boundary conditions' values imposed for the Hot Near-sonic Jet simulations

simulate such a flow field the first step was to modify the boundary conditions in the near-sonic validation simulation by imposing a proper temperature at the nozzle's exit.

All the adopted values for an aircraft exhaust gas refer to [10]. So, to have an exit temperature of $T_J = 580K$ as in the case of a real emission flow, the isentropic relation:

$$T_t = T_J \cdot \left(1 + \frac{\gamma - 1}{2} Ma^2 \right) \quad (2.1)$$

allowed to compute the total temperature to be imposed at the inlet of our domain, whose value turned out to be $T_t = 692.625K$. Moreover, although validation data for this specific flow are not available, there is plenty of reasons for thinking that the results of this simulation can be considered somehow reliable. As previously pointed out, the same mesh configuration and resolutions have been used for simulating both a hot subsonic flow and a cold near-sonic flow. Therefore, simulating a hot near-sonic flow on the same grids should also give results that are at least good and representative, if not totally correct. Moreover, thanks to the availability of grids with different resolution levels, a mesh convergence study can also be performed. However this section had the only aims to describe the case set up and give the idea behind every choice, but all the details about the results will be fully covered in Section 5.1. Boundary conditions are reported in Figure 10, while the free-stream conditions are unchanged with respect to the other cases previously described, so the reference is Figure 9.

2.2.4 CASE 04 - Flight free-stream conditions

Once a realistic temperature has been applied to the emission gas, proper values of pressure and temperature for the free-stream air should be imposed. So far the flow simulated took into account the conditions of the experiment carried out by NASA, pretty close to standard air at zero altitude. However these values are different when considering real flight conditions. Moreover by adjusting the free-stream pressure also the exhaust flow will have a proper pressure value. The reason why also these results are expected to be reliable result is that simulations mainly depend on the ratios between the inlet conditions and the free-stream temperature and pressure values, which are unchanged as only depending on the flow Mach number. However,

```

% ----- COMPRESSIBLE FREE-STREAM DEFINITION -----%
%
% Mach number (non-dimensional, based on the free-stream values)
MACH_NUMBER= 0.01
%
% Angle of attack (degrees, only for compressible flows)
AOA= 0
%
% Side-slip angle (degrees, only for compressible flows)
SIDESLIP_ANGLE= 0.0
%
% Init option to choose between Reynolds (default) or thermodynamics quantities
% for initializing the solution (REYNOLDS, TD_CONDITIONS)
INIT_OPTION= TD_CONDITIONS
%
% Free-stream option to choose between density and temperature (default) for
% initializing the solution (TEMPERATURE_FS, DENSITY_FS)
FREESTREAM_OPTION= TEMPERATURE_FS
%
% Free-stream pressure (101325.0 N/m^2, 2116.216 psf by default)
FREESTREAM_PRESSURE= 23800
%
% Free-stream temperature (288.15 K, 518.67 R by default)
FREESTREAM_TEMPERATURE= 219
%
FREESTREAM_VISCOSITY=1.853E-5
%
% Reynolds length (1 m, 1 inch by default)
REYNOLDS_LENGTH= 1.0
%
% Compressible flow non-dimensionalization (DIMENSIONAL, FREESTREAM_PRESS_EQ_ONE,
%                                     FREESTREAM_VEL_EQ_MACH, FREESTREAM_VEL_EQ_ONE)
REF_DIMENSIONALIZATION= FREESTREAM_PRESS_EQ_ONE

```

Figure 11: Flight free-stream conditions imposed to the Hot Near-sonic jet simulations

again, this idea will be supported by a mesh convergence study. Figure 11 and Figure 12 show the free-stream and boundary conditions values used in the simulation. Free-stream values for flight condition have been extrapolated from the International Standard Atmosphere table [11]. To simulate a common case, properties at 11000m altitude have been considered.

```

% ----- BOUNDARY CONDITION DEFINITION -----%
%
% Navier-Stokes (no-slip), constant heat flux wall marker(s) (NONE = no marker)
% Format: ( marker name, constant heat flux (J/m^2), ... )
MARKER_HEATFLUX= ( wall,0 )
%
% Far-field boundary marker(s) (NONE = no marker)
MARKER_FAR= ( farfield, lat_inlet )
%
% Inlet boundary type (TOTAL_CONDITIONS, MASS_FLOW)
INLET_TYPE= TOTAL_CONDITIONS
%
% Read inlet profile from a file (YES, NO) default: NO
SPECIFIED_INLET_PROFILE= NO
%
% File specifying inlet profile
INLET_FILENAME= inlet.dat
%
% Inlet boundary marker(s) with the following formats (NONE = no marker)
% Total Conditions: (inlet marker, total temp, total pressure, flow_direction_x,
%                   flow_direction_y, flow_direction_z, ... ) where flow_direction is
%                   a unit vector.
% Mass Flow: (inlet marker, density, velocity magnitude, flow_direction_x,
%            flow_direction_y, flow_direction_z, ... ) where flow_direction is
%            a unit vector.
% Incompressible: (inlet marker, temperature, velocity magnitude, flow_direction_x,
%                flow_direction_y, flow_direction_z, ... ) where flow_direction is
%                a unit vector.
MARKER_INLET= ( inflow, 692.6253552, 44291.8, 1, 0, 0 )
%
% Outlet boundary marker(s) (NONE = no marker)
% Format: ( outlet marker, back pressure (static), ... )
MARKER_OUTLET= ( outflow, 23800 )

```

Figure 12: Boundary conditions for the Hot Near-sonic jet simulations in flight free-stream conditions.

2.2.5 CASE 05 - Aircraft's exhaust simulation

Last modification to be applied to simulate the realistic conditions of an aircraft's emission gas flow is the smallest but at the same time the most delicate. So far all the test cases involved a flow developing in quiescent air. This is however not the case for such a configuration, as the aircraft is actually travelling at high speed into air. It can be simulated on a CFD base

by imposing a velocity for the free-stream air of the same magnitude but opposite in sign with respect to airplane's speed. Common practice for aircraft external aerodynamics simulations is to impose a free-stream Mach number of 0.85. Boundary conditions are the same reported in Section 2.2.4, whereas the free-stream is now described by the values reported in Figure 13.

```

% ----- COMPRESSIBLE FREE-STREAM DEFINITION -----%
%
% Mach number (non-dimensional, based on the free-stream values)
MACH_NUMBER= 0.85
%
% Angle of attack (degrees, only for compressible flows)
AOA= 0
%
% Side-slip angle (degrees, only for compressible flows)
SIDESLIP_ANGLE= 0.0
%
% Init option to choose between Reynolds (default) or thermodynamics quantities
% for initializing the solution (REYNOLDS, TD_CONDITIONS)
INIT_OPTION= TD_CONDITIONS
%
% Free-stream option to choose between density and temperature (default) for
% initializing the solution (TEMPERATURE_FS, DENSITY_FS)
FREESTREAM_OPTION= TEMPERATURE_FS
%
% Free-stream pressure (101325.0 N/m^2, 2116.216 psf by default)
FREESTREAM_PRESSURE= 23800
%
% Free-stream temperature (288.15 K, 518.67 R by default)
FREESTREAM_TEMPERATURE= 219
%
FREESTREAM_VISCOSITY=1.853E-5
%
% Reynolds length (1 m, 1 inch by default)
REYNOLDS_LENGTH= 1.0
%
% Compressible flow non-dimensionalization (DIMENSIONAL, FREESTREAM_PRESS_EQ_ONE,
% FREESTREAM_VEL_EQ_MACH, FREESTREAM_VEL_EQ_ONE)
REF_DIMENSIONALIZATION= FREESTREAM_PRESS_EQ_ONE

```

Figure 13: Flight free-stream conditions including the imposition of the aircraft's speed.

TABLE VII: Boundary conditions comparison between all simulations

Boundary conditions					
	CASE 01	CASE 02	CASE 03	CASE 04	CASE 05
Ma_{free}	0.01	0.01	0.01	0.01	0.85
T_{free} [K]	294.45	294.45	294.45	219	219
p_{free} [Pa]	98595	98595	98595	23800	23800
$p_{t,in}$ [Pa]	108654.4	183485.295	183485.295	44291.8	44291.8
$T_{t,in}$ [K]	534	294.45	692.625	692.625	692.625
p_{out} [Pa]	98595	98595	98595	23800	23800

TABLE VIII: Nozzle's exit quantities comparison between all simulations

Nozzle exit					
	CASE 01	CASE 02	CASE 03	CASE 04	CASE 05
$Ma_{x=0}$	0.376	0.985	0.985	0.985	0.985
$T_{x=0}$ [K]	519.32	246.89	580	580	580

This condition represents a very critical change from a CFD point of view, so that the intent of this work is at the end to present the current status of such a case with the new tool SU2, to give a representative solution and finally to leave a solid base where to start from for future work. All simulations' relevant data and boundary conditions are reported together in Table VII and Table VIII to give a compact and complete overview.

CHAPTER 3

CURRENT STATUS AND BEST PRACTICE

One of the main goals of this project is to give a wide and detailed feedback on SU2 current status after a very deep testing in the turbulent round jet configuration. The idea is to both provide new users some sort of guidelines showing what settings at the moment are the most reliable and on the other hand to report some possible imperfections the code still holds, hoping this can be a good contribution for developers to spot which areas to work the most on to keep improving this amazing tool. That is the reason why all the steps moved into the software with relevant results will be presented. This section will show the whole path from the very first results to the final adjustments that allowed obtaining very important and precise results. Some introductory information is needed to better understand the approximations that could be applied to this test case. It is important to keep in mind that this flow configuration can be considered to a good approximation an axisymmetric flow. This means that it is acceptable considering to have the same solution in each radial section of the 3D flow laying on the jet centerline axis. It is common practice in these cases to exploit such features to run lighter simulations. In this way only a small part of the domain is used and so much less data are calculated and saved afterwards, reducing significantly the simulations run-time and the memory occupied. All simulations reported in the following sections refer to the first test case, the Hot Subsonic Jet. Once the set up to have good results have been found, it has been used to run all the other cases.

3.1 3D one-degree mesh

The first attempt was to reproduce the test case in the exact same way NASA did, as their results are considered as reference for verification. So the first aspect to analyze is the adopted domain's structure. The configuration they adopted involves a rotation around the centerline axis of a 2D meshed plane to obtain a 3D domain. However, the axisymmetric property of the problem allows to only rotate the plane of one degree and then impose proper boundary conditions on the lateral planes. This implies having a single layer of cells in circumferential direction, as generally CFD codes need this kind of configuration to solve a 2D case. Figure 2 and Figure 4 help figuring out the domain's shape, which is also represented and clearly visible in Figure 14. On the NASA websites the grids' files are available but in file formats that SU2 does not support. At first the rotated mesh was basically just exported in a different format. Then, as results were not as expected, other attempts involved using the 2D plane and rotating it directly on the software to obtain the 3D configuration. Other variants of this standard configuration were tested: using more than one degree rotation and/or more than one layer of circumferential cells. Second point to focus on is related to boundary conditions. Using only a one-degree portion of a 360° full domain implies two lateral radial planes to be at the boundary of the computational field. Only by applying a proper condition on these surfaces the axisymmetric approximation can be imposed. Indications from code developers found on the CFD online forum have been considered to implement the case, since as previously mentioned no official user guide documentation is available for the software yet. The suggested practice involves imposing a symmetry boundary condition on the two planes, as they intersect on the



Figure 14: One-degree 3D domain configuration.

centerline axis which is the symmetry geometric feature for a round jet (axisymmetric flow). Other attempt has been to use a periodic boundary condition on the two faces, but in this particular case all simulations diverged.

The result came out incorrect and it is reported as complete velocity field in Figure 15 with a zoom in the area of major interest, the centerline at the nozzle exit in Figure 16. The variable has been presented in its non-dimensional form as common practice for a round jet, since it also is the same convention followed by NASA in reporting both experiments and simulations results. The velocity is divided by the centerline ($r = 0$) velocity value at the nozzle exit

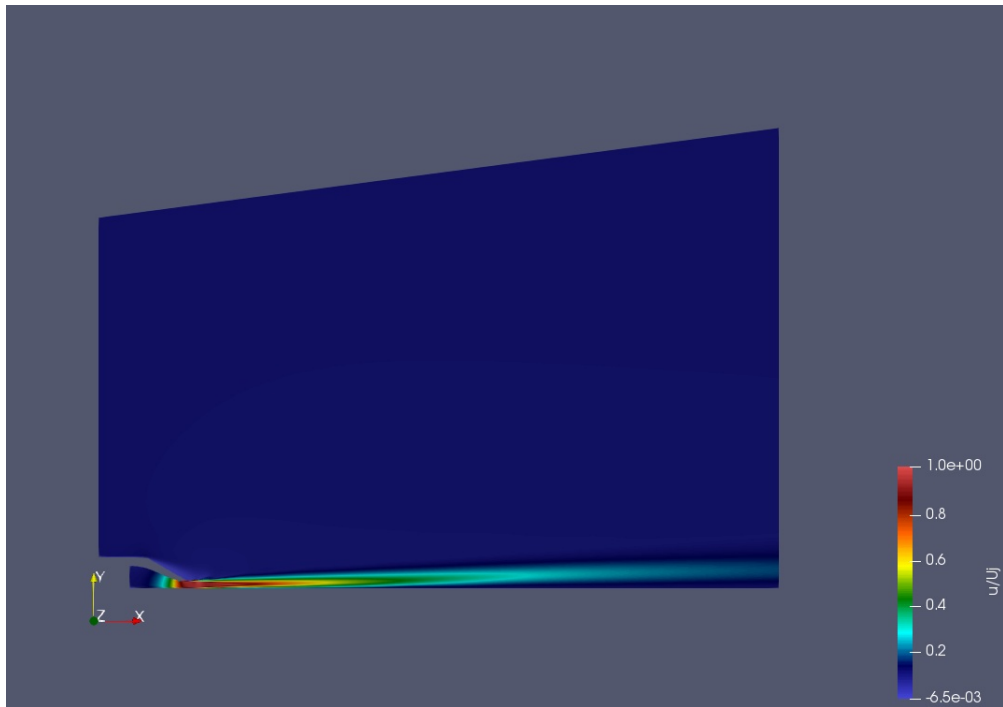


Figure 15: Non-dimensional velocity flow field result obtained with the one-degree domain configuration.

($x = 0$), denominated as U_J . This flow field should be compared to the one reported by NASA in Figure 3, considering that Figure 15 and Figure 16 just show half a section of the whole computational domain, so that their lower edge is actually the centerline of the jet. It is easy to spot that something is clearly going wrong in proximity of the centerline axis, which is indeed the most critical part of the whole simulation and where the symmetry condition holds. The velocity field shows a flow somehow detaching from the centerline, where instead the highest velocity is reached. This result suggests there is margin of improvement in the

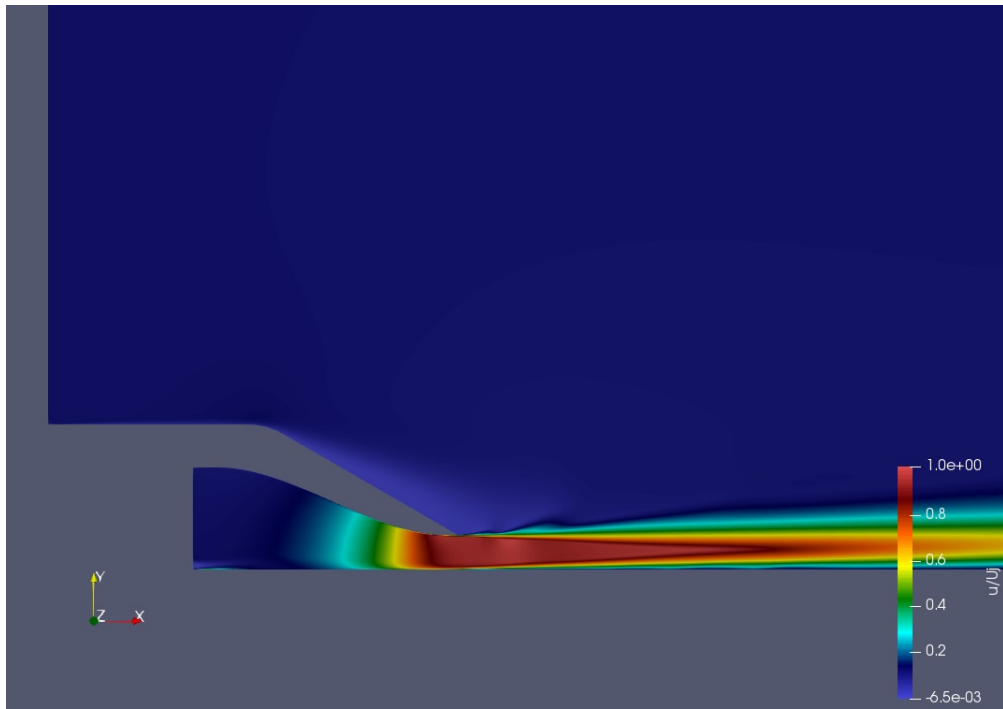


Figure 16: Centerline zoom of the non-dimensional velocity flow field result obtained with the one-degree domain configuration.

particular implementation of the symmetry boundary conditions applied to an axisymmetric geometry.

3.2 2D mesh

The second configuration that has been tested is again something suggested by the code developers. SU2 provides a function called “axisymmetric” which is able to solve an axisymmetric 3D problem on a two-dimensional grid. So the idea was to exploit this feature and solve the case on a real 2D domain, represented by half a section of the whole domain as shown in Figure 17. This case differs a bit from all the others as, being a 2D configuration, boundaries are

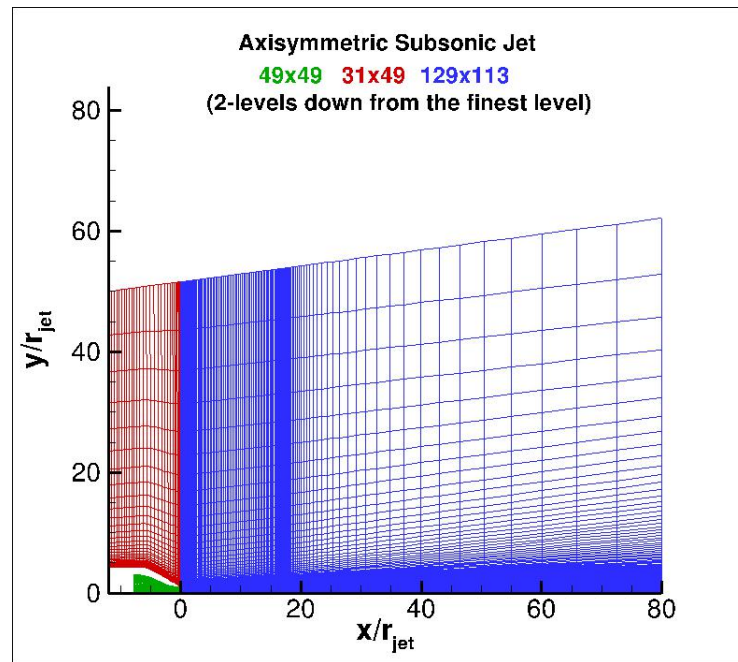


Figure 17: Two dimensional grid.

represented by edges rather than surfaces. The axisymmetric function requires the definition of a symmetry axis identified by the symmetry boundary condition. Therefore, the whole bottom edge of the domain has been set as symmetry boundary, being the centerline of the flow.

The result in this case represents a big improvement compared to the one described in the previous section. The fluid field shape is now feasible: nothing nonphysical happens at any point of the domain. Moreover, this configuration reduces dramatically the run-time of the simulation, reason why this axisymmetric feature available in SU2 is really powerful. However, results' values are still not really precise. In this case together with the flow field shown in Figure 18 and Figure 19, it is interesting to take a look at the velocity profile along the

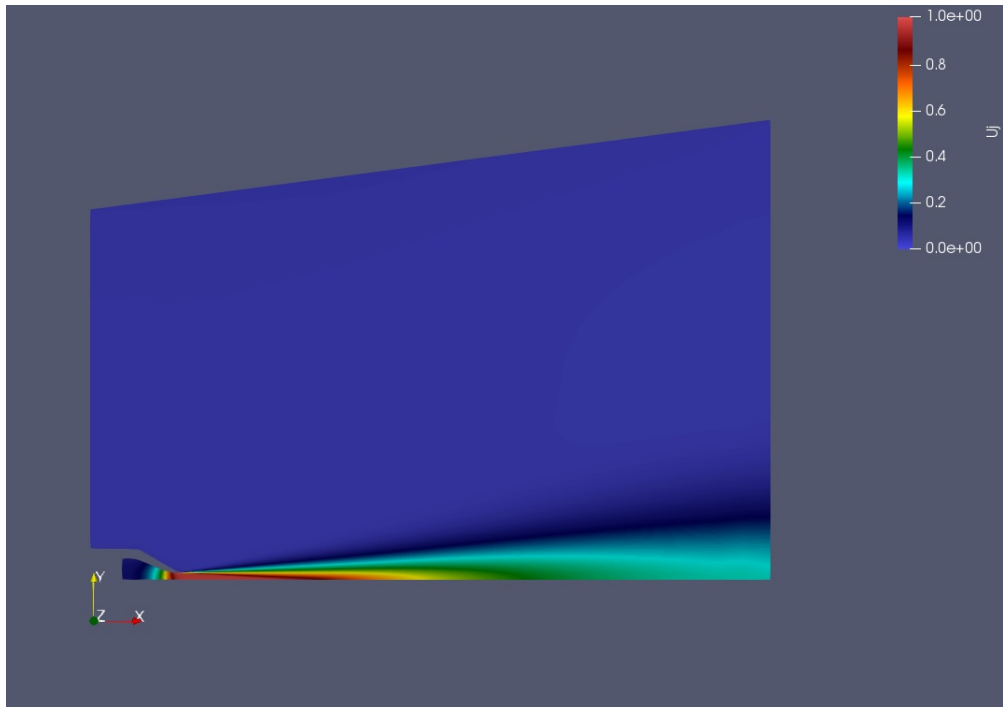


Figure 18: Non-dimensional velocity flow field result obtained with the 2D domain configuration.

centerline reported in Figure 20. Here the first real comparison between results is presented, as the two curves obtained from the simulations with SA and SST models are plotted together with the same results obtained by NASA and the experimental data. Curves extracted from SU2 results deviate quite a lot from the reference ones, as the velocity does not decrease at a sufficiently high rate.

The figures show a big and clear improvement compared to the one-degree mesh case (Figure 15 and Figure 16). The 2D axisymmetric tool is really amazing in terms of total computational time, as it would make possible to run such simulations very fast also on local machines.

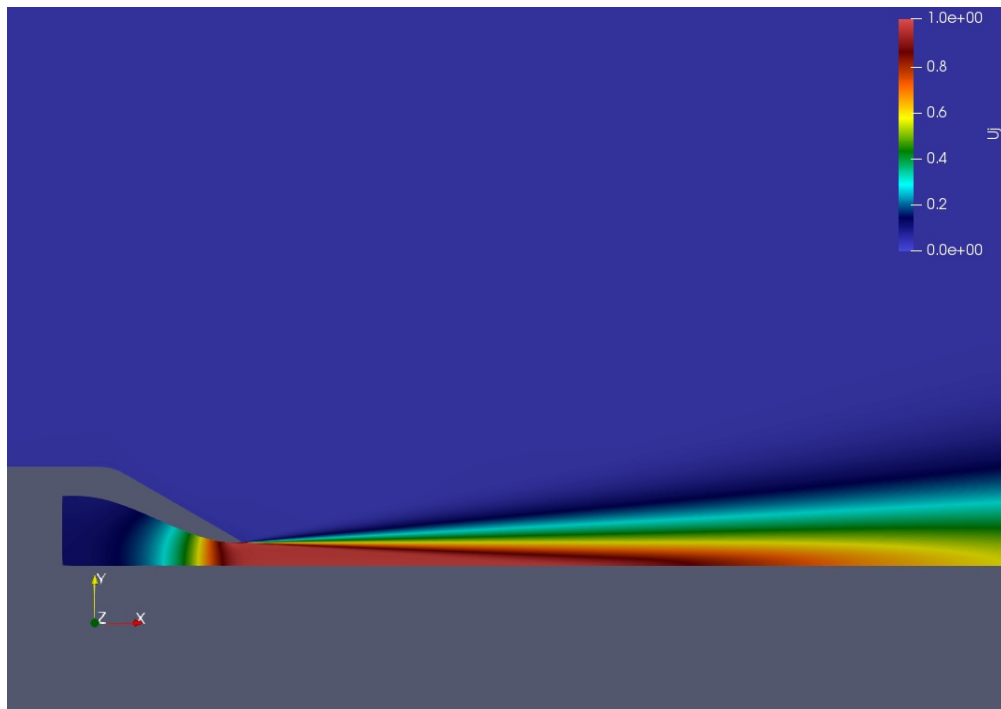


Figure 19: Centerline zoom of the non-dimensional velocity flow field result obtained with the 2D domain configuration.

Grids reduce to just few thousands elements. To give a comparison, a full scale 3D case would comprehend between 600 thousands up to more than 13 millions cells! The mismatch between the curves though is nothing negligible. It was not feasible in this particular configuration to obtain properly satisfying results, meaning there is still a limit in the usability of this feature. The tool shows however great potential and results that are at least feasible and not that far from being correct. It seems absolutely worth it to keep improving its implementation, in order to also be able to obtain more precise results. Considering this and the previous case, it seems clear that the implementation of all kind of symmetric approximations is what further needs to

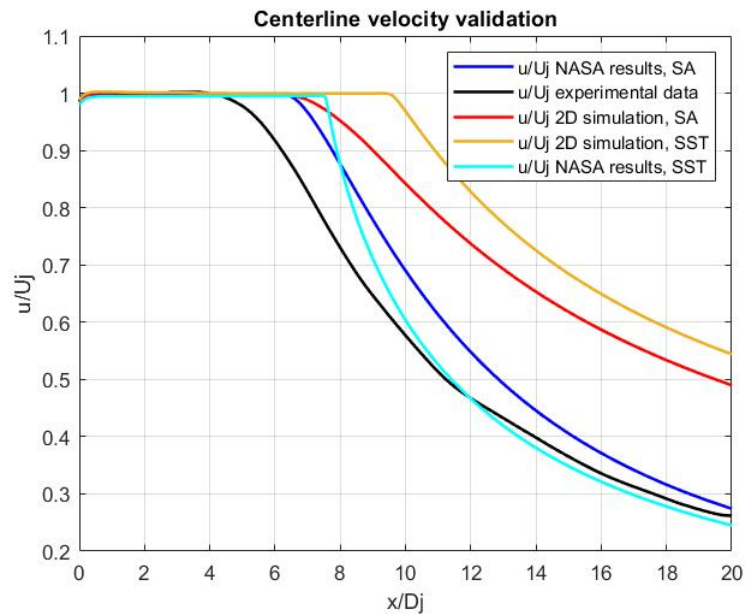


Figure 20: Centerline axial velocity profile for the 2D configuration.

be developed. It would definitely be greatly useful for users to keep improving these features. At the current status, results should be carefully double checked to assess their reliability.

3.3 3D mesh - Dimensional form of the Navier-Stokes equation

Once the full testing of all possible ways to exploit the axisymmetric characteristic of the flow has been covered, the complete 3D problem was resolved. So in this case the mesh is a 360° revolution of the 2D domain whose schematic representation is given by Figure 14. However, the meshing process required some important steps in order to reach a structure such that the solver was able to correctly use the domain's discretization. Full details about it will be provided at the end of this chapter in Section 3.5. It is just important so far to keep in

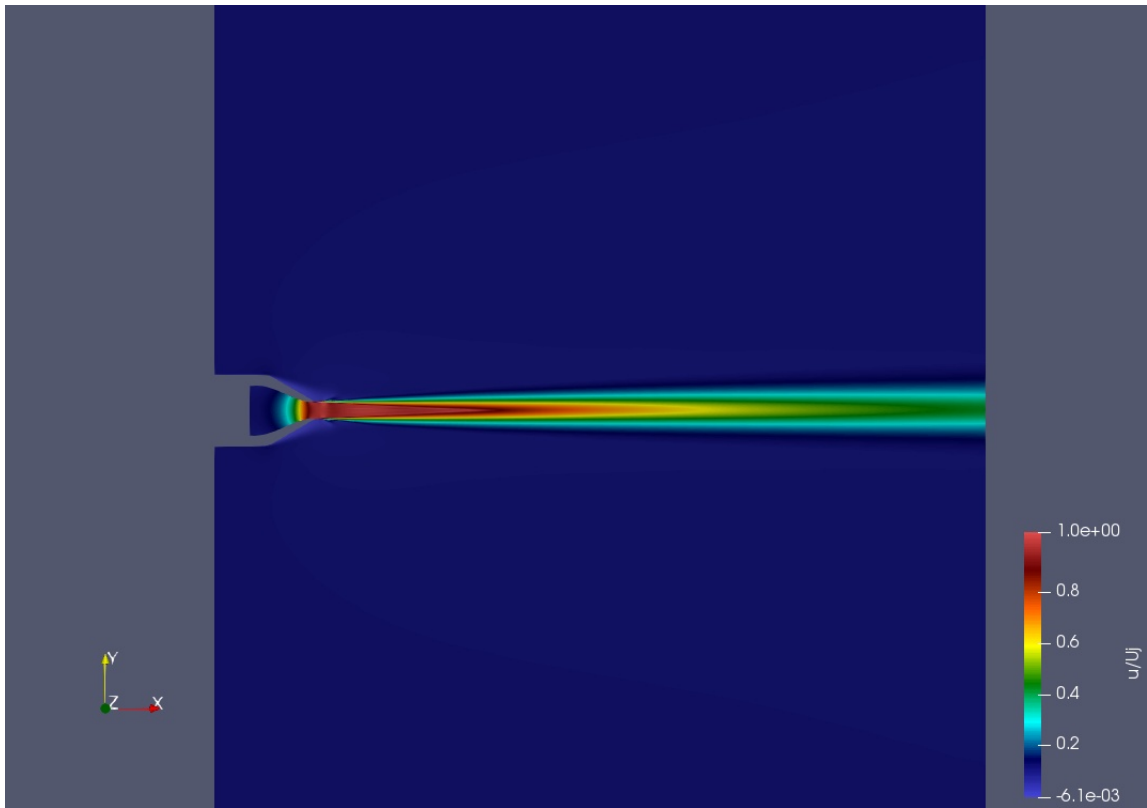


Figure 21: Non-dimensional velocity flow field result obtained with the 3D domain configuration in the dimensional form of the equations.

mind that the meshes adopted in the results shown in this section are exactly the same that have been used to obtain all the correct results shown in Chapter 4 and Chapter 5. Actually, between the results presented here and the simulations reported in Chapter 4 and Chapter 5, there is only one different setting: the equations in this case here have been solved in their dimensional form. Results show an unexpected substantial difference whether the equations are solved in their dimensional or non-dimensional form. Figure 21 shows the non-dimensional

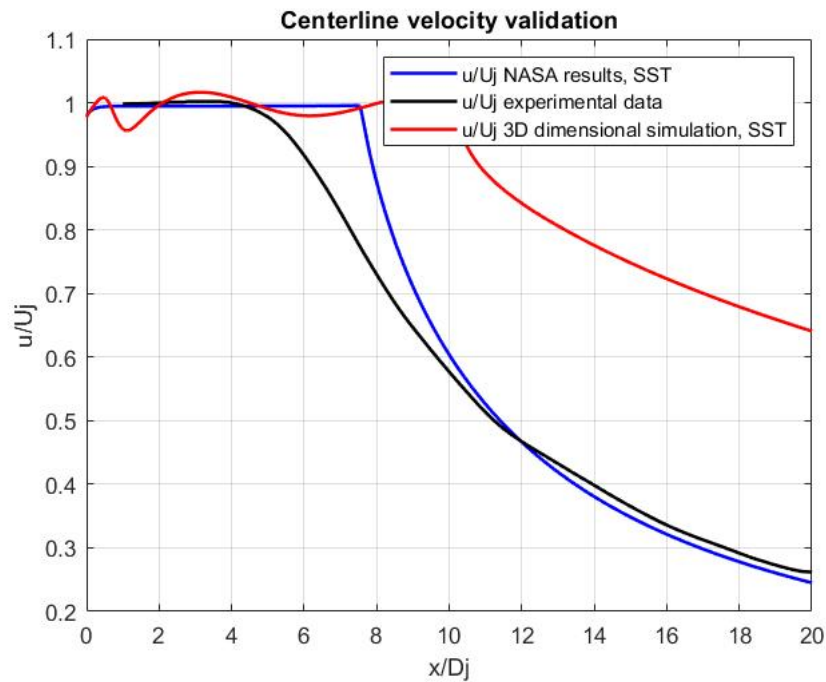


Figure 22: Centerline axial velocity profile for the 3D configuration in dimensional form of the equations.

velocity field and Figure 22 the non-dimensional velocity profile along the centerline obtained with SST turbulence model in comparison with NASA results and experimental data. The lack of precision in this case is pretty large. The curve lays far from the reference ones and some instability in the results is also visible. The flow field appears different than what expected, if one compares Figure 21 and Figure 3. The flow does not spread in radial direction, it remains very narrow around the centerline. Moreover, the rate at which the velocity decreases along the centerline is much lower than expected. The latter is the same imperfection spotted in Section 3.2 but of even higher intensity. Results in Section 3.2 have been obtained in the non-

dimensional form of the equations as it already represented a big improvement if compared to the results on the same 2D domain but with the equations in dimensional form. Generally speaking, solving the equations in non-dimensional form reduces the numerical dissipation, so that one would expect higher precision. However, the difference is really wide and it is hard to understand why. Recommendation for users would finally be to fully rely on the non-dimensional solver, as it allows obtaining extremely precise results. There are two possible ways the non-dimensionalization can be performed in SU2: using as a reference either the pressure or the velocity. In both cases results are really close, both options show a good behaviour. Let's focus on the way all the reference values for non-dimensionalization are calculated. Non-dimensionalization uses some of the values imposed at the free-stream as reference quantities, so that the idea is that specific values at the free-stream will be set as one rather than holding their physical magnitude. According to choice, some variables will be directly divided by their corresponding values at free-stream and the remaining will be calculated imposing the relevant fluid dynamics relations, which are the perfect gas law $p/\rho = RT$, the Mach number definition $Ma = u/\sqrt{\gamma RT}$ and the Reynolds number definition $Re = uL/\nu$. The Reynolds number is also calculated by the solver itself using the quantities imposed at free-stream, including the reference length (refer to Figure 6 as one of the possible examples). Therefore the difference between the two options is that one considers the velocity magnitude at the free-stream to be one and calculates pressure through the relations or vice versa the pressure is set to one and the velocity calculated. In all cases, together the chosen quantity also the temperature and density will be set to one. Then one should remember also that the Mach number is imposed and the

TABLE IX: Pressure non-dimensional equations: reference quantities calculation

Imposed quantities				
Pressure	Temperature	Density	Mach	Reynolds
$p_{ref} = p_{free}$	$T_{ref} = T_{free}$	$\rho_{ref} = \rho_{free}$	Ma	Re

Calculated quantities		
Gas constant	Velocity magnitude	Viscosity
$R_{ref} = R$	$U_{ref} = \frac{U_{free}}{Ma\sqrt{\gamma}}$	$\nu = \frac{U_{free}U_{ref}}{Re}$

gas constant γ is itself non-dimensional. A schematic of all the reference values is reported in Table IX for pressure non-dimensionalization and Table X for velocity non-dimensionalization. The suffix *ref* indicates the reference quantity, so that for example the code will then solve for the velocity in terms of U/U_{ref} .

TABLE X: Velocity non-dimensional equations: reference quantities calculation

Imposed quantities				
Velocity magnitude	Temperature	Density	Mach	Reynolds
$U_{ref} = U_{free}$	$T_{ref} = T_{free}$	$\rho_{ref} = \rho_{free}$	Ma	Re

Calculated quantities		
Gas constant	Pressure	Viscosity
$R_{ref} = \frac{1}{Ma^2\gamma R}$	$p_{ref} = \frac{p_{free}}{\gamma} \cdot \frac{R_{ref}}{R}$	$\nu = \frac{1}{Re}$

3.4 Best practice overview

This is a short recap of all that has been discussed in details in the previous sections, with the intention to give a compact overview of all the settings that after a deep study turned out to be those who give the most reliable results. First of all, it is important to solve the equations in their non-dimensional form, whether non-dimensionalization is performed through pressure or velocity. Then, another important hint coming from testing is to still not use any axisymmetric approximations. Although there is more than one possibility implemented, simulations are really tricky to handle in this configuration and results may turn out to be not precise. Therefore, the flow has been completely solved in the whole 3D domain. This is for sure a compromise in terms of run-time but also the safest choice to obtain reliable results. Finally, a good improvement is also achievable by using the ROE numerical scheme. Other methods such as JST are still able to give good results, implying this is no major factor in the simulation. However the ROE numerical method allowed to get the closest to reality among all the possible ones, since it involves the least numerical dissipation. Therefore last hint would be to adopt the ROE numerical scheme to get even closer to reality, even though the two main factors to keep into account are the configuration of the domain (3D) and the form of the equations (non-dimensional).

3.5 Mesh generation

The mesh generation process is one of the keys to be able to properly run the simulations. As previously mentioned, the starting bases are the grids provided by NASA. The reason behind it is to have the fairest possible comparison between software. However, this does not mean that

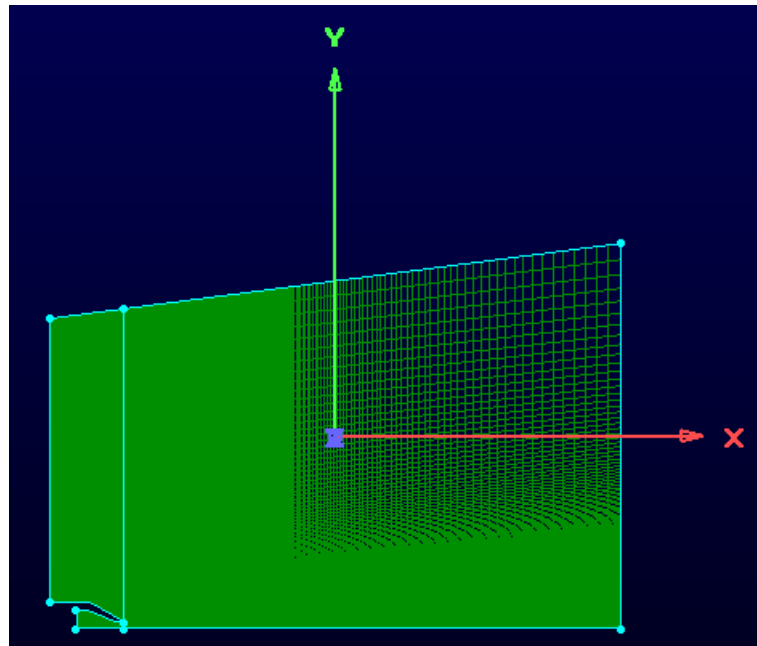


Figure 23: 2D mesh domain.

the grids have been just downloaded and adopted, but some manipulation was required on all of them to make them suitable for working with SU2. Therefore, in the end only the meshes overall structure and resolution of the original grids are still there, so that the results dependence on the grid should not be different than it was for NASA. The final mesh configuration will look pretty different to allow SU2 to properly work but not in a way results should be influenced by these modifications. So let's take a look at the steps involved in the meshing process. The starting point is a 2D grid looking like Figure 23. Pictures show the finest mesh level. It is hard to spot the mesh structure in all the figures, but the main objective of this section is to show the process leading to the final meshes. The resolution of the grids is always something very similar

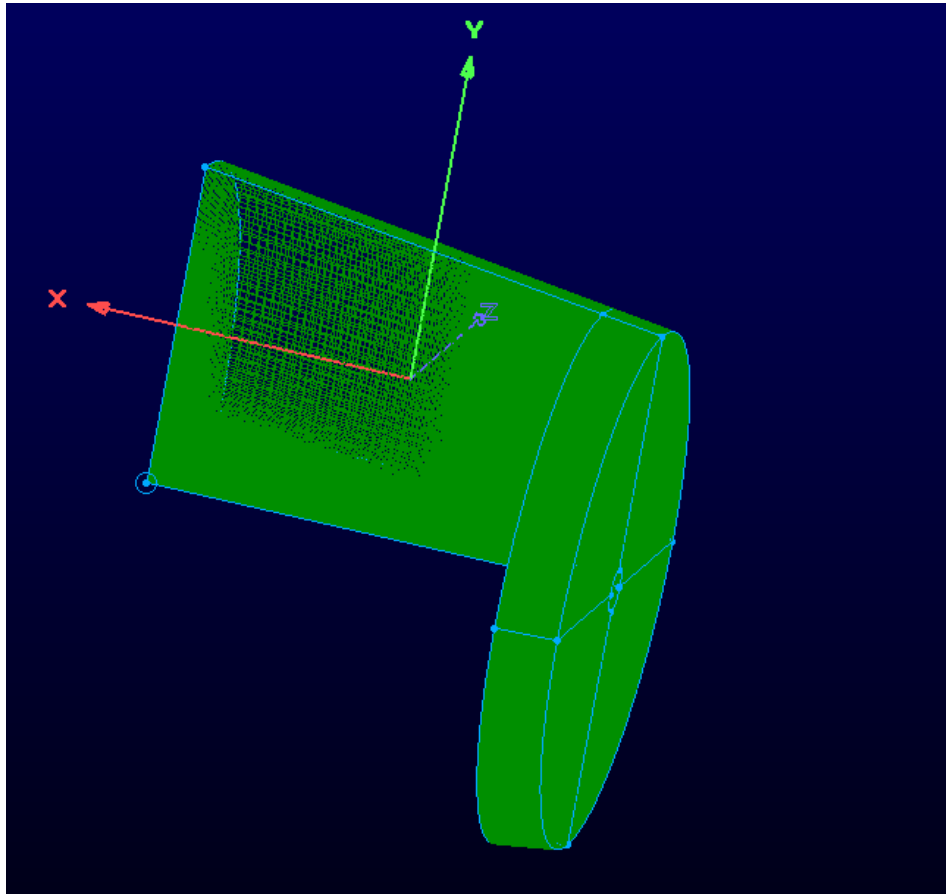


Figure 24: Mesh rotation process.

to Figure 17. This 2D domain must be then rotated. The rotation was not performed directly 360° . Since it will be necessary to split the mesh into four equal blocks and the reason why will be shown soon, the rotation was performed through four 90° steps. Here the circumferential resolution of the mesh has to be chosen. Results have been obtained using meshes with three different resolution levels, which will be called fine, medium and coarse grids for sake of easy understanding. For the fine level mesh a 2° circumferential resolution has been adopted, while

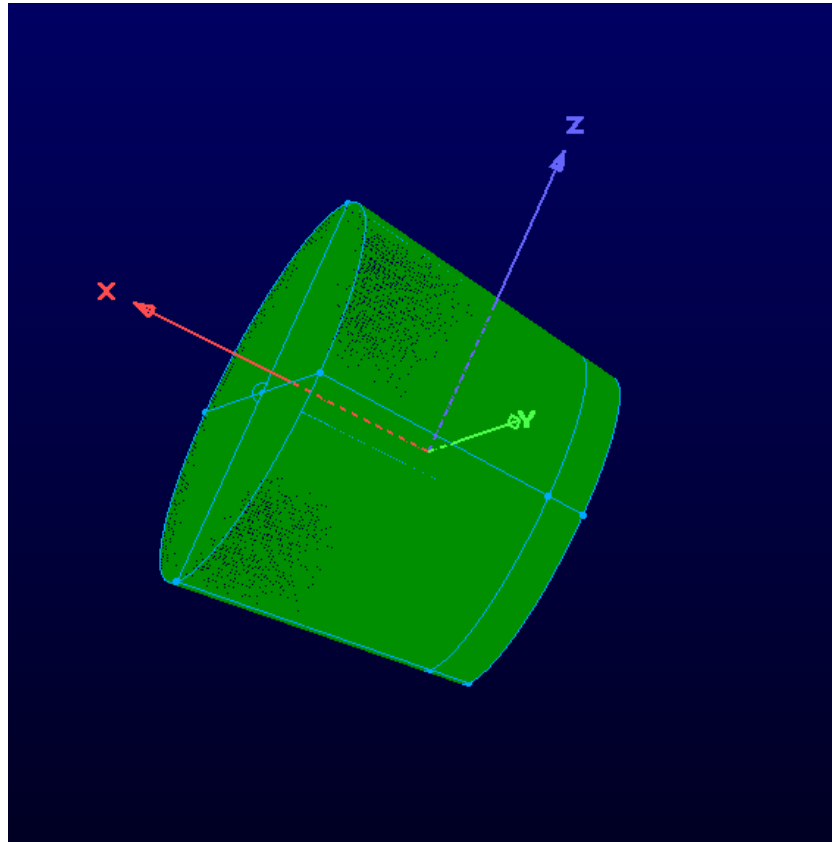


Figure 25: Complete mesh rotation.

medium and coarse meshes have 3° instead. The rotation process can be better figured out by taking a look at Figure 24 and Figure 25. Figure 24 also shows how the 2D domain is first split in three different parts and then each of them is rotated separately. The three different regions are the nozzle, the far-field upstream the nozzle exit and the far-field downstream the nozzle exit. This can be visualized in the 2D view of Figure 23 where one can easily see a vertical line in correspondence of the nozzle exit. Now the key point for the meshing process

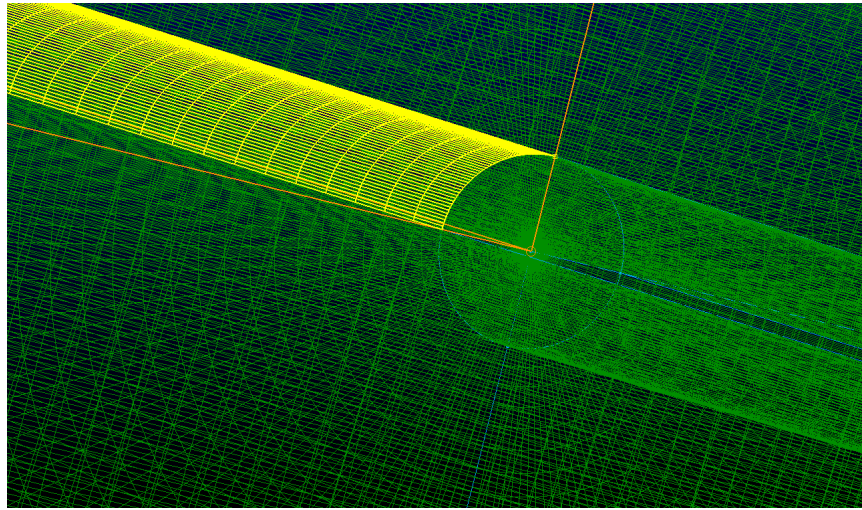


Figure 26: Mesh blocks splitting.

will be described. All the cells have six boundary surfaces but those on the centerline, as the rotation implies one surface to collapse into a single line. This is something that does not allow the software to properly work. So the idea is in simple words to empty a cylindrical area the centerline throughout the whole domain and then fill it back again with cells. This is done by splitting each of the blocks and then deleting the one laying on the centerline. Considering Figure 26, the block will be split in two parts, one above the yellow surface and one below it. The one below, being the one laying on the centerline, must be deleted. Keeping in mind every block represents just one fourth of the mesh in circumferential direction, after all four blocks of each of the three domain regions is split like in Figure 26 and the inner blocks deleted, an empty cylinder is left around the centerline. Now, next step is to create two circular domains at the boundaries of this empty region. The reason why it was necessary to perform the rotation in

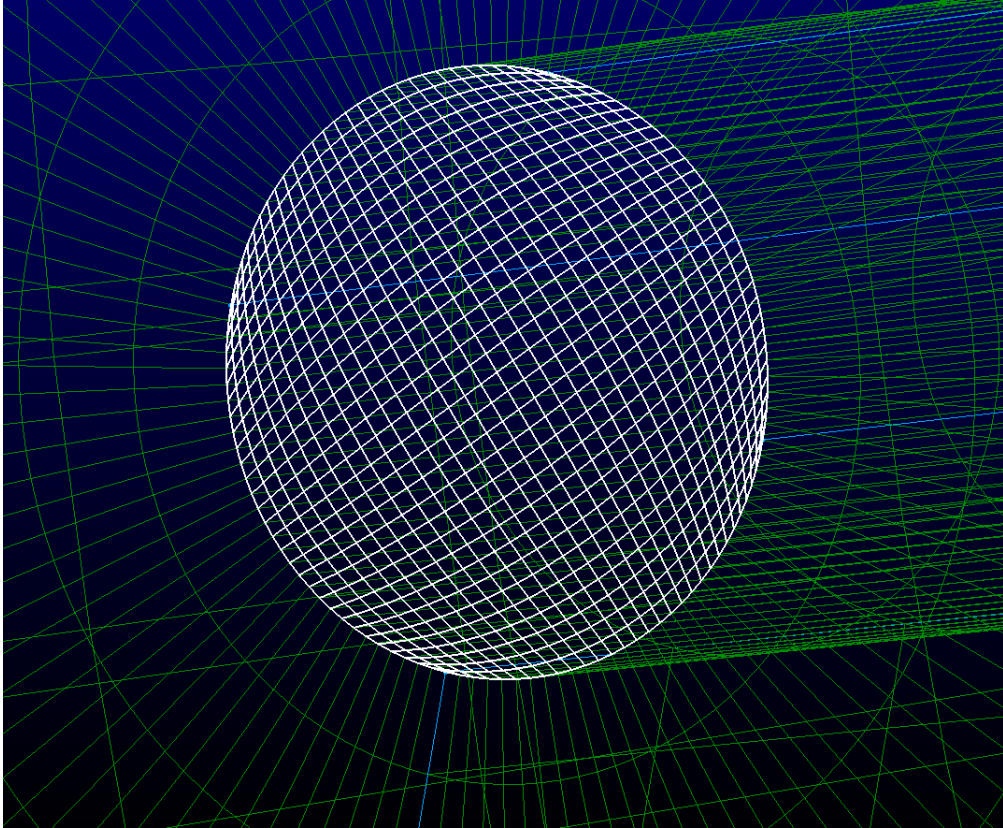


Figure 27: Mesh surface at the empty region boundary.

four 90° steps is that four edges are needed to fill a domain in Pointwise. So automatically, by having four different rotating blocks and then four different split blocks, four edges are created where a domain must be generated. This domain is shown in Figure 27. Once the two domains are created, selecting those and the inner surfaces of the current hollow domain (which are just like the yellow surfaces in Figure 26) a block can be created to properly fill the empty region. However, Figure 27 shows another critical point. It is possible to see how some grid elements in the white surface are very stretched and flat. This would produce a very high area ratio

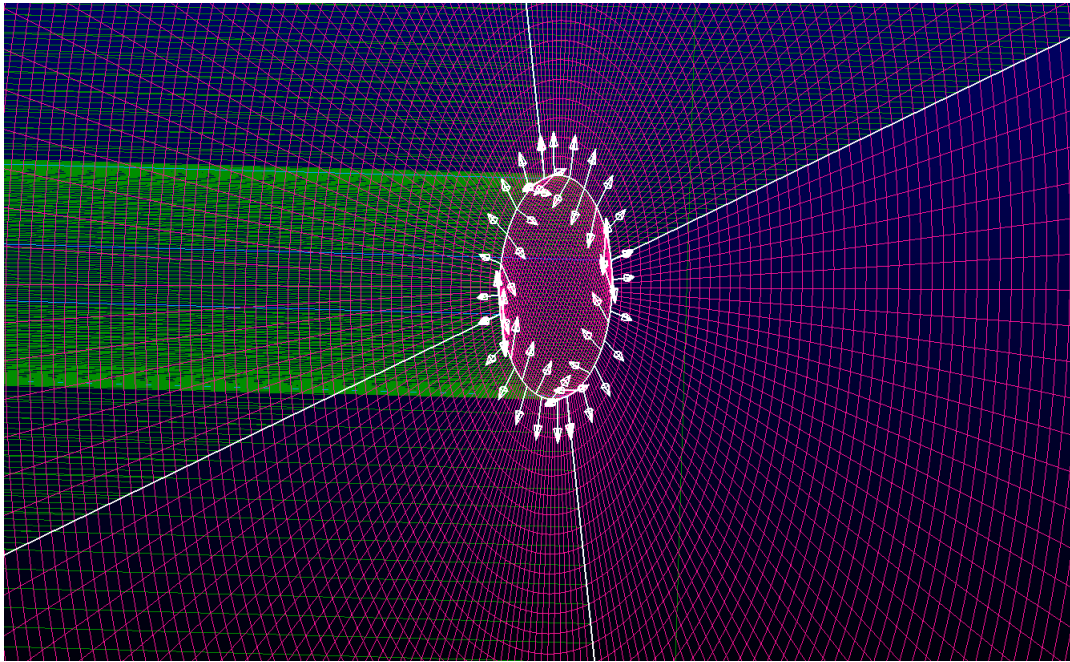


Figure 28: Solve operation on axial boundary domains.

and consequently volume ratio when creating the blocks, which is nothing desirable for a good quality mesh. So to overcome this problem it is necessary to perform a "solve" operation on the two boundary domains. By selecting all the faces showed in pink in Figure 28, some solving iterations have been performed on them. What this procedure will do is to slightly adjust the domains shape so as to get to a better configuration in terms of area ratio. The final result is shown in Figure 29. The transition between the meshes obtained by rotation and the filling of the empty region now is much smoother, no grid elements have a stretched look so that the quality of the mesh is now good. Once the internal block is generated, the mesh is finally ready.

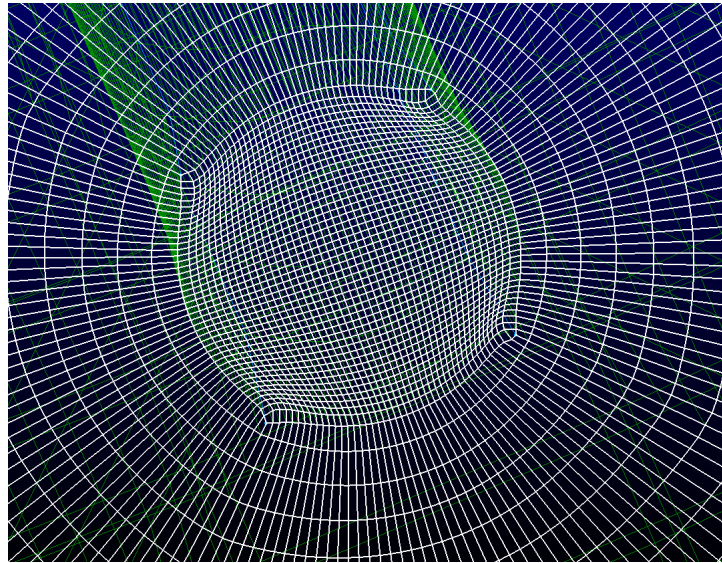


Figure 29: Axial boundary domain after performing solve operation.

3.5.1 Boundary domains

This small section is meant to better show the different boundary domains and point out what boundary condition has been imposed on each of them. The light green domain in Figure 30 is the inlet of the nozzle, where an inflow boundary condition has been applied with proper values of total pressure, total temperature and flow direction (axial, so along x direction). On the purple and yellow domains in Figure 32 the far-field properties are imposed. Then, the orange surface in Figure 31 is the outlet of the domain, so that an outflow condition must be applied. The only imposition required is the back pressure on that surface, which in this case just corresponds to the far-field pressure. Finally, the walls of the nozzles are the blue surfaces in Figure 33. Here a no-slip condition will be applied. As previously mentioned simulations

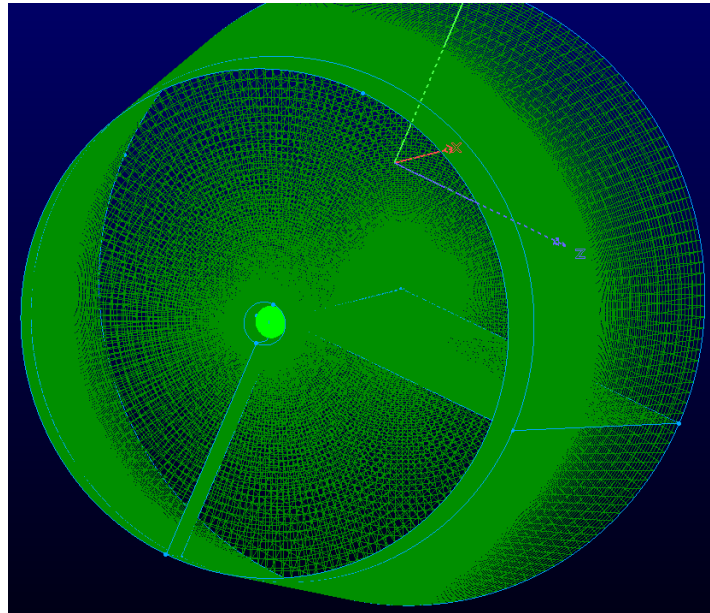


Figure 30: Nozzle's inlet boundary.

TABLE XI: Number of total elements for the different adopted grids

Number of cells		
Coarse	Medium	Fine
641 924	2 479 397	13 322 858

were run on three different grids with different mesh resolution levels, which will be named respectively fine, medium and coarse. The structure they hold is the same, what changes is just the number of elements on the 2D starting plane (Figure 17) and therefore in the end in the whole grid. Moreover, the circumferential element size of the fine mesh is 2° , while for the medium and coarse meshes it is 3° . Table XI reports the number of total cells for each grid.

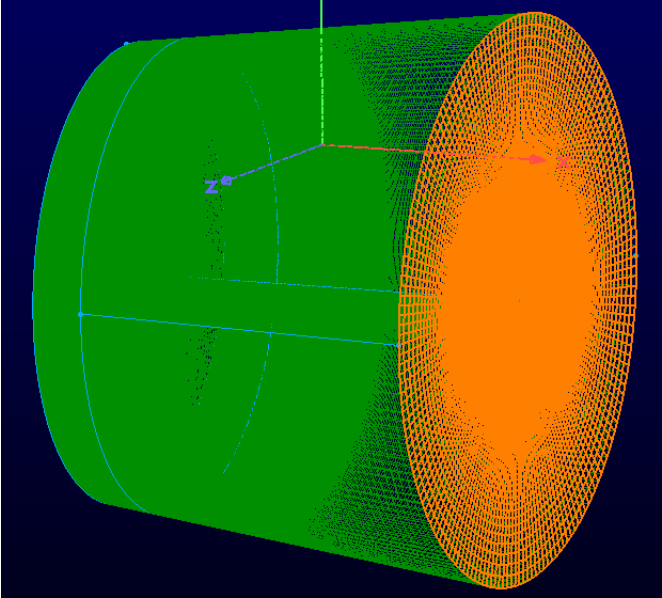


Figure 31: Domain's outflow boundary.

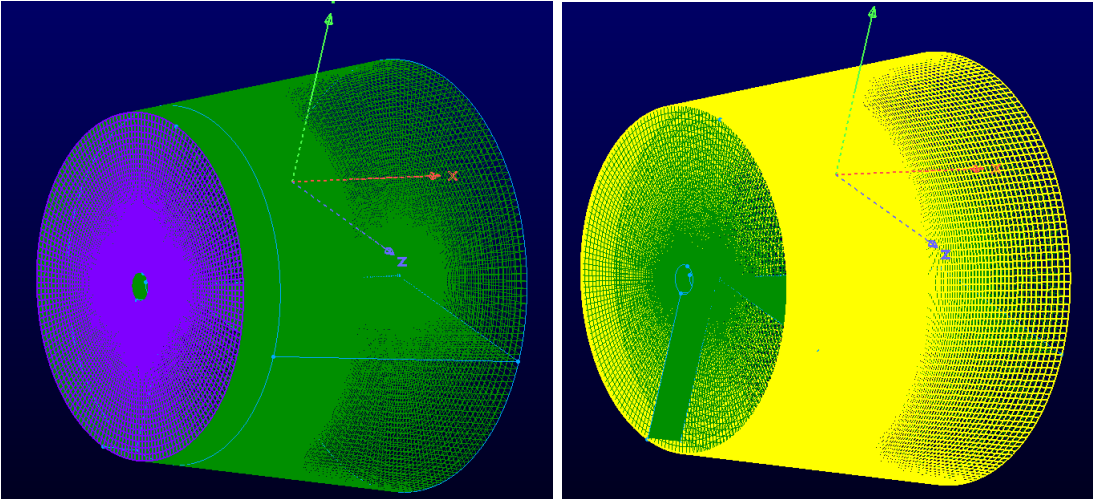


Figure 32: Far-field boundaries.

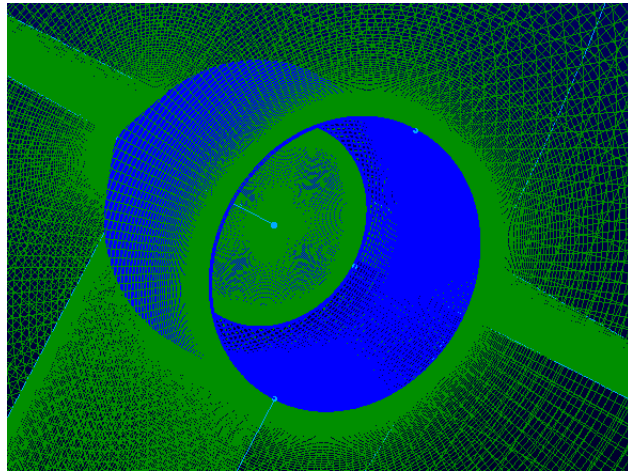


Figure 33: Nozzle's walls.

CHAPTER 4

VALIDATION RESULTS

This section is dedicated to show the validation and verification of the code. All the useful flow field pictures and profiles are reported. The main quantity this study is focused on is the flow velocity, in terms of both axial u and radial v component. According to common practice, all the values are in their non-dimensional form, which means the dimensional profiles are always divided by the centerline axial fluid velocity at the nozzle exit, namely $U_J = u(x = 0, r = 0)$. In this chapter results will be presented for the two validation cases, Hot Subsonic and Near-sonic turbulent round jet, using both the SST and SA turbulence models. These four cases will show a good comparison between the results obtained on SU2 in the configuration previously explained in details, the NASA results and experimental data. This shows the reliability of the simulations on SU2 representing both validation and verification of the code for such a fluid flow. Results consist in non-dimensional velocity profiles. Only the axial velocity plot is useful along the centerline, while on different radial sections both the axial and radial velocity components profiles are shown. To help giving a clear understanding of where in the flow the different radial profiles are extracted, a picture of the fluid flow with an arrow in the specific line will also be shown. Radial sections of interest are $x = 2D$, $x = 5D$, $x = 10D$ and $x = 15D$, where D is the nozzle exit section diameter. One thing to be pointed out is the way the radial profiles have been obtained and a difference that will be clear in the corresponding plots between the results presented for this thesis and those obtained by NASA. Especially in proximity of the

symmetry axis, results show more oscillations compared to the perfectly smooth ones obtained by NASA. The reason is NASA solved the fluid flow imposing perfect axisymmetry, so that this leads to smooth curves. However, axisymmetry is a very good and close approximation but not a perfect characteristic of the flow. That is why when solving the complete 3D configuration, one cannot expect to extract perfectly smooth profiles at any section. Actually, the profile on a single section are much less smooth than those presented. The way those curves have been obtained is by extracting radial profiles on 8 different lines at any section and then averaging all the curves. To better figure out what this means, if one thinks of the 360° domain at the same section x there is infinite possible lines where a radial profile of velocity can be extracted. The idea behind axisymmetry is that on average, any radial profile should be almost the same. This can be translated in a property that would hold if one takes an average on all infinite radial lines. This might look in the graphs as an imperfections, but actually represents a further prove of the good behaviour of the code in this particular configuration if results are interpreted in the right way. It would not be feasible to have a smooth profile on every section. On the other hand, by adding up more and more profiles to be averaged the results indeed smooth down. This is what one would expect in an axisymmetric flow, therefore it should be considered as a further element of validation and correctness of the results.

4.0.1 CASE 01 - Hot-Subsonic turbulent round jet results

4.0.1.1 CASE 01 - Spalart-Almaras turbulence model results

First presented result is the Hot Subsonic turbulent round jet simulation using the Spalart-Almaras turbulence model. One should not be surprised that results are not perfectly matching

the experimental results. Turbulence models hold necessarily approximations that might force results to slightly deviate from reality. Moreover, the SA model is not the most appropriate for this configuration, being a one-equation model whose strong approximation fits much better external aerodynamic cases. However, it is important to test the behaviour also of this model and to compare it with both the NASA results and the results obtained using the SST turbulence model. Results in general are very close to the NASA ones. It is also pleasant to notice how sometimes the profiles obtained with the finest mesh are indeed even closer to the experimental data curves than the results obtained by NASA.

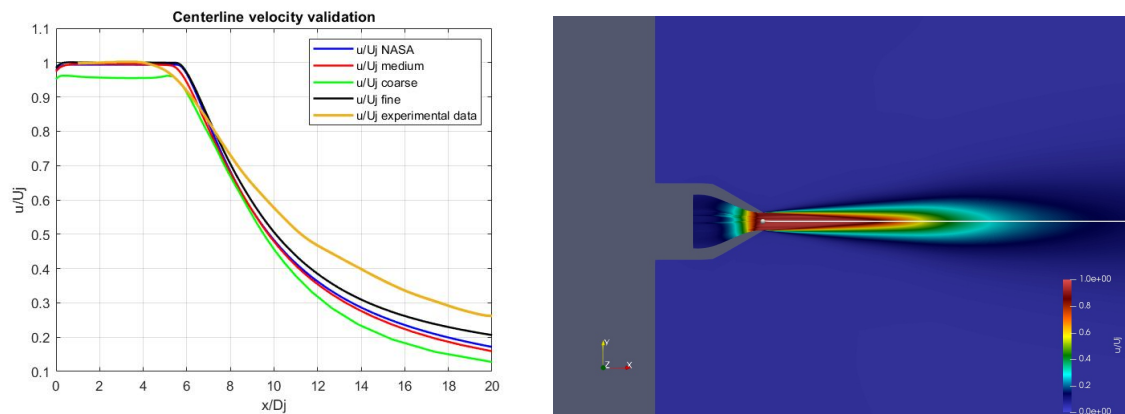


Figure 34: SA results: axial velocity profile along centerline for the Hot Subsonic jet.

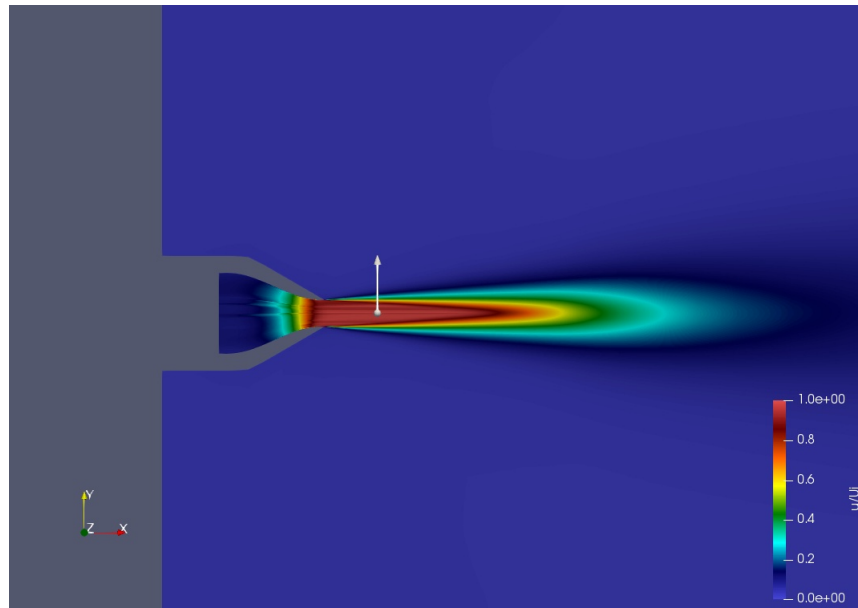


Figure 35: $X = 2D$ line representation on the fluid flow of the Hot Subsonic jet.

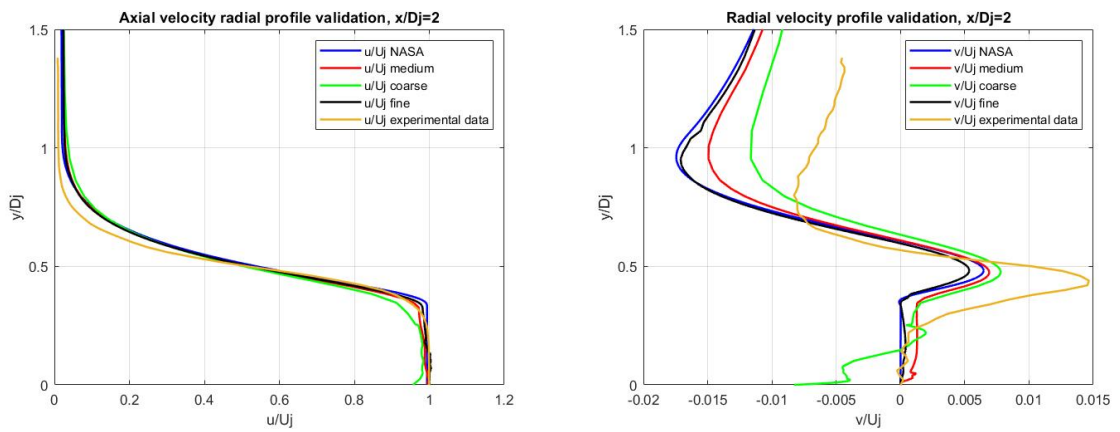


Figure 36: SA results: axial (left) and radial (right) velocity radial profiles at $x = 2D$ for the Hot Subsonic jet.

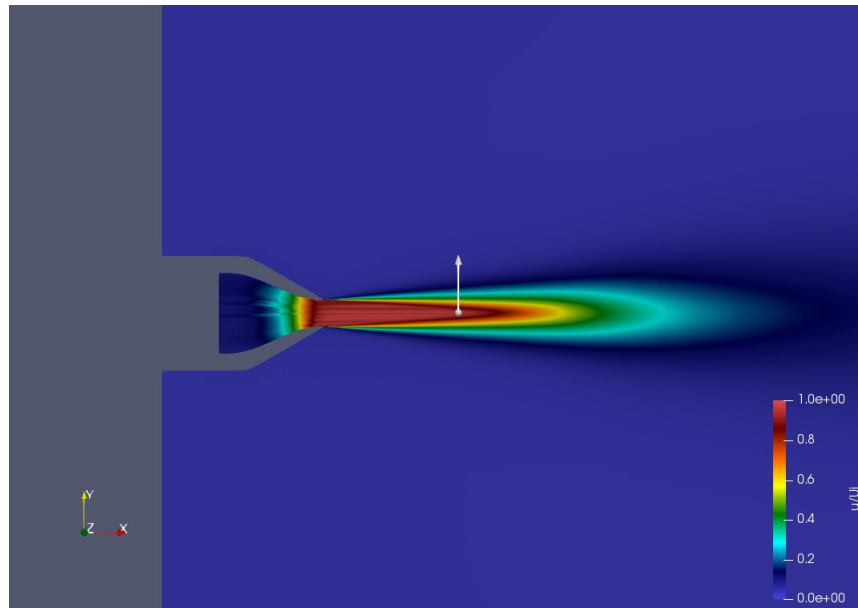


Figure 37: $X = 5D$ line representation on the fluid flow of the Hot Subsonic jet.

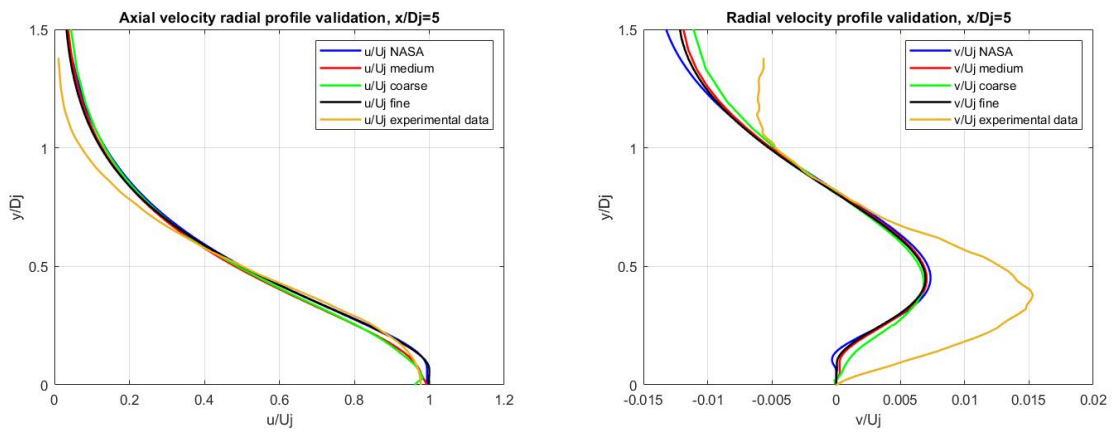


Figure 38: SA results: axial (left) and radial (right) velocity radial profiles at $x = 5D$ for the Hot Subsonic jet.

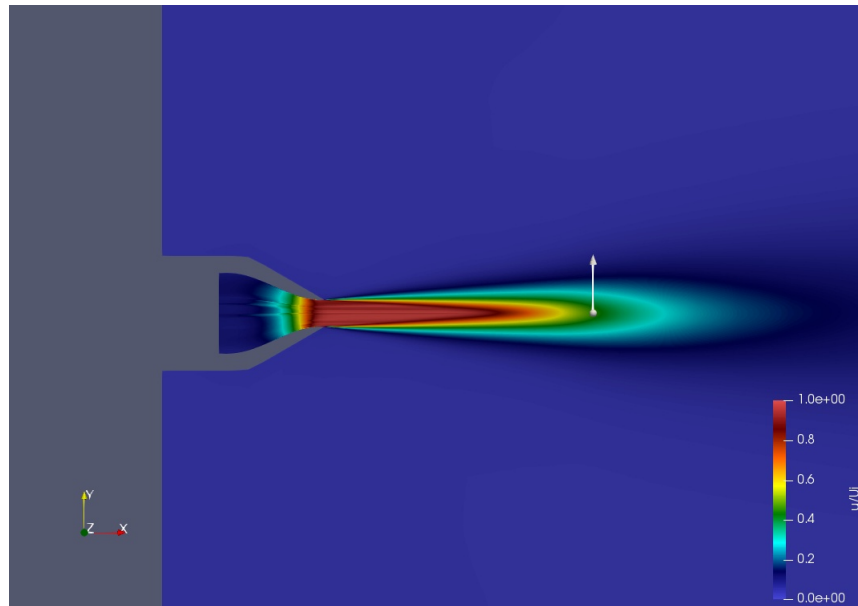


Figure 39: $X = 10D$ line representation on the fluid flow of the Hot Subsonic jet.

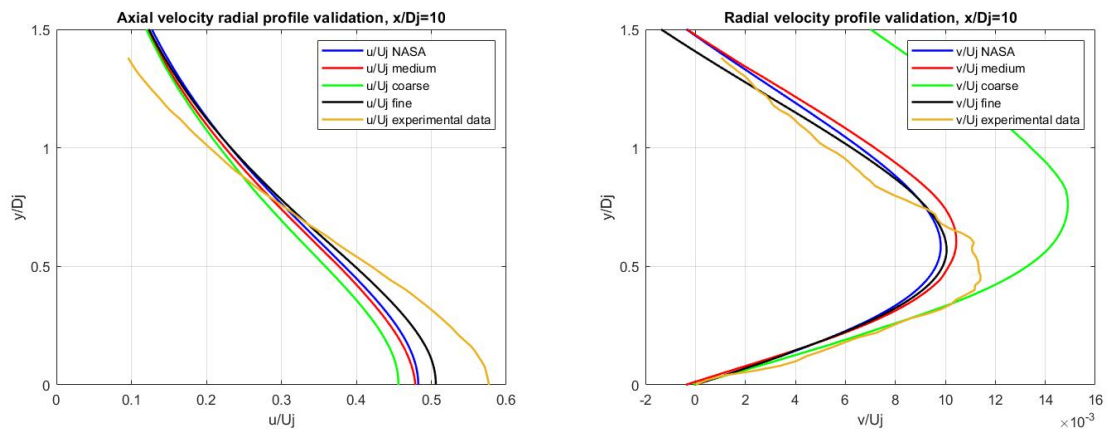


Figure 40: SA results: axial (left) and radial (right) velocity radial profiles at $x = 10D$ for the Hot Subsonic jet.

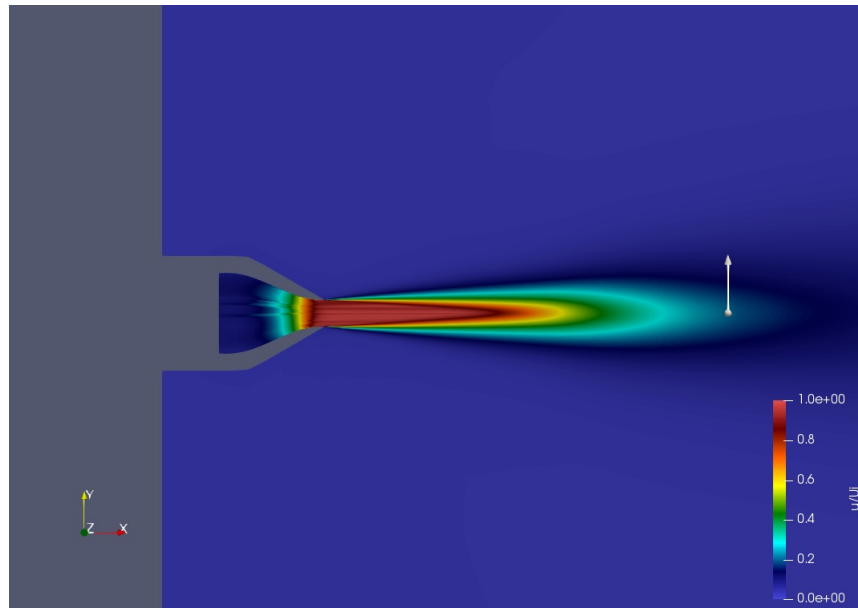


Figure 41: $X = 15D$ line representation on the fluid flow of the Hot Subsonic jet.

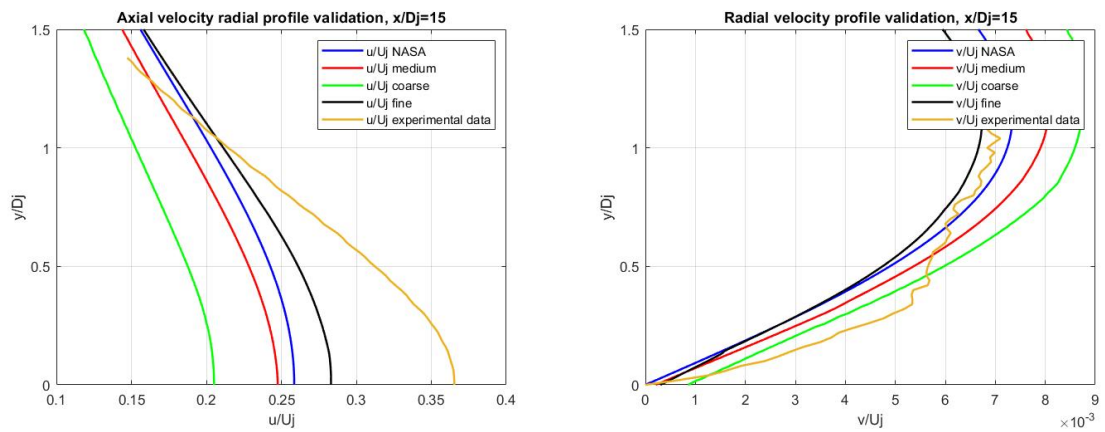


Figure 42: SA results: axial (left) and radial (right) velocity radial profiles at $x = 15D$ for the Hot Subsonic jet.

4.0.1.2 CASE 01 -Menter Shear Stress Transport (SST) model results

The SST turbulence model is the most appropriate for this fluid flow configuration. Profiles look indeed much closer to reality if compared to the results obtained with Spalart-Almaras turbulent model. This is another important aspect to validate to confirm the good behaviour of both the turbulence models. Again, all the curves will show a good correspondence with those obtained by NASA. Here only the velocity profiles as there is no clearly visible difference in the fluid flow with the SA case: it can only be appreciated by comparing the curves.

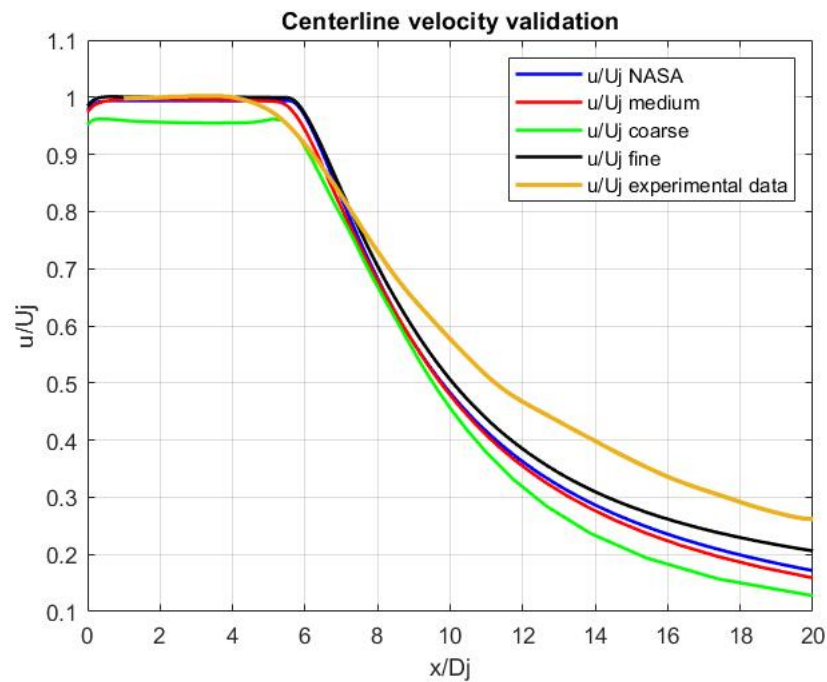


Figure 43: SST results: axial velocity profile along centerline for the Hot Subsonic jet.

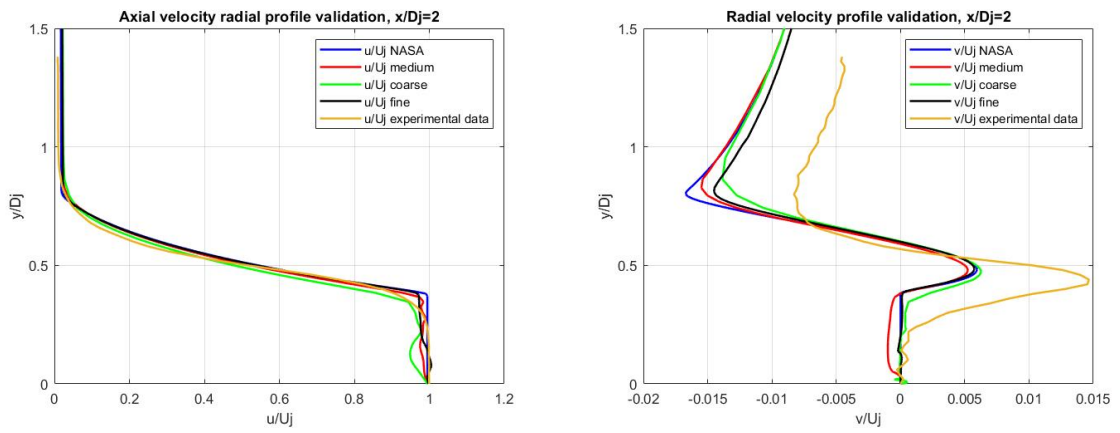


Figure 44: SST results: axial (left) and radial (right) velocity radial profiles at $x = 2D$ for the Hot Subsonic jet.

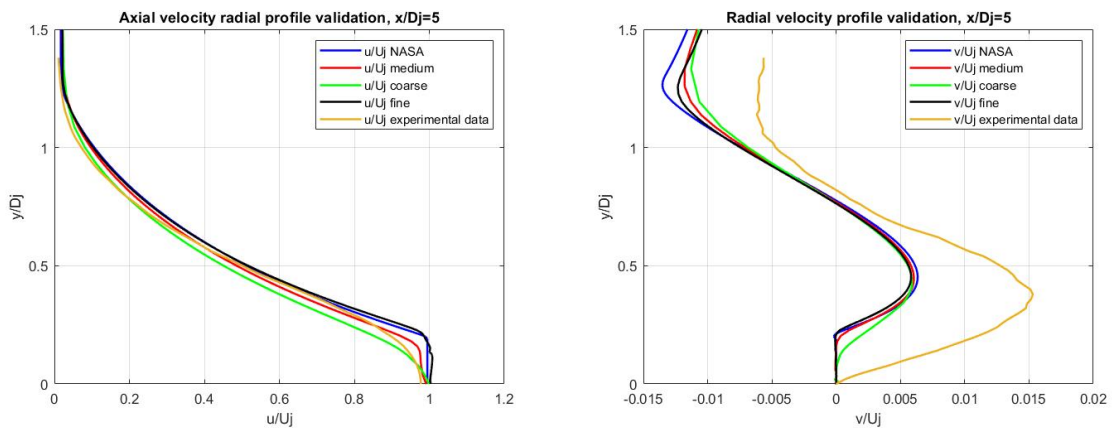


Figure 45: SST results: axial (left) and radial (right) velocity radial profiles at $x = 5D$ for the Hot Subsonic jet.

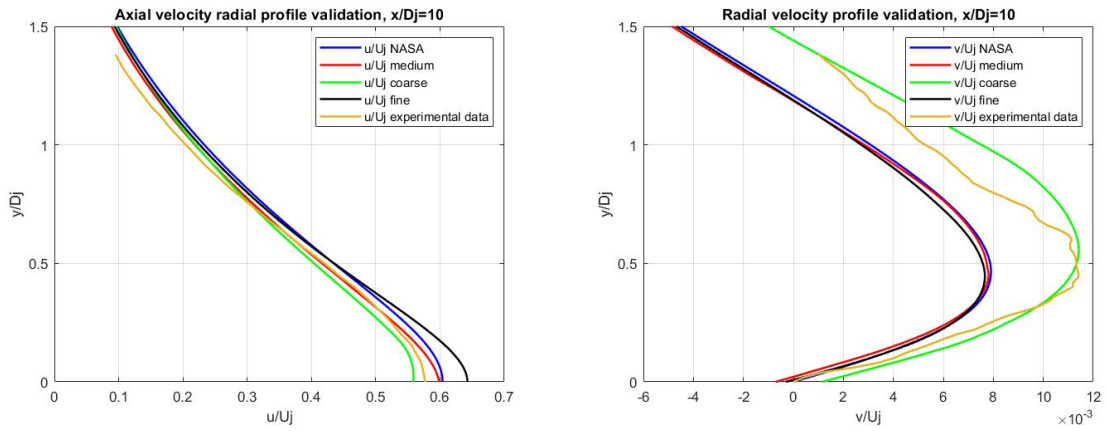


Figure 46: SST results: axial (left) and radial (right) velocity radial profiles at $x = 10D$ for the Hot Subsonic jet.

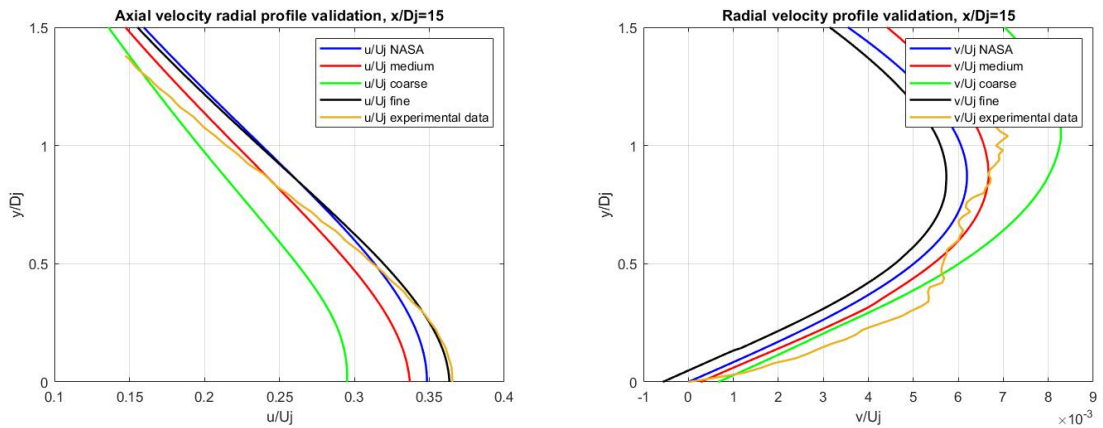


Figure 47: SST results: axial (left) and radial (right) velocity radial profiles at $x = 15D$ for the Hot Subsonic jet.

4.0.2 CASE 02 - Near-sonic turbulent round jet results

The second validation case will be presented in this section. Results will be presented following the same structure previously adopted. This is the case of a low temperature near-sonic turbulent jet. Again results obtained with SA will be shown before the SST ones. All previous considerations about the models still hold. Results look again very precise, matching closely the NASA ones. So both in both cases verification and validation turned out to be successful. Mesh convergence looks even more evident in this test cases, as all curves are really close to each other.

4.0.2.1 CASE 02 - Spalart-Almaras turbulence model results

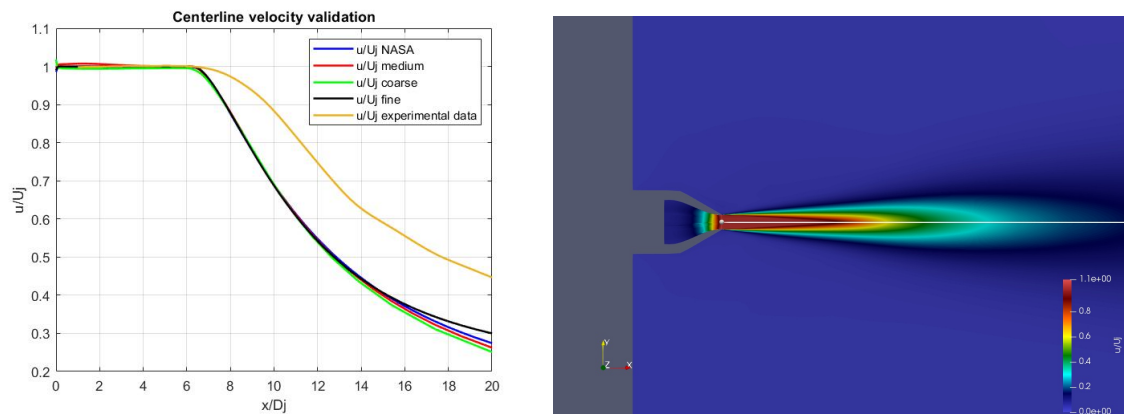


Figure 48: SA results: axial velocity profile along centerline for the Near-sonic jet.

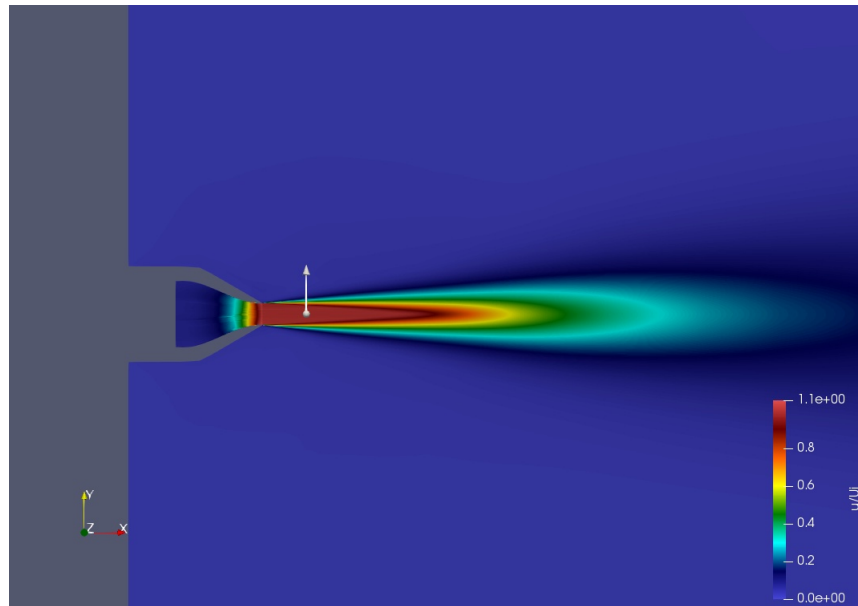


Figure 49: $X = 2D$ line representation on the fluid flow of the Near-sonic jet.

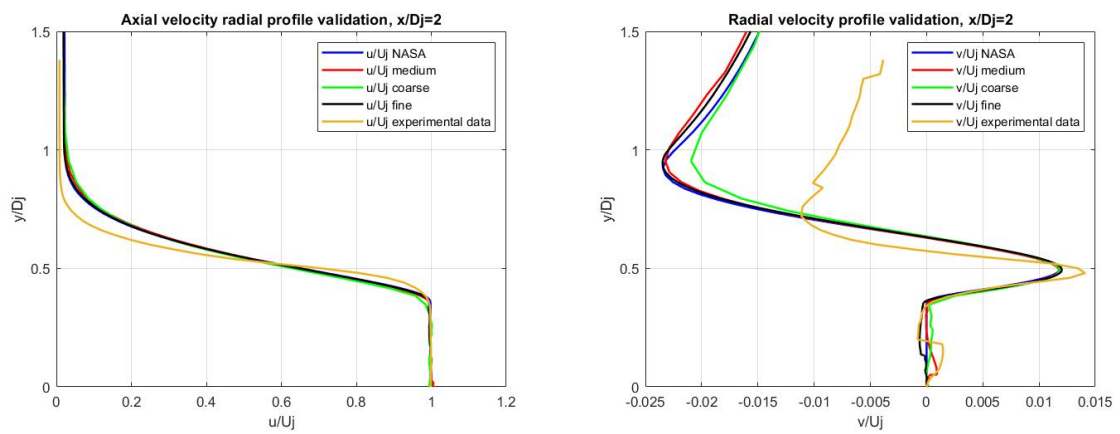


Figure 50: SA results: axial (left) and radial (right) velocity radial profiles at $x = 2D$ for the Near-sonic jet.

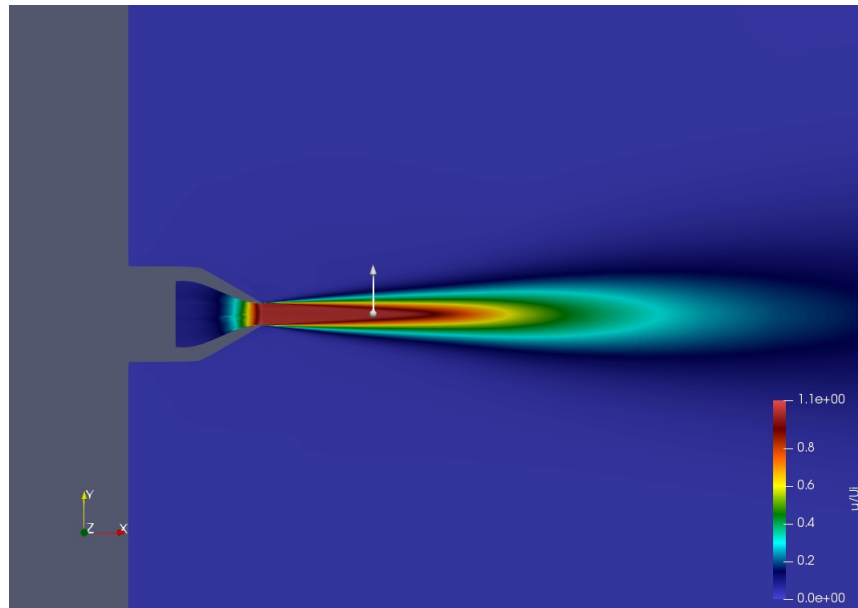


Figure 51: $X = 5D$ line representation on the fluid flow of the Near-sonic jet.

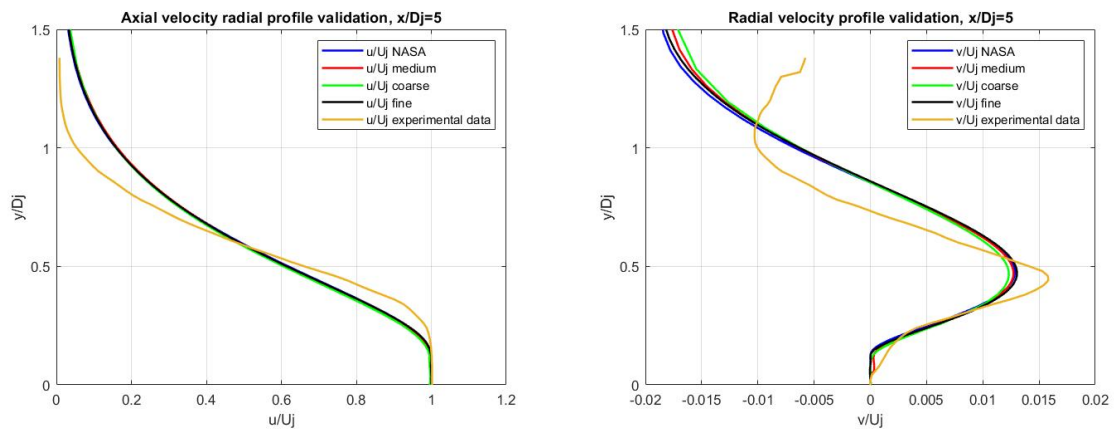


Figure 52: SA results: axial (left) and radial (right) velocity radial profiles at $x = 5D$ for the Near-sonic jet.

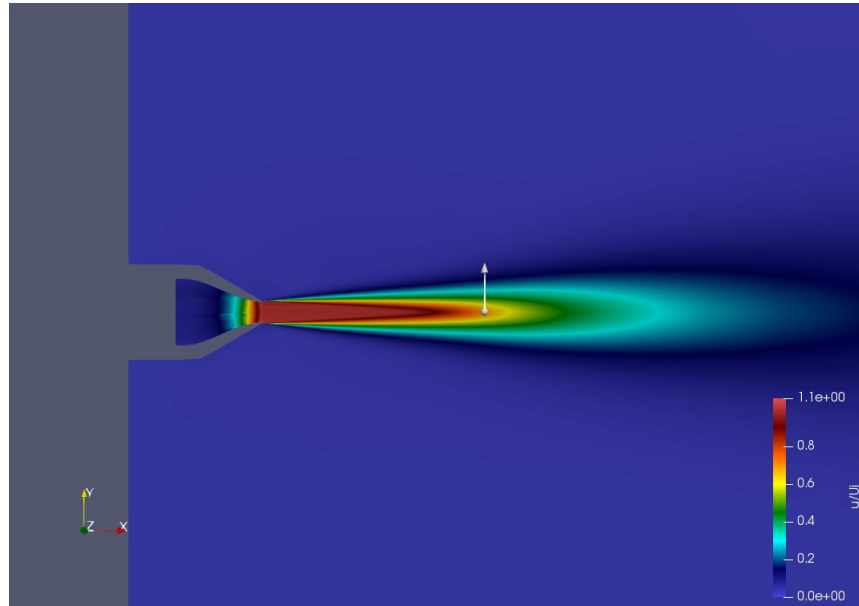


Figure 53: $X = 10D$ line representation on the fluid flow of the Near-sonic jet.

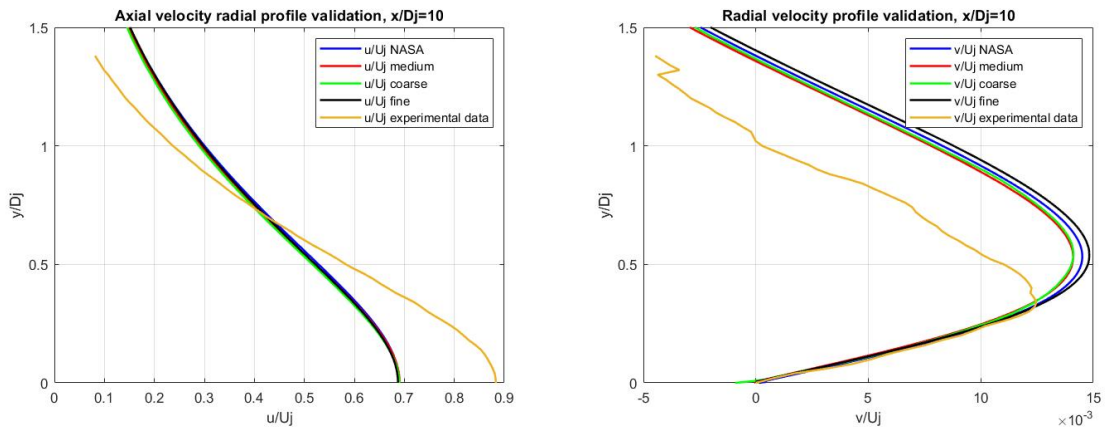


Figure 54: SA results: axial (left) and radial (right) velocity radial profiles at $x = 10D$ for the Near-sonic jet.

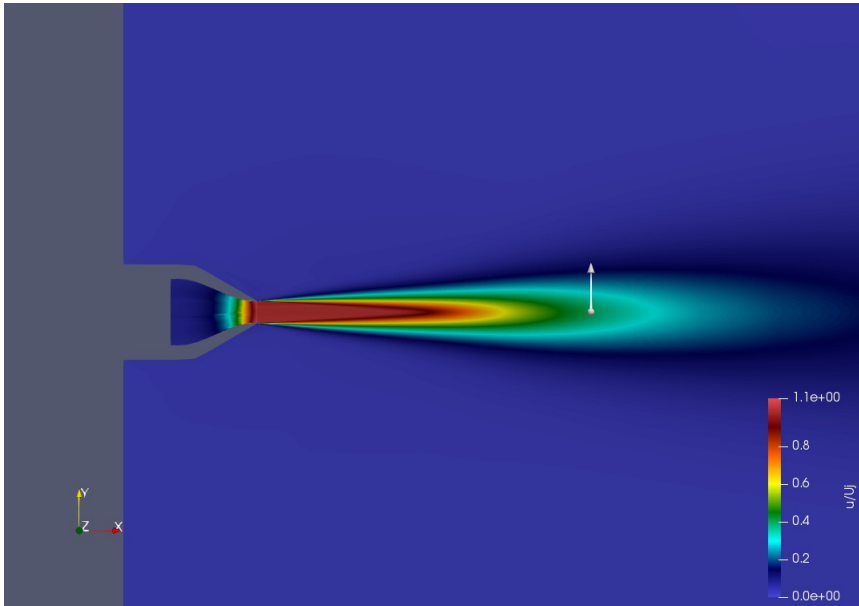


Figure 55: $X = 15D$ line representation on the fluid flow of the Near-sonic jet.

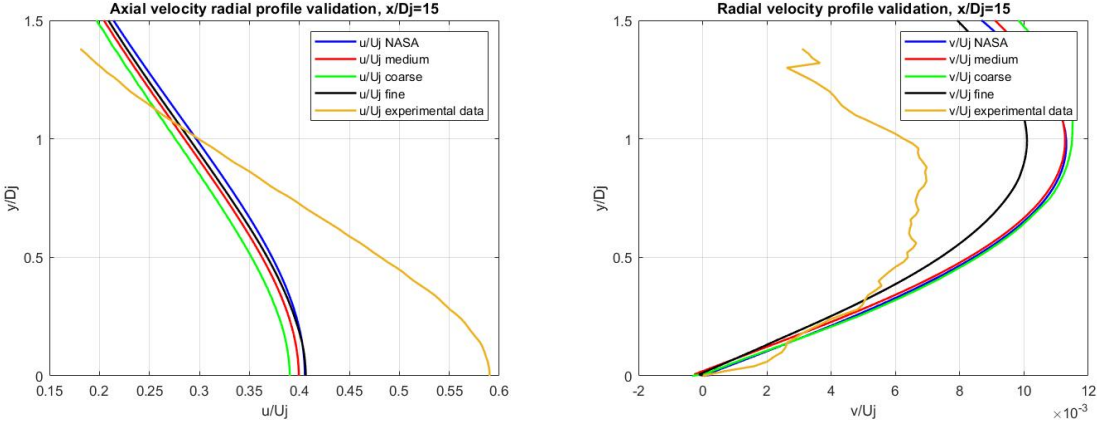


Figure 56: SA results: axial (left) and radial (right) velocity radial profiles at $x = 15D$ for the Near-sonic jet.

4.0.2.2 CASE 02 - Menter Shear Stress Transport (SST) model results

Here the results obtained using the SST turbulence model are reported. Even in this configuration curves look closer to experimental data than SA ones, as expected, proving again a good and stable behavior of the solver. Moreover the profiles match very well with those extracted from NASA's simulations. What can be noticed in the following plots is that results on the coarsest mesh sometimes deviate from the others.

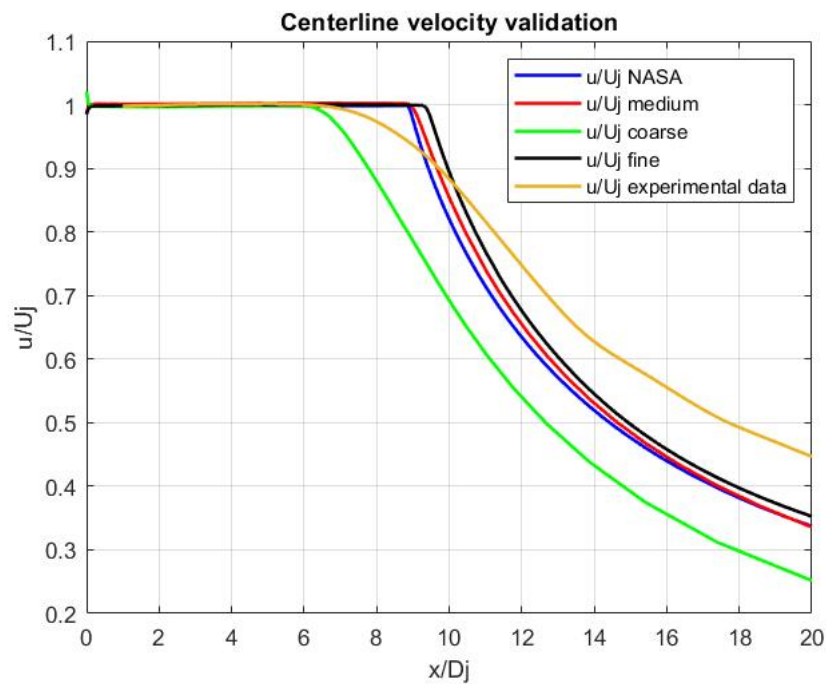


Figure 57: SST results: axial velocity profile along centerline for the Near-sonic jet.

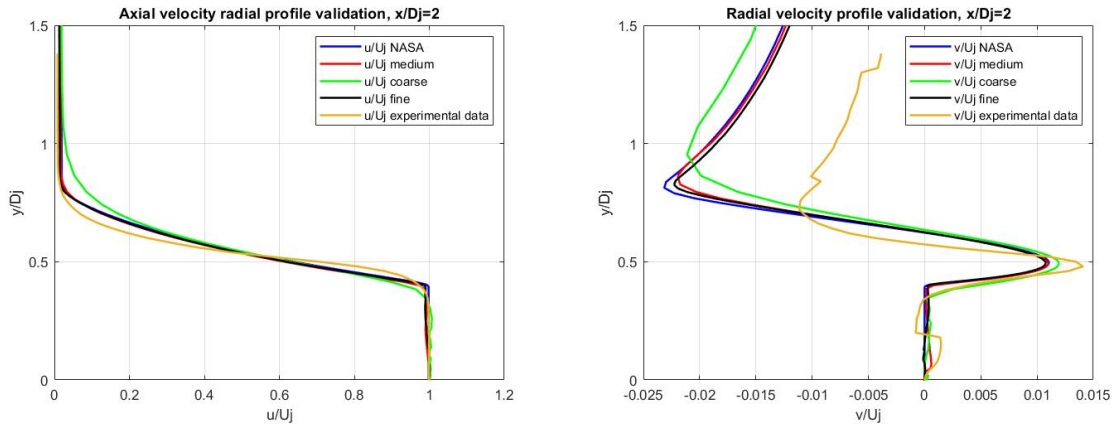


Figure 58: SST results: axial (left) and radial (right) velocity radial profiles at $x = 2D$ for the Near-sonic jet.

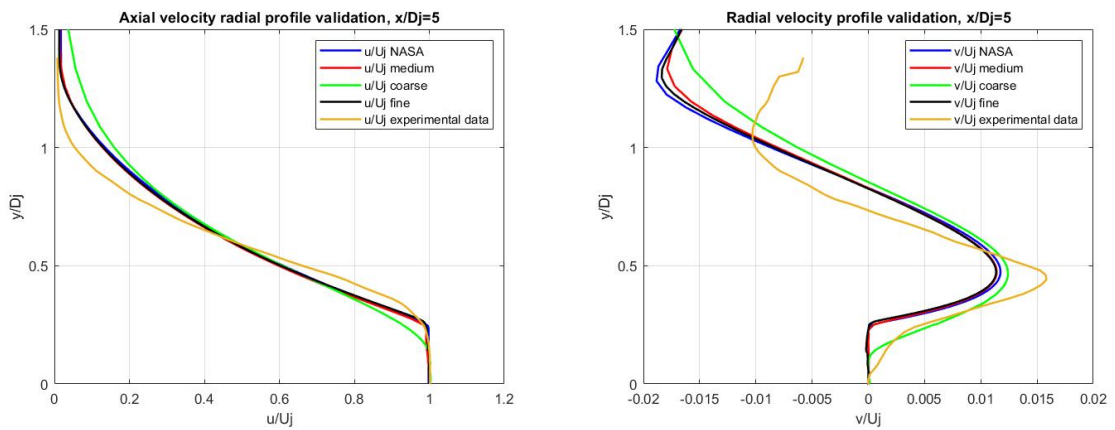


Figure 59: SST results: axial (left) and radial (right) velocity radial profiles at $x = 5D$ for the Near-sonic jet.

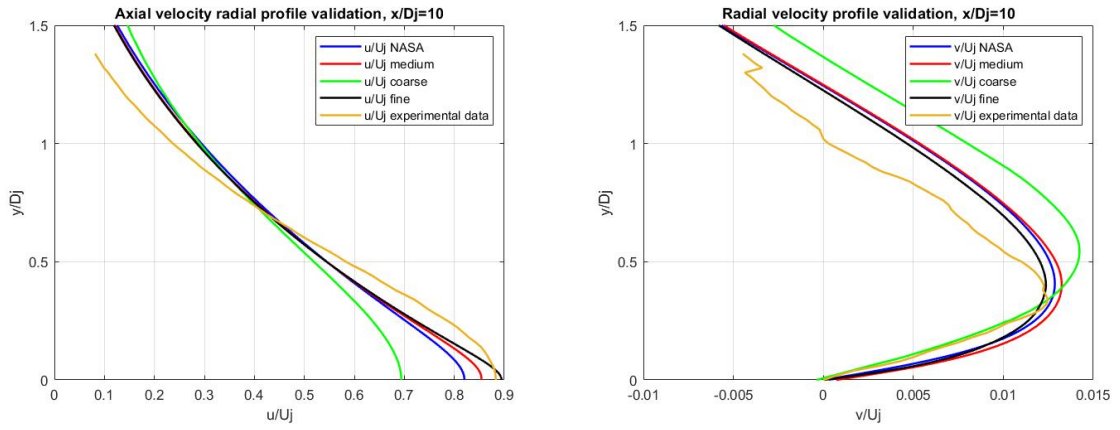


Figure 60: SST results: axial (left) and radial (right) velocity radial profiles at $x = 10D$ for the Near-sonic jet.

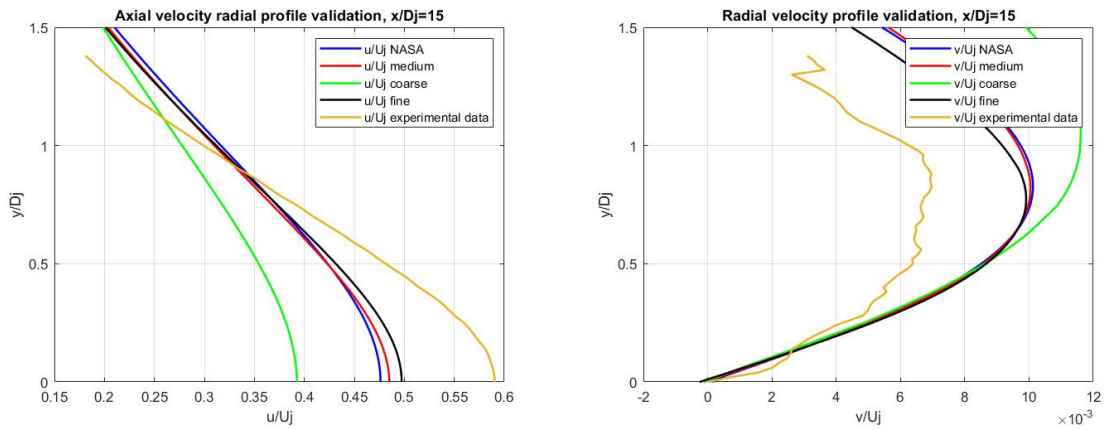


Figure 61: SST results: axial (left) and radial (right) velocity radial profiles at $x = 15D$ for the Near-sonic jet.

CHAPTER 5

ANALYSIS OF OTHER TURBULENT ROUND JETS CONFIGURATIONS

Once the best settings to be used on SU2 for proper results on this configuration have been found and once it has been proven that results are reliable through the previous validation and verification cases, more interesting test cases have been considered as already described in Section 2.2. The ideal goal of this project was to accurately simulate the exhaust gas of a generic aircraft's engine. Main problem to be faced is the nature of the software itself: being a recent, open-source free software with very little literature available, it was possible to only figure out throughout the project what was indeed realistically feasible. The best way to proceed was then to move some intermediate steps between the validation cases and the exhaust simulation. This is meant to have a double goal: to give a pretty wide range of interesting results for turbulent round jets and to allow finding the critical aspects where attention should be focused on for future work.

5.1 CASE 03 - Hot near-sonic turbulent round jet results

The first configuration comes from a combination of the two validation cases. The exhaust gas flow of an aircraft's engine is a hot sonic jet. Therefore, this simulation was run using the same Mach number at the nozzle exit adopted in the Near-sonic configuration but also imposing to the jet a realistic temperature for an aircraft's exhaust gas flow. In this case no validation

data are available. However, there is plenty of reasons to think the results are absolutely reliable. First of all, this configuration is nothing more than a combination of the two validation cases, where results have been already proved to be correct. Moreover, the case was again conducted on all three mesh levels to check the mesh dependency of the results. Most results show a clear mesh convergence, being the different curves closely overlapping. In the closest area to the nozzle exit results match very precisely in the three different mesh levels. This is because the focus of the simulations is mainly to check what happens in that zone and so the mesh is clearly finer there. Finally, again simulations were run with both SA and SST configurations. As expected, results look much coherent and smoother when adopting the Menter Shear Stress Transport model. This is one more proof that the behaviour of the solver is very stable also in this new configuration and allows believing the results are correct.

5.1.1 CASE 03 - Spalart-Almaras turbulence model results

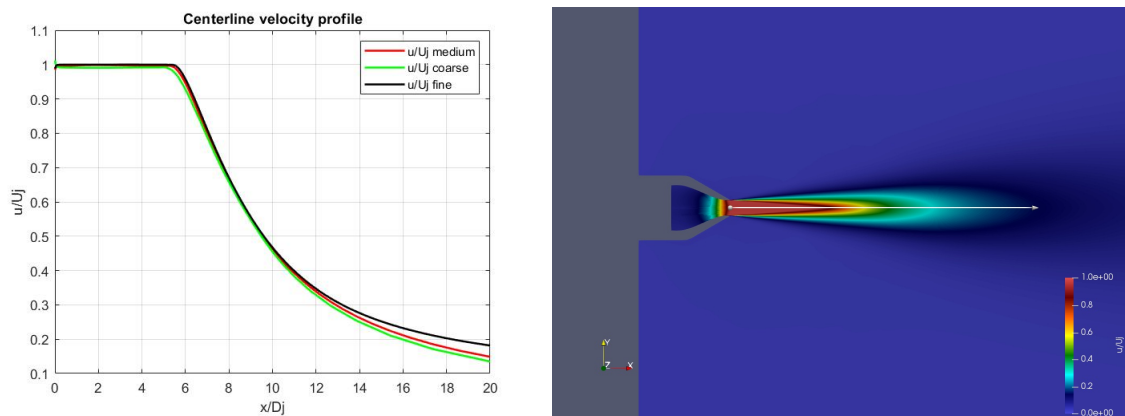


Figure 62: SA results: axial velocity profile along centerline for the Hot Near-sonic jet.

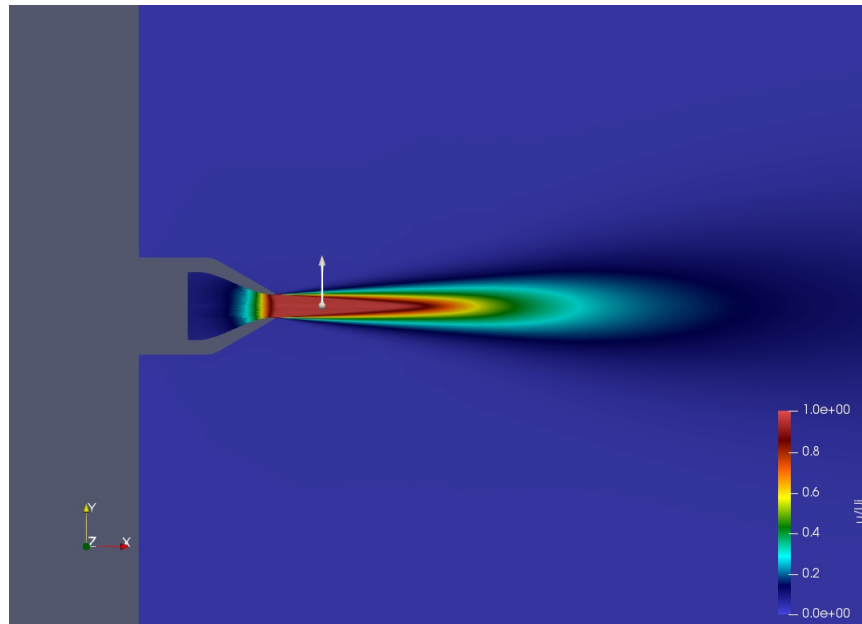


Figure 63: $X = 2D$ line representation on the fluid flow of the Hot Near-sonic jet.

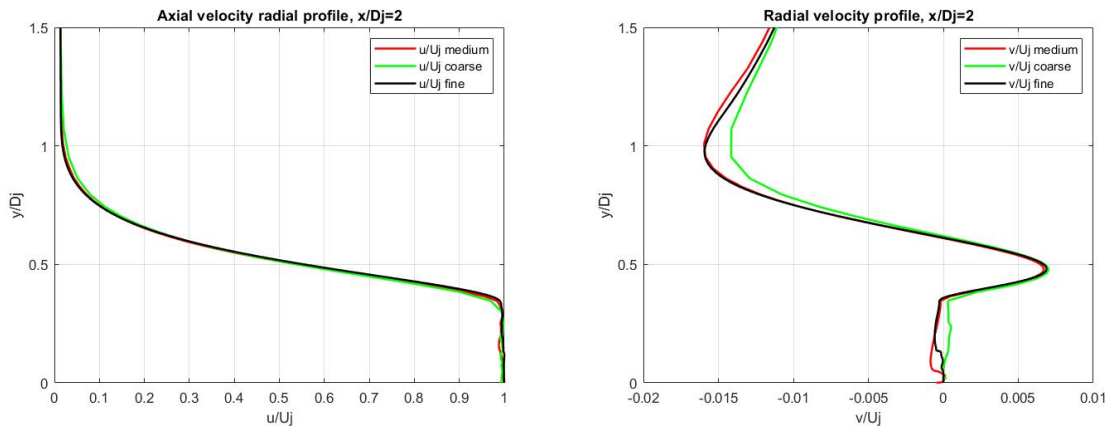


Figure 64: SA results: axial (left) and radial (right) velocity radial profiles at $x = 2D$ for the Hot Near-sonic jet.

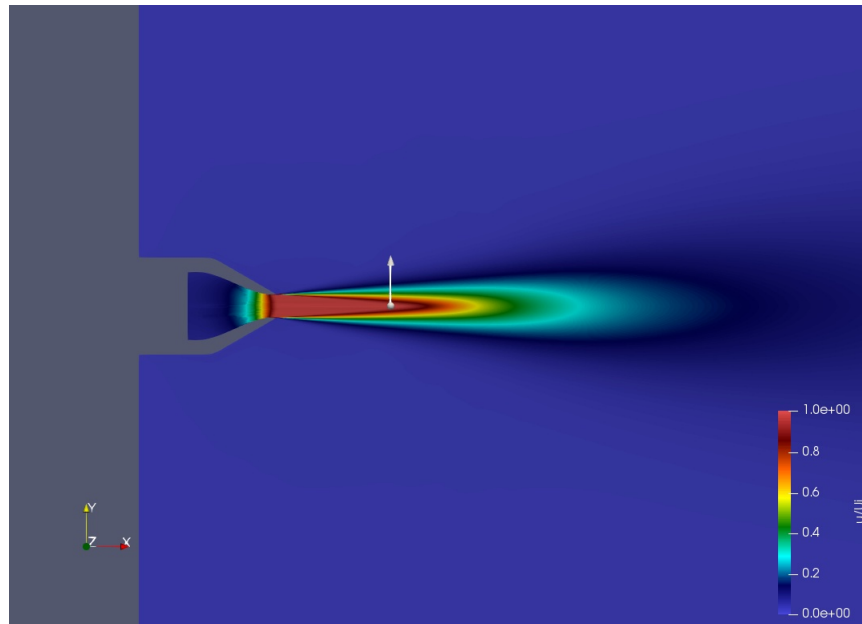


Figure 65: $X = 5D$ line representation on the fluid flow of the Hot Near-sonic jet.

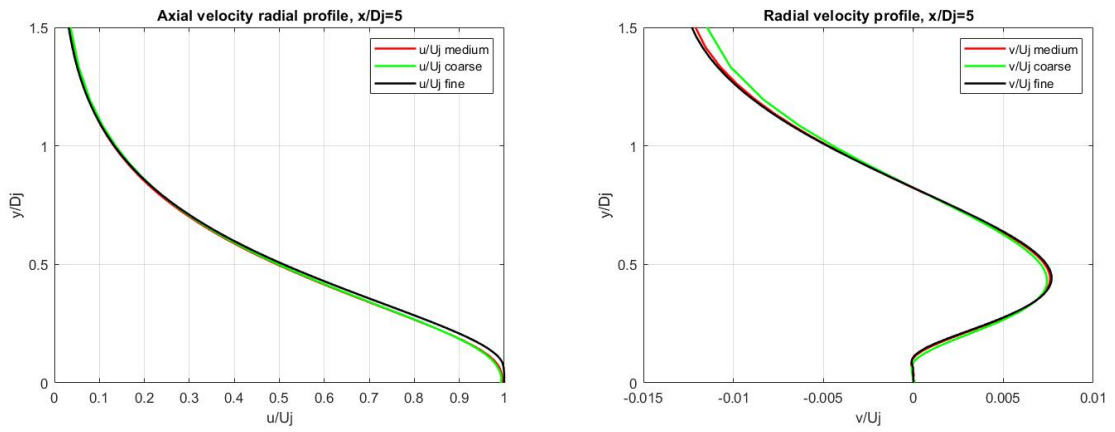


Figure 66: SA results: axial (left) and radial (right) velocity radial profiles at $x = 5D$ for the Hot Near-sonic jet.

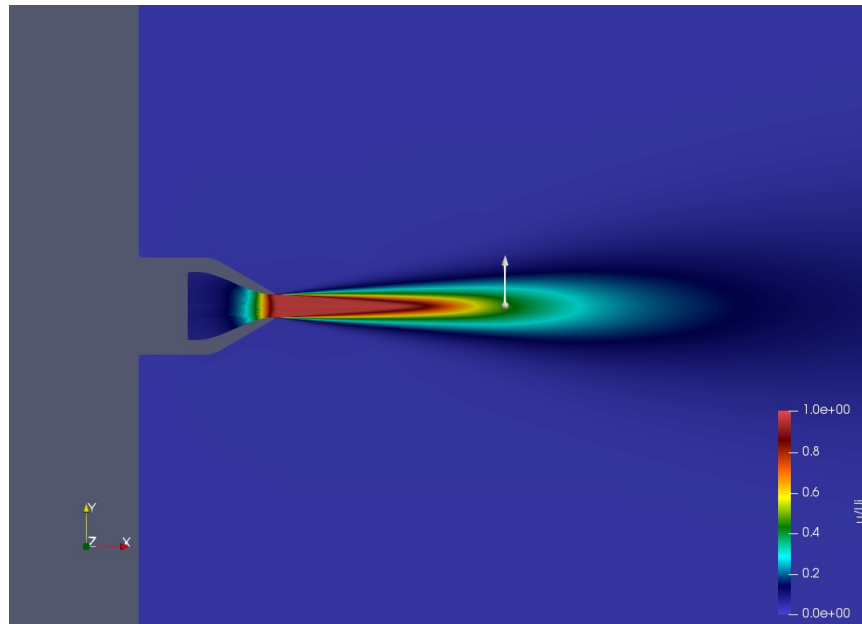


Figure 67: $X = 10D$ line representation on the fluid flow of the Hot Near-sonic jet.

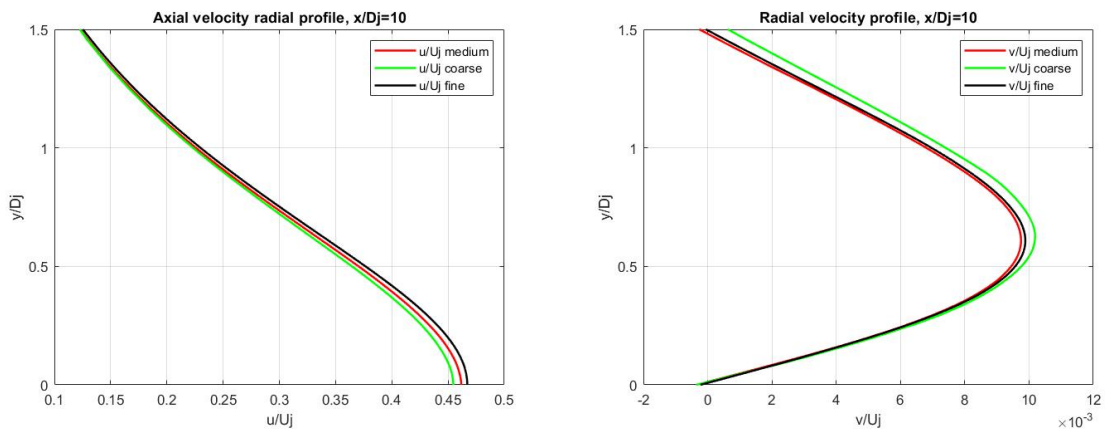


Figure 68: SA results: axial (left) and radial (right) velocity radial profiles at $x = 10D$ for the Hot Near-sonic jet.

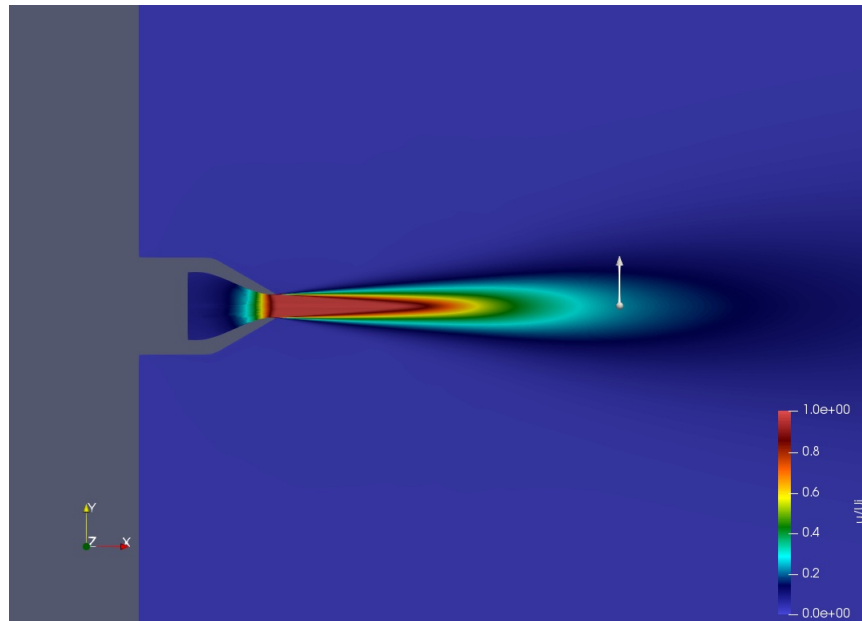


Figure 69: $X = 15D$ line representation on the fluid flow of the Hot Near-sonic jet.

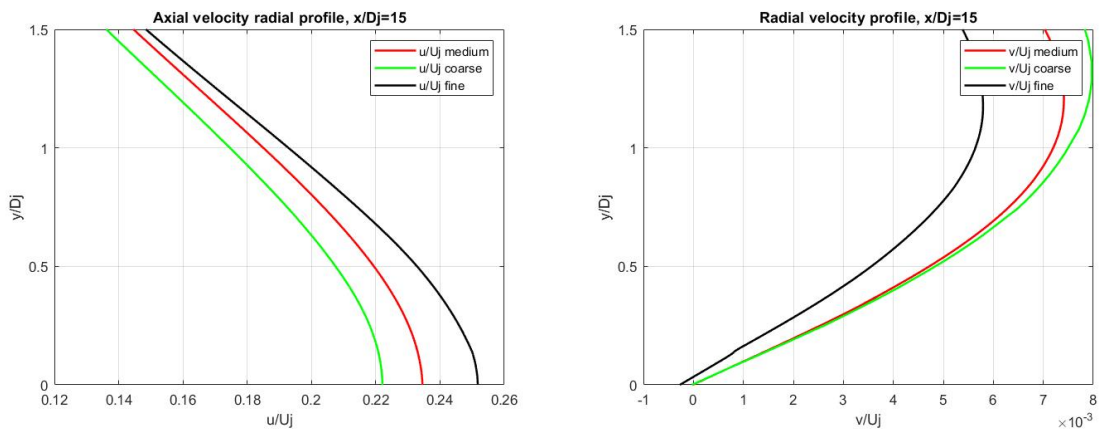


Figure 70: SA results: axial (left) and radial (right) velocity radial profiles at $x = 15D$ for the Hot Near-sonic jet.

5.1.2 CASE 03 - Menter Shear Stress Transport (SST) model results

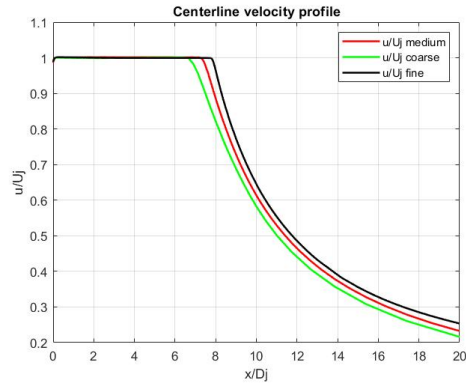


Figure 71: SST results: axial velocity profile along centerline for the Hot Near-sonic jet.

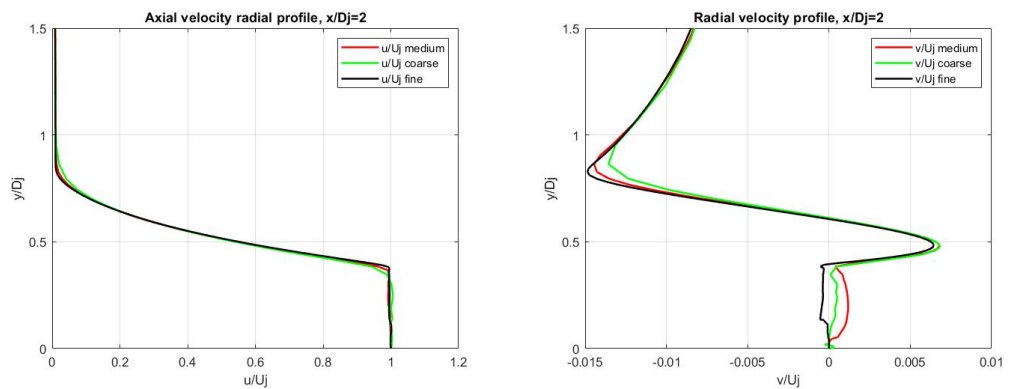


Figure 72: SST results: axial (left) and radial (right) velocity radial profiles at $x = 2D$ for the Hot Near-sonic jet.

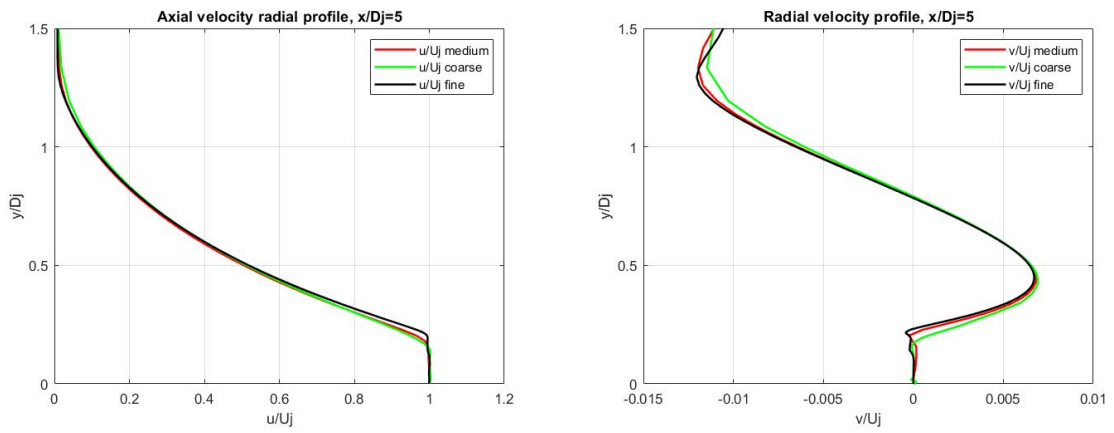


Figure 73: SST results: axial (left) and radial (right) velocity radial profiles at $x = 5D$ for the Hot Near-sonic jet.

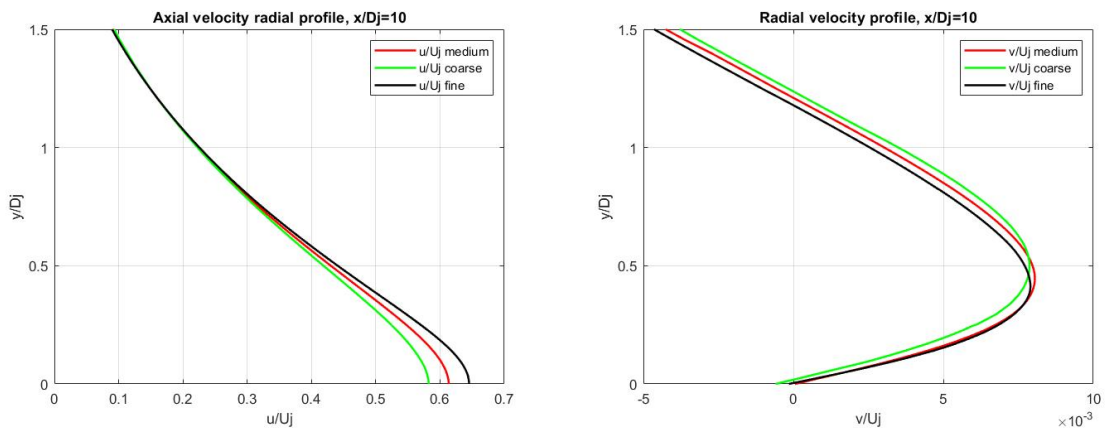


Figure 74: SST results: axial (left) and radial (right) velocity radial profiles at $x = 10D$ for the Hot Near-sonic jet.

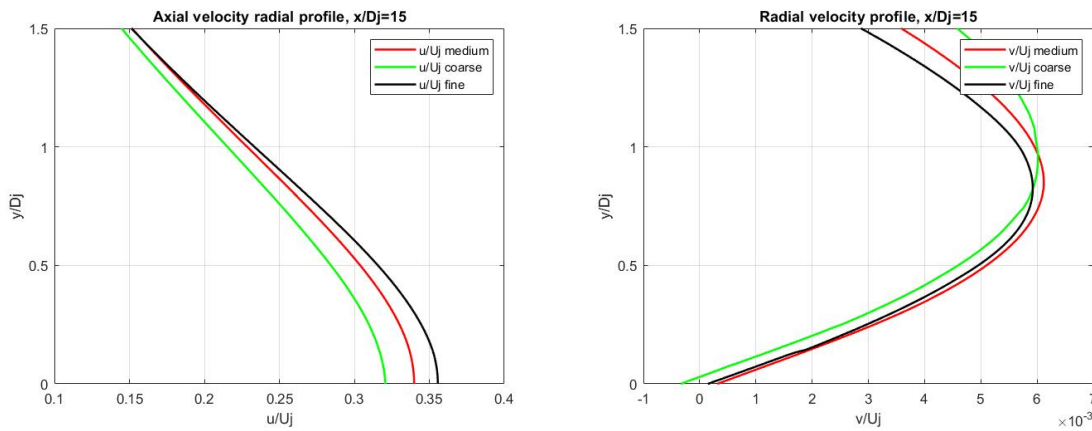


Figure 75: SST results: axial (left) and radial (right) velocity radial profiles at $x = 15D$ for the Hot Near-sonic jet.

5.2 CASE 04 - Flight free-stream conditions results

All the previous simulations were run in free-stream conditions corresponding to atmospheric air at sea level. The next modification to be applied is therefore to impose to the test case a proper environment during flight considering a reference altitude 11000m. Standard values are provided as International Standard Atmosphere properties and are available at [11]. Being the only modification with respect to the previous case the free-stream thermodynamic conditions, namely pressure and temperature, results should still be reliable. Indeed all curves show a very similar behaviour to all cases run so far. Mesh convergence is clear, especially close to the nozzle exit. Simulations with SST turbulence model gave better results than those run with the Spalart-Almaras one. Therefore, all the reasons to think these results are absolutely reliable are there. In particular, this configuration retains a double role. First of all, as previously

mentioned, it is one important step moved towards the realistic simulation of an aircraft's exhaust gas flow. Only one step is now missing, which is the most delicate one and will be discussed in Section 5.3. Moreover, in the idea of analysing in general the behaviour of turbulent round jets, this simulations are important to show what happens to the results when changing the thermodynamic state of the environment where the jet is developing.

5.2.1 CASE 04 - Spalart-Almaras turbulence model results

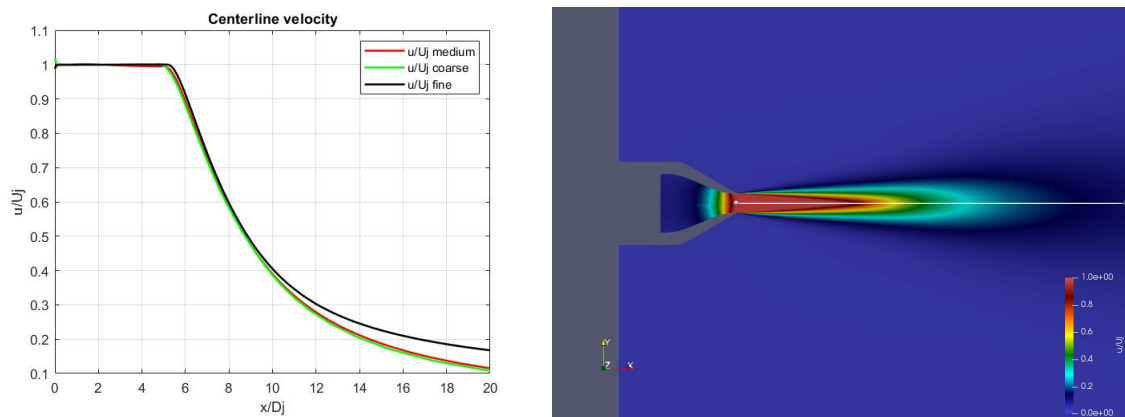


Figure 76: SA results: axial velocity profile along centerline for the Hot Near-sonic jet in flight free-stream conditions.

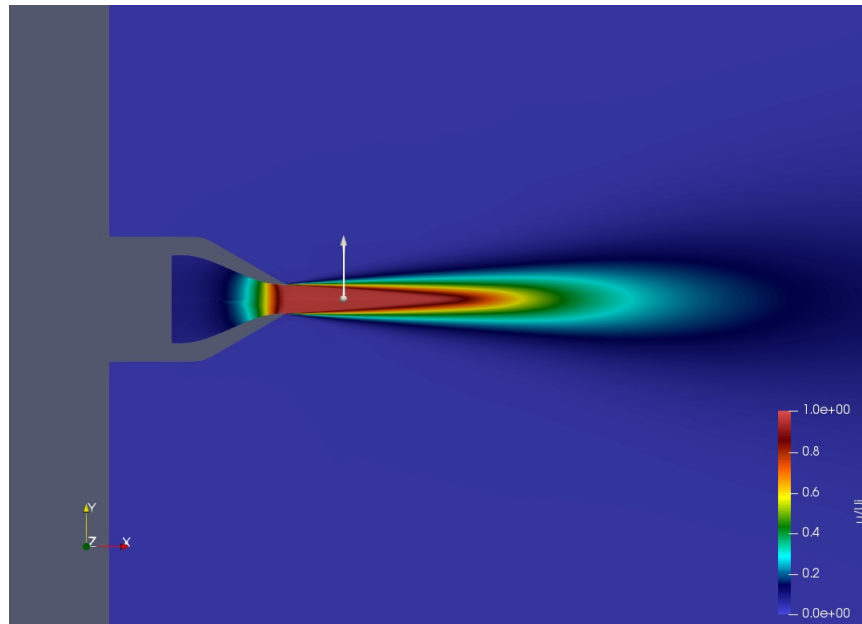


Figure 77: $X = 2D$ line representation on the fluid flow of the Hot Near-sonic jet in flight free-stream conditions.

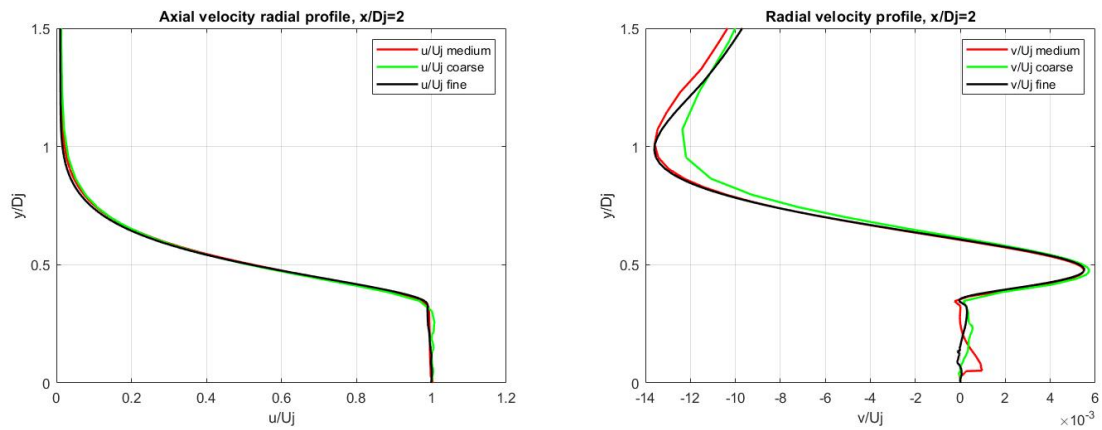


Figure 78: SA results: axial (left) and radial (right) velocity radial profiles at $x = 2D$ for the Hot Near-sonic jet in flight free-stream conditions.

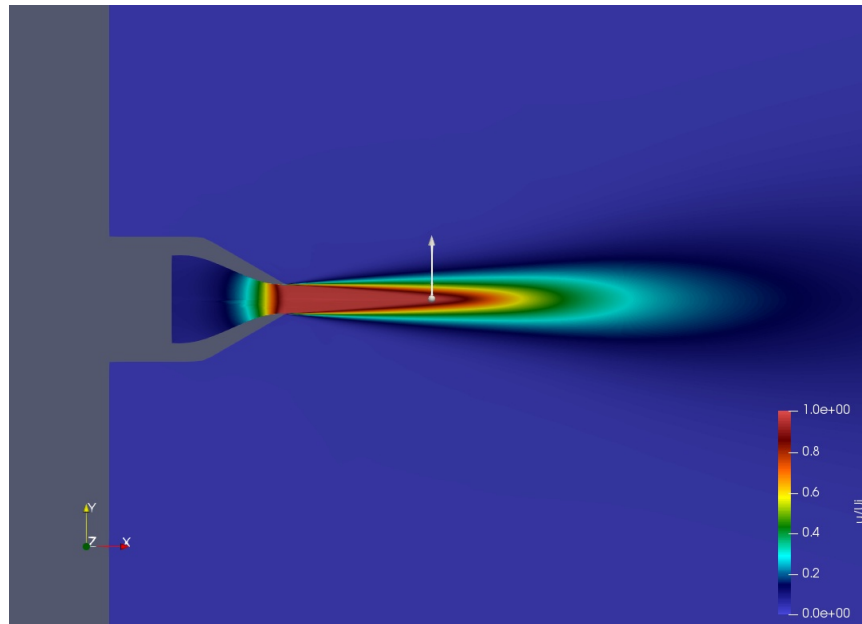


Figure 79: $X = 5D$ line representation on the fluid flow of the Hot Near-sonic jet in flight free-stream conditions.

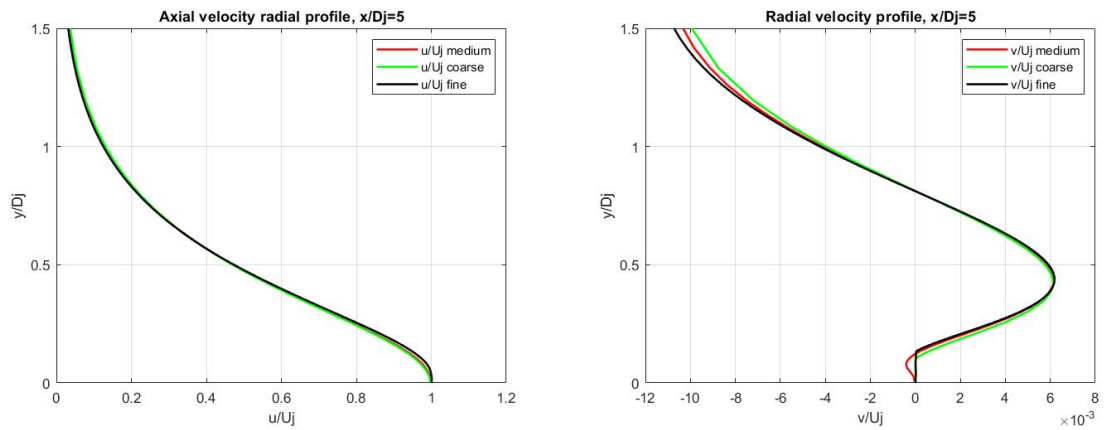


Figure 80: SA results: axial (left) and radial (right) velocity radial profiles at $x = 5D$ for the Hot Near-sonic jet in flight free-stream conditions.

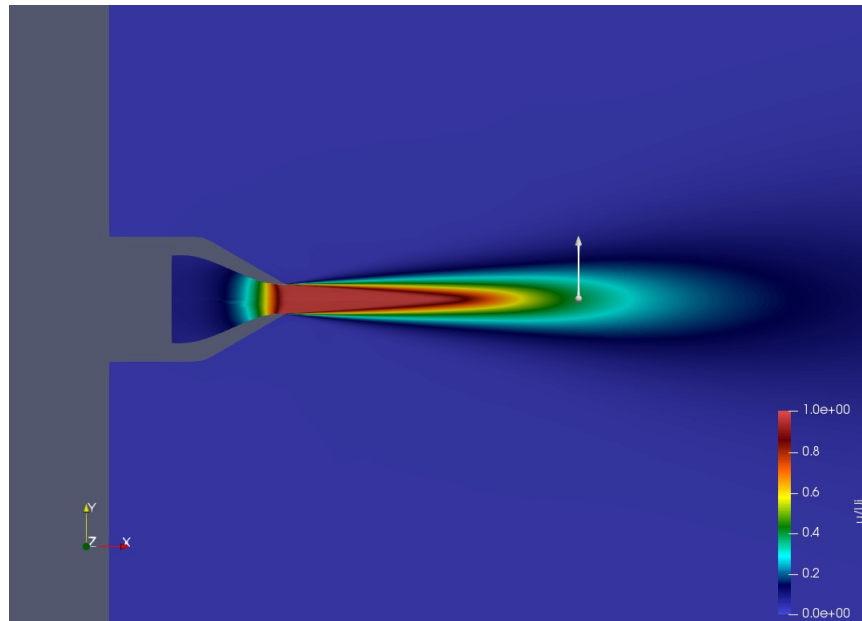


Figure 81: $X = 10D$ line representation on the fluid flow of the Hot Near-sonic jet in flight free-stream conditions.

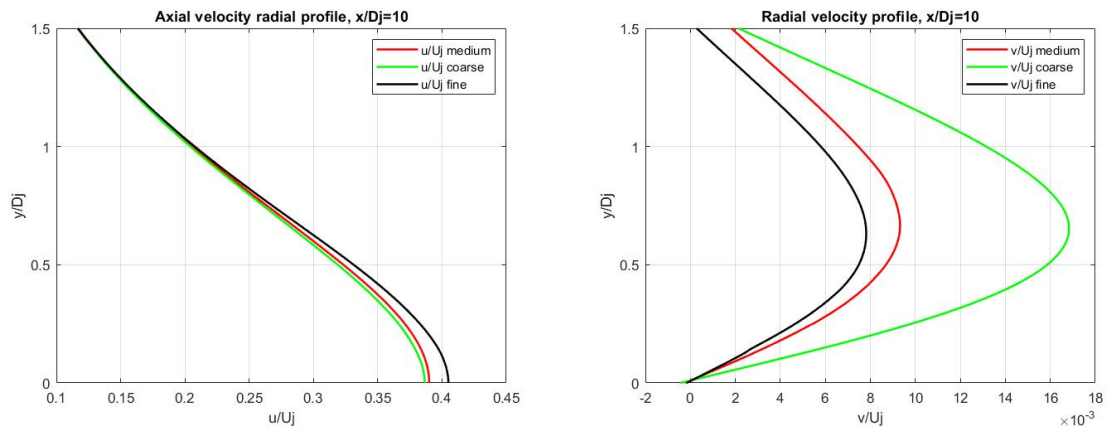


Figure 82: SA results: axial (left) and radial (right) velocity radial profiles at $x = 10D$ for the Hot Near-sonic jet in flight free-stream conditions.

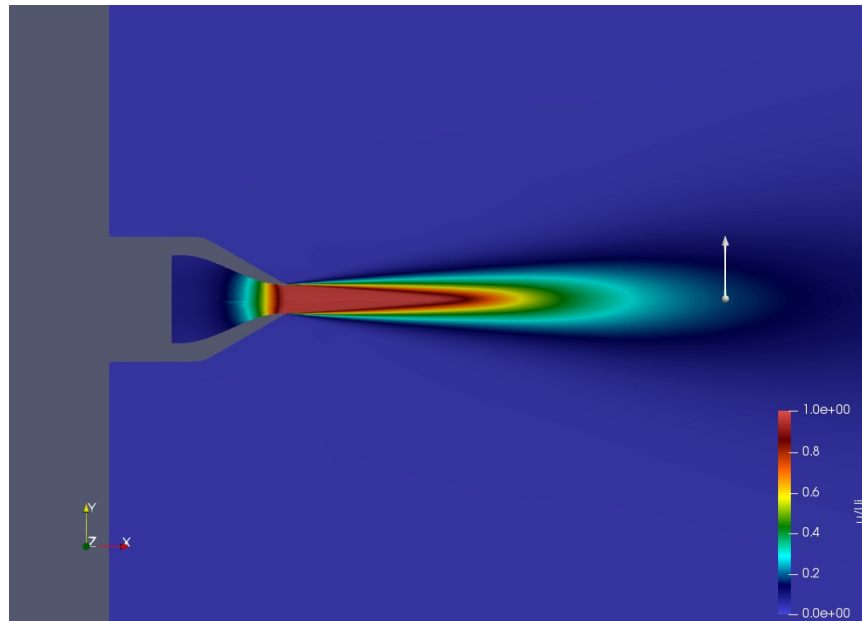


Figure 83: $X = 15D$ line representation on the fluid flow of the Hot Near-sonic jet in flight free-stream conditions.

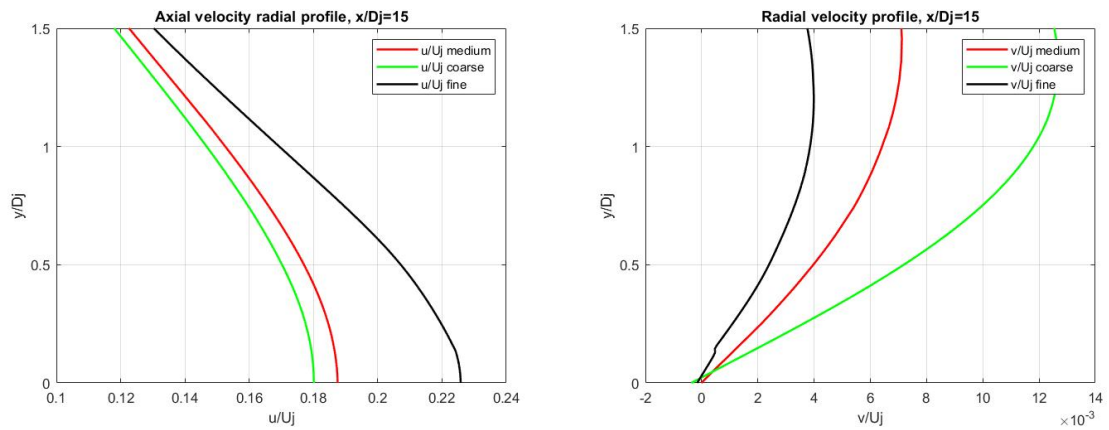


Figure 84: SA results: axial (left) and radial (right) velocity radial profiles at $x = 15D$ for the Hot Near-sonic jet in flight free-stream conditions.

5.2.2 CASE 04 - Menter Shear Stress Transport (SST) model results

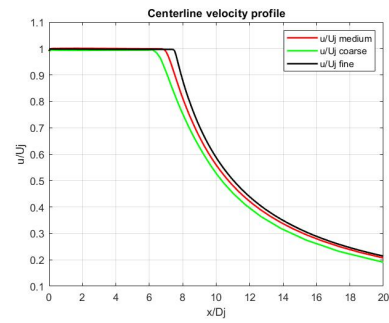


Figure 85: SST results: axial velocity profile along centerline for the Hot Near-sonic jet in flight free-stream conditions.

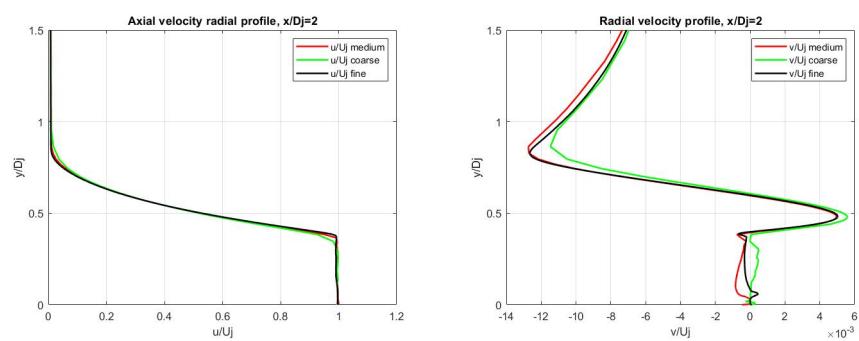


Figure 86: SST results: axial (left) and radial (right) velocity radial profiles at $x = 2D$ for the Hot Near-sonic jet in flight free-stream conditions.

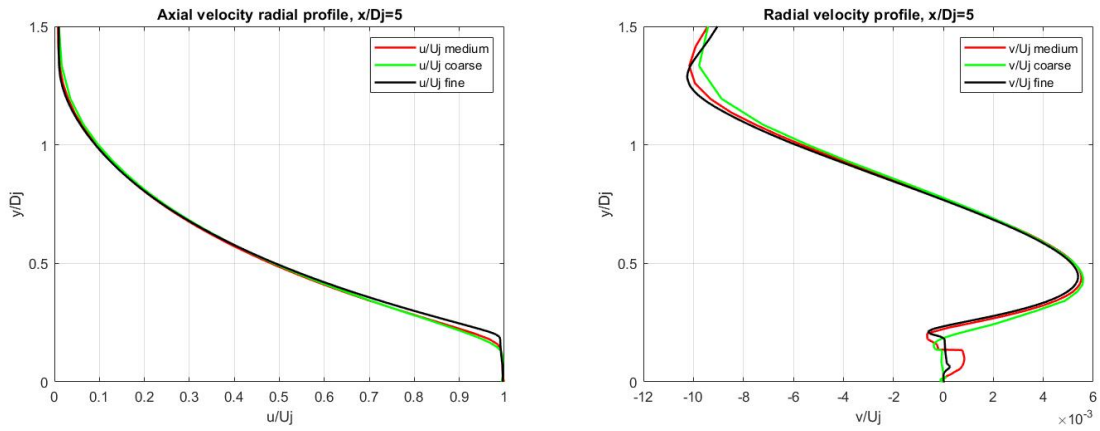


Figure 87: SST results: axial (left) and radial (right) velocity radial profiles at $x = 5D$ for the Hot Near-sonic jet in flight free-stream conditions.

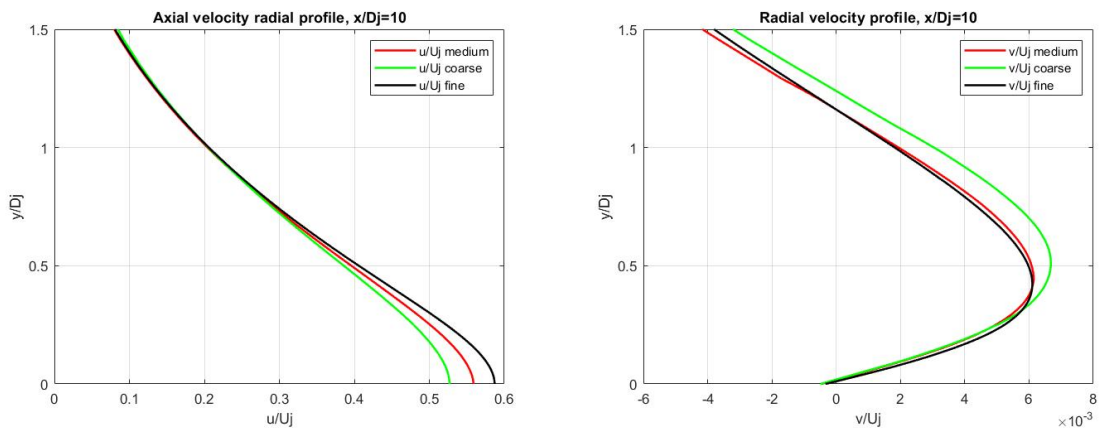


Figure 88: SST results: axial (left) and radial (right) velocity radial profiles at $x = 10D$ for the Hot Near-sonic jet in flight free-stream conditions.

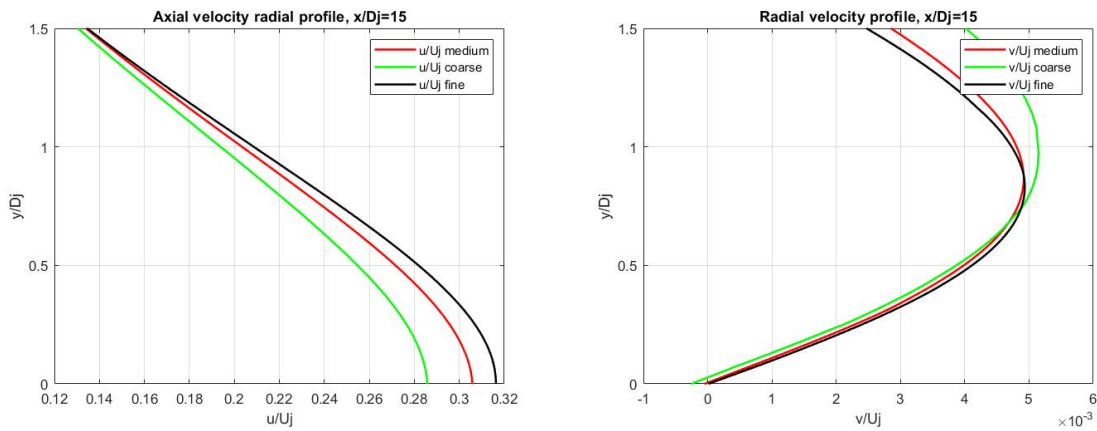


Figure 89: SST results: axial (left) and radial in flight free-stream conditions(right) velocity radial profiles at $x = 15D$ for the Hot Near-sonic jet.

5.3 CASE 05 - Aircraft's Exhaust

There is one more condition to be applied to the previous simulation to obtain a realistic aircraft's exhaust fluid flow. All the other cases simulated a still nozzle spraying into still air. This is however not the real condition, as usually an aircraft is travelling with a Mach number of $Ma = -0.85$ (negative sign comes from coordinates convention). The way this can be implemented into a CFD case is to impose that the environment air is moving with the same Mach number but in the opposite direction. So what needs to be finally assigned is a Mach number of $Ma = 0.85$ to the free-stream air. This increases significantly the whole fluid flow speed, resulting in a very severe condition for the solver's computation. A whole deep study should be dedicated to only this case to obtain a correct solution. Therefore, results reported in this section can be considered as representative of the fluid flow, but not

fully precise. They will be here presented in terms of Mach number (rather than velocity) and pressure. These two parameters are the most helpful in spotting all the main characteristics and possible uncertainties of the results. Clear differences between curves obtained using different mesh levels can be highlighted, meaning mesh convergence was not reached and simulations on medium and coarse mesh levels have to be considered not reliable. So the fine mesh level results will be taken as reference for this test case. Moreover, the results also substantially differ if using the Spalart-Allmaras or the Shear Stress Transport turbulent model. When considering the Mach number, one important element that gives a first feeling of the results' quality is the value at the nozzle exit ($x = 0$). To be fully correct, it should reach 0.985. In both SA and SST curves, the corresponding value gets closer and closer to the desired one as the mesh level gets finer, which is the first positive sign that the solution is pointing in the right direction. Only exception to this is the profile obtained with the coarse mesh level and SST turbulence model, which has a closer value to 0.985 at the nozzle exit but however shows a clearly unstable and incorrect behavior. This might suggest that on one hand the SST model is able to reproduce the most realistic results, as expected, but on the other hand it requires a higher discretization precision to correctly solve the fluid flow. This aspect was hard to catch in most of the previous cases, as even with the coarsest mesh level results were usually very reliable. However, when mesh convergence is not reached like in this test case, it is clear how results diverge much more from a feasible solution. The positive conclusion of comparing different mesh levels is that overall there is a common trend in the curves: as a finer mesh is considered, results all seem

to be moving in the same direction. This means the solver is still not able to produce precise results with the current meshes, but it is showing a proper behavior.

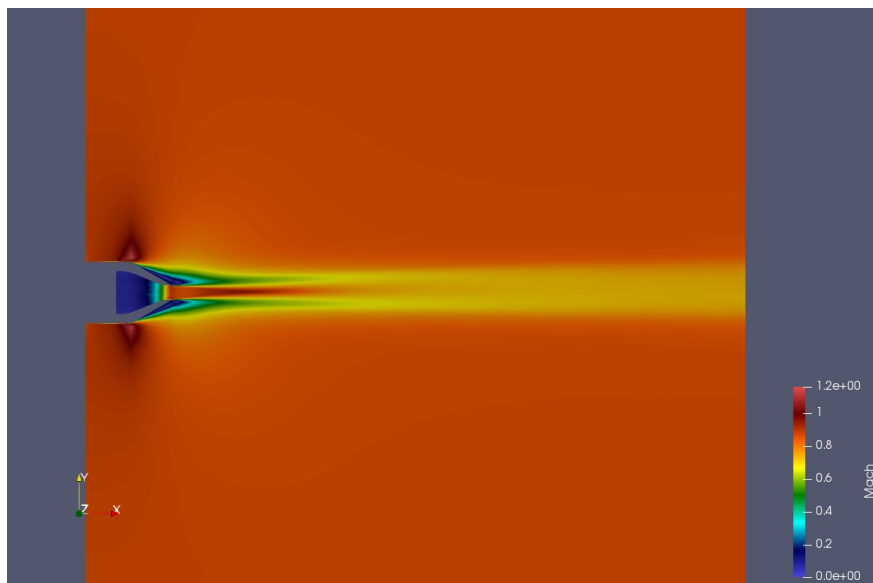


Figure 90: Mach number flow field for the aircraft's exhaust simulation.

It is very hard to assess how close these results are to a correct solution with no reference benchmark available. It can still be useful considering some clear flow macro-features to trace the current status of the results. In Figure 90 the flow in terms of Mach number is represented. Figure 91 represents instead the pressure field and shows clear pressure oscillations throughout the domain. In any other simulations that had been run before the pressure field was always uniform. This test case instead is dealing with an entire fluid flow close to a sonic condition,

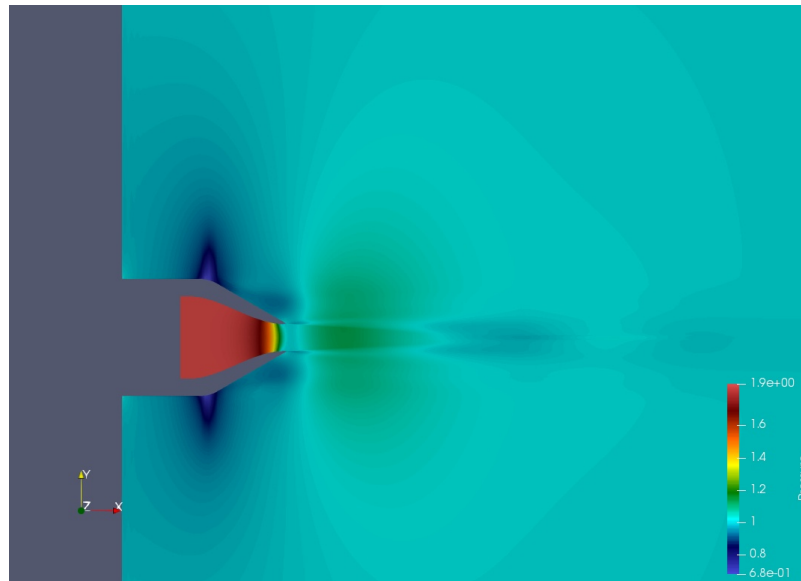


Figure 91: Pressure field for the aircraft's exhaust simulation.

also locally turning supersonic, which is a reasonable factor that could cause the alteration of the pressure field. It is not clear how exactly pressure oscillations should look like, what their intensity should be, how they should be distributed, what exactly they are locally due to. Comparing all results, what can be noticed from Figure 93, Figure 92 and Figure 94 is that all curves show a first oscillation right downstream the nozzle exit, representing a post-expansion of the fluid. The usual trend is that the oscillation has a lower intensity as the discretization gets finer and finer, always keeping in mind that the SST - coarse mesh result has to be considered completely unreliable. Moreover, this is the only pressure oscillation affecting curves obtained with coarse and medium mesh levels. Simulation on the finest mesh level instead clearly show more oscillations around $x = 8 - 10D$. Results differ quite a lot if using the Spallart-Allmaras

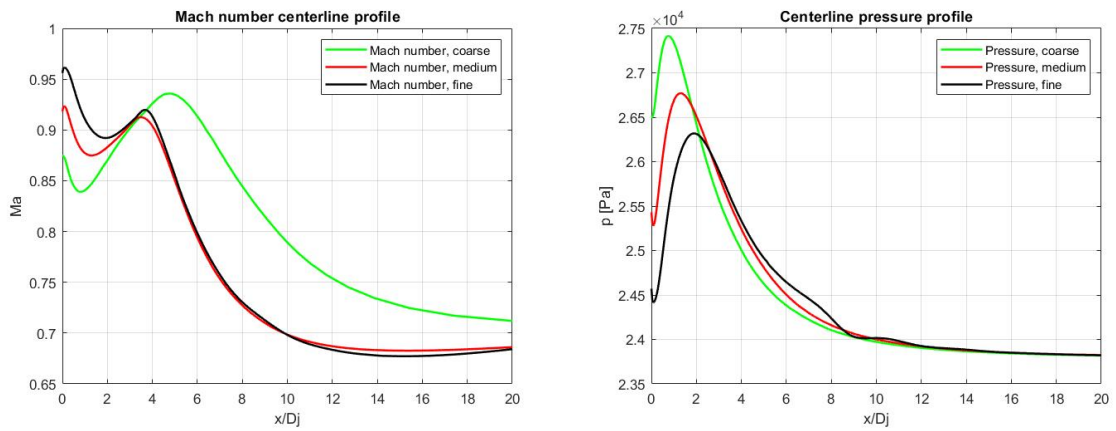


Figure 92: SA results: Mach (left) and pressure (right) centerline profiles for the aircraft's exhaust simulation.

or Shear Stress Transport turbulence models. This oscillation retains greater intensity in the the SST curve, while it is much smaller on the SA one. Figure 94 also show pretty different mach profiles obtained with the two models. There is a common trend though. Looking back at Figure 34, Figure 43, Figure 48 and Figure 57 all simulation curves always lay below the experimental data, so in the simulation the fluid slows down faster than in reality. Moreover, the SA results always show even more this behavior compared to the SST ones. This last point is something that also happens in the aircraft's exhaust simulation and it is clearly visible in Figure 94. Finally, these are all the possible considerations that can be extracted from this test case. The main aim of this section was to give a first representative solution of this flow. The results' discussion might also be very useful for future work, as it points out explicitly where uncertainties lay giving then a clear idea of what to focus on.

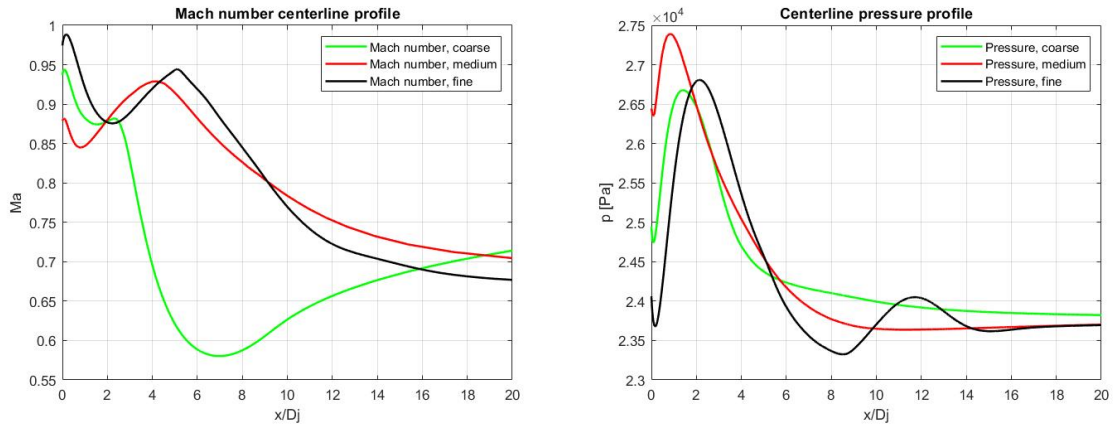


Figure 93: SST results: Mach (left) and pressure (right) centerline profiles for the aircraft's exhaust simulation.

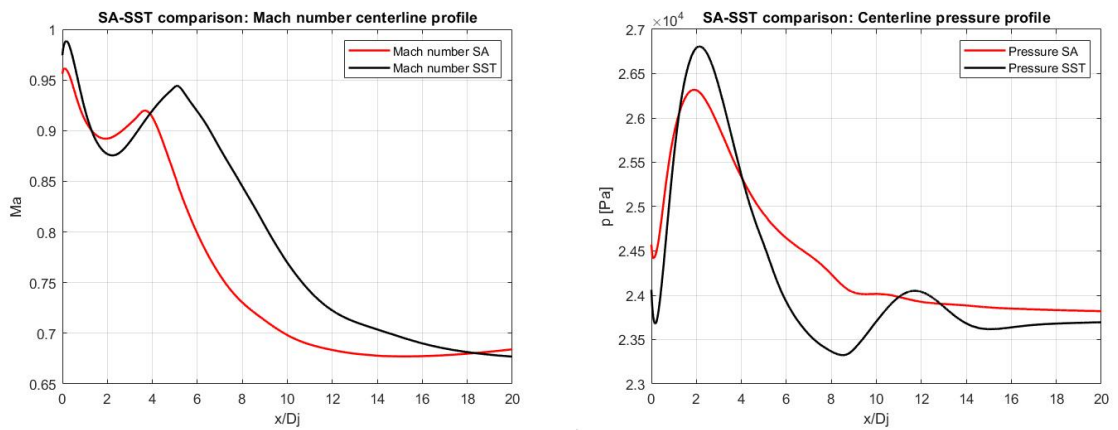


Figure 94: SA - SST results comparison: Mach (left) and pressure (right) centerline profiles for the aircraft's exhaust simulation on the finest grid level.

CHAPTER 6

CONCLUSIONS

Open-source CFD codes are amazing resources for development in this field of application. These tools are free to use and develop, reason why every person's and project's contribution is fundamental for their growth. This work aims at being a contribution for SU2 as a support of the incredible job that has been carried out at Stanford University. The code is very recent and in full development, but already shows some great capabilities. All the cases presented show how to better exploit this software for simulating turbulent round jets. The idea behind the project was to give two main contributions. First of all it can be used as a small user guide for everybody who is interested in simulating the analysed flow configuration using SU2. Chapter 3 reports current status of all the features of interest and a final suggested best practice in Section 3.4, supported by validation results in Chapter 4. Second goal was to give a feedback to code developers about what is already very well implemented and where there is more margin for improvement.

A turbulent round jet is a very common flow topology. Although the apparently simple geometry, its turbulent nature leads to a non trivial treatment of the problem. Therefore analytical solutions are available only under strong assumptions and only in the fully turbulent region (far enough from the nozzle exit). CFD is again a useful way to get a wide treatment of this fluid dynamic phenomenon. It makes possible to explore different configurations in terms of fluid properties. The price to pay is a relatively small computational cost, which is a big

advantage compared to real experiments. That is why another key idea of this project is to present a range of different results.

Finally, another desired goal was to get as close as possible to a real test case: a general aircraft's exhaust fluid flow. That is why the range of round jets that have been analysed moved step by step from some validation cases to the ultimate case of a flow downstream an airplane's engine. This is not a closed chapter but one of the most important input for future work.

6.1 Future work

Three interesting projects could be developed using this thesis as an input.

The first would be an hands on the code project. Some features that still apparently need further development have been presented. The idea is to get a feeling on the software implementation and to subsequently find possible ways to improve it. This would be greatly useful to both the SU2 developers and the whole CFD community.

Second hint could be further increasing the range of turbulent round jets to be analysed and running multiple cases with very small differences. In this way it will be possible to better spot each parameter's influence, qualitatively and quantitatively, and possibly get to a semi-analytical description based on the many results obtained.

Last idea would be to solely focus on simulating reliably an aircraft's exhaust gas fluid flow on SU2. First it would be necessary to create a base of comparison to be able to direct results in the right way. Then, starting from the case set-up provided by this thesis, a fine mesh convergence study would be required to finally get to correct results.

APPENDICES

Appendix A

CONFIGURATION FILE: AIRCRAFT'S EXHAUST SIMULATION

The appendix reports the configuration file used to set up the Aircraft's Exhaust jet simulation, whose results are reported in Section 5.3.

```

%%%%%%%%%%%%%%%%%%%%%%%%%%%%%%%%%%%%%%%%%%%%%%%%%%%%%%%%%%%%%%%%%%%%%%%%
%
% SU2 configuration file
% Case description: -----
% Author: -----
% Institution: -----
% Date: -----
% File Version 6.1.0 "Falcon"
%
%%%%%%%%%%%%%%%%%%%%%%%%%%%%%%%%%%%%%%%%%%%%%%%%%%%%%%%%%%%%%%%%%%%%%%%%

% ----- DIRECT, ADJOINT, AND LINEARIZED PROBLEM DEFINITION -----%
%
% Physical governing equations (EULER, NAVIER_STOKES, POISSON_EQUATION,
%
%                               WAVE_EQUATION, HEAT_EQUATION, FEM_ELASTICITY)

```

Appendix A (continued)

```
%  
PHYSICAL_PROBLEM= NAVIER_STOKES  
  
%  
% Specify turbulence model (NONE, SA, SA_NEG, SST, SA_E, SA_COMP, SA_E_COMP)  
KIND_TURB_MODEL= SST  
  
%  
% Mathematical problem (DIRECT, CONTINUOUS_ADJOINT, DISCRETE_ADJOINT)  
MATH_PROBLEM= DIRECT  
  
%  
% Regime type (COMPRESSIBLE, INCOMPRESSIBLE)  
REGIME_TYPE= COMPRESSIBLE  
  
%  
% Axisymmetric simulation, only compressible flows (NO, YES)  
AXISYMMETRIC= NO  
  
%  
% Restart solution (NO, YES)  
RESTART_SOL= YES  
  
%  
% System of measurements (SI, US)  
% International system of units (SI): ( meters, kilograms, Kelvins,  
% Newtons = kg m/s^2, Pascals = N/m^2,
```

Appendix A (continued)

```

%                               Density = kg/m^3, Speed = m/s,
%                               Equiv. Area = m^2 )
% United States units (US): ( inches, slug, Rankines, lbf = slug ft/s^2,
%                               psf = lbf/ft^2, Density = slug/ft^3,
%                               Speed = ft/s, Equiv. Area = ft^2 )
SYSTEM_MEASUREMENTS= SI

% ----- COMPRESSIBLE FREE-STREAM DEFINITION -----%
%
% Mach number (non-dimensional, based on the free-stream values)
MACH_NUMBER= 0.85
%
% Angle of attack (degrees, only for compressible flows)
AOA= 0
%
% Side-slip angle (degrees, only for compressible flows)
SIDESLIP_ANGLE= 0.0
%
% Init option to choose between Reynolds (default) or thermodynamics
% quantities for initializing the solution (REYNOLDS, TD_CONDITIONS)
INIT_OPTION= TD_CONDITIONS

```

Appendix A (continued)

```
%  
  
% Free-stream option to choose between density and temperature (default)  
  
% for initializing the solution (TEMPERATURE_FS, DENSITY_FS)  
  
FREESTREAM_OPTION= TEMPERATURE_FS  
  
%  
  
% Free-stream pressure (101325.0 N/m^2, 2116.216 psf by default)  
  
FREESTREAM_PRESSURE= 23800  
  
%  
  
% Free-stream temperature (288.15 K, 518.67 R by default)  
  
FREESTREAM_TEMPERATURE= 219  
  
%  
  
FREESTREAM_VISCOSITY=1.853E-5  
  
%  
  
% Reynolds number (non-dimensional, based on the free-stream values)  
  
REYNOLDS_NUMBER= 220529.4638  
  
%  
  
% Reynolds length (1 m, 1 inch by default)  
  
REYNOLDS_LENGTH= 1.0  
  
%  
  
% Compressible flow non-dimensionalization (DIMENSIONAL,  
%     FREESTREAM_PRESS_EQ_ONE, FREESTREAM_VEL_EQ_MACH,
```

Appendix A (continued)

```

%                                FREESTREAM_VEL_EQ_ONE)
REF_DIMENSIONALIZATION= FREESTREAM_PRESS_EQ_ONE

% ----- REFERENCE VALUE DEFINITION -----%
%
% Reference origin for moment computation (m or in)
REF_ORIGIN_MOMENT_X = 0.25
REF_ORIGIN_MOMENT_Y = 0.00
REF_ORIGIN_MOMENT_Z = 0.00
%
% Reference length for moment non-dimensional coefficients (m or in)
REF_LENGTH= 1.0
%
% Reference area for non-dimensional force coefficients (0 implies automatic
% calculation) (m^2 or in^2)
REF_AREA= 1.0
%
% Aircraft semi-span (0 implies automatic calculation) (m or in)
SEMI_SPAN= 0.0

% ---- IDEAL GAS, POLYTROPIC, VAN DER WAALS AND PENG ROBINSON CONSTANTS -----%

```

Appendix A (continued)

```
%  
% Fluid model (STANDARD_AIR, IDEAL_GAS, VW_GAS, PR_GAS,  
%           CONSTANT_DENSITY, INC_IDEAL_GAS)  
FLUID_MODEL= IDEAL_GAS  
%  
% Ratio of specific heats (1.4 default and the value is hardcoded  
%           for the model STANDARD_AIR, compressible only)  
GAMMA_VALUE= 1.4  
%  
% Specific gas constant (287.058 J/kg*K default and this value is hardcoded  
%           for the model STANDARD_AIR, compressible only)  
GAS_CONSTANT= 287.058  
%  
% Critical Temperature (131.00 K by default)  
CRITICAL_TEMPERATURE= 131.00  
%  
% Critical Pressure (3588550.0 N/m^2 by default)  
CRITICAL_PRESSURE= 3588550.0  
%  
% Acentric factor (0.035 (air))  
ACENTRIC_FACTOR= 0.035
```

Appendix A (continued)

```
% ----- VISCOSITY MODEL -----%  
  
%  
  
% Viscosity model (SUTHERLAND, CONSTANT_VISCOSITY).  
  
VISCOSITY_MODEL= SUTHERLAND  
  
%  
  
% Sutherland Viscosity Ref (1.716E-5 default value for AIR SI)  
  
MU_REF= 1.716E-5  
  
%  
  
% Sutherland Temperature Ref (273.15 K default value for AIR SI)  
  
MU_T_REF= 273.15  
  
%  
  
% Sutherland constant (110.4 default value for AIR SI)  
  
SUTHERLAND_CONSTANT= 110.4  
  
  
% ----- THERMAL CONDUCTIVITY MODEL -----%  
  
%  
  
% Conductivity model (CONSTANT_CONDUCTIVITY, CONSTANT_PRANDTL).  
  
CONDUCTIVITY_MODEL= CONSTANT_PRANDTL  
  
%  
  
% Molecular Thermal Conductivity that would be constant (0.0257 by default)
```

Appendix A (continued)

```
KT_CONSTANT= 0.0257
```

```
%
```

```
% Laminar Prandtl number (0.72 (air), only for CONSTANT_PRANDTL)
```

```
PRANDTL_LAM= 0.72
```

```
%
```

```
% Turbulent Prandtl number (0.9 (air), only for CONSTANT_PRANDTL)
```

```
PRANDTL_TURB= 0.7
```

```
% ----- BOUNDARY CONDITION DEFINITION -----%
```

```
%
```

```
% Navier-Stokes (no-slip), constant heat flux wall marker(s)
```

```
% (NONE = no marker)
```

```
% Format: ( marker name, constant heat flux (J/m^2), ... )
```

```
MARKER_HEATFLUX= ( wall,0 )
```

```
%
```

```
% Far-field boundary marker(s) (NONE = no marker)
```

```
MARKER_FAR= ( farfield )
```

```
%
```

```
% Symmetry boundary marker(s) (NONE = no marker)
```

```
% MARKER_SYM= ( simmetry )
```

```
%
```

Appendix A (continued)

```
% Inlet boundary type (TOTAL_CONDITIONS, MASS_FLOW)

INLET_TYPE= TOTAL_CONDITIONS

%

% Read inlet profile from a file (YES, NO) default: NO

SPECIFIED_INLET_PROFILE= NO

%

% File specifying inlet profile

INLET_FILENAME= inlet.dat

%

% Inlet boundary marker(s) with the following formats (NONE = no marker)

% Total Conditions: (inlet marker, total temp, total pressure,
%                   flow_direction_x, flow_direction_y, flow_direction_z, ... )
%                   where flow_direction is a unit vector.

% Mass Flow: (inlet marker, density, velocity magnitude,
%            flow_direction_x, flow_direction_y, flow_direction_z, ... )
%            where flow_direction isa unit vector.

% Incompressible: (inlet marker, temperature, velocity magnitude,
%                 flow_direction_x,flow_direction_y, flow_direction_z, ... )
%                 where flow_direction is a unit vector.

MARKER_INLET= ( inflow, 692.6253552, 44291.8, 1, 0, 0 )

%
```

Appendix A (continued)

```
% Outlet boundary marker(s) (NONE = no marker)

% Format: ( outlet marker, back pressure (static), ... )

MARKER_OUTLET= ( outflow, 23800 )

% ----- COMMON PARAMETERS DEFINING THE NUMERICAL METHOD -----%
%
% Numerical method for spatial gradients (GREEN_GAUSS, WEIGHTED_LEAST_SQUARES)

NUM_METHOD_GRAD= GREEN_GAUSS

%
% CFL number (initial value for the adaptive CFL number)

CFL_NUMBER= 20

%
% Adaptive CFL number (NO, YES)

CFL_ADAPT= NO

%
% Parameters of the adaptive CFL number (factor down, factor up,
%                                     CFL min value, CFL max value )

CFL_ADAPT_PARAM= ( 1.5, 0.5, 1.25, 50.0 )

%
% Maximum Delta Time in local time stepping simulations

MAX_DELTA_TIME= 1E6
```

Appendix A (continued)

```

%
% Runge-Kutta alpha coefficients
RK_ALPHA_COEFF= ( 0.66667, 0.66667, 1.000000 )
%
% Objective function in gradient evaluation (DRAG, LIFT, SIDEFORCE, MOMENT_X,
%
%           MOMENT_Y, MOMENT_Z, EFFICIENCY,
%
%           EQUIVALENT_AREA, NEARFIELD_PRESSURE,
%
%           FORCE_X, FORCE_Y, FORCE_Z, THRUST,
%
%           TORQUE, TOTAL_HEATFLUX,
%
%           MAXIMUM_HEATFLUX,
%
%           INVERSE_DESIGN_PRESSURE,
%
%           INVERSE_DESIGN_HEATFLUX,
%
%           SURFACE_TOTAL_PRESSURE,
%
%           SURFACE_MASSFLOW,
%
%           SURFACE_STATIC_PRESSURE,
%
%           SURFACE_MACH)
% For a weighted sum of objectives: separate by commas, add OBJECTIVE_WEIGHT
% and MARKER_MONITORING in matching order.
OBJECTIVE_FUNCTION= DRAG
%
% List of weighting values when using more than one OBJECTIVE_FUNCTION.

```

Appendix A (continued)

```
% Separate by commas and match with MARKER_MONITORING.

OBJECTIVE_WEIGHT = 1.0

% ----- SLOPE LIMITER AND DISSIPATION SENSOR DEFINITION -----%
%
% Monotonic Upwind Scheme for Conservation Laws (TVD) in the
%       flow equations. Required for 2nd order upwind schemes (NO, YES)
MUSCL_FLOW= NO
%
% Slope limiter (NONE, VENKATAKRISHNAN, VENKATAKRISHNAN_WANG,
%               BARTH_JESPERSEN, VAN_ALBADA_EDGE)
SLOPE_LIMITER_FLOW= VENKATAKRISHNAN
%
% Monotonic Upwind Scheme for Conservation Laws (TVD) in the
%       turbulence equations. Required for 2nd order upwind schemes (NO, YES)
MUSCL_TURB= NO
%
% Slope limiter (NONE, VENKATAKRISHNAN, VENKATAKRISHNAN_WANG,
%               BARTH_JESPERSEN, VAN_ALBADA_EDGE)
SLOPE_LIMITER_TURB= VENKATAKRISHNAN
%
```

Appendix A (continued)

```

% Monotonic Upwind Scheme for Conservation Laws (TVD) in the adjoint
%      flow equations. Required for 2nd order upwind schemes (NO, YES)
MUSCL_ADJFLOW= NO
%
% 1st order artificial dissipation coefficients for
%      the LaxFriedrichs method ( 0.15 by default )
LAX_SENSOR_COEFF= 0.15
%
% 2nd and 4th order artificial dissipation coefficients for
%      the JST method ( 0.5, 0.02 by default )
JST_SENSOR_COEFF= ( 0.5, 0.02 )
%
% 1st order artificial dissipation coefficients for
%      the adjoint LaxFriedrichs method ( 0.15 by default )
ADJ_LAX_SENSOR_COEFF= 0.15
%
% 2nd, and 4th order artificial dissipation coefficients for
%      the adjoint JST method ( 0.5, 0.02 by default )
ADJ_JST_SENSOR_COEFF= ( 0.5, 0.02 )

% ----- LINEAR SOLVER DEFINITION -----%
```

Appendix A (continued)

```
%  
  
% Linear solver or smoother for  
  
% implicit formulations (BCGSTAB, FGMRES, SMOOTHER_JACOBI,  
%  
%             SMOOTHER_ILU, SMOOTHER_LUSGS,  
%  
%             SMOOTHER_LINELET)  
  
LINEAR_SOLVER= FGMRES  
  
%  
  
% Preconditioner of the Krylov linear solver (ILU, LU_SGS, LINELET, JACOBI)  
  
LINEAR_SOLVER_PREC= ILU  
  
%  
  
% Linael solver ILU preconditioner fill-in level (0 by default)  
  
LINEAR_SOLVER_ILU_FILL_IN= 0  
  
%  
  
% Minimum error of the linear solver for implicit formulations  
  
LINEAR_SOLVER_ERROR= 1E-10  
  
%  
  
% Max number of iterations of the linear solver for the implicit formulation  
  
LINEAR_SOLVER_ITER= 10  
  
% ----- MULTIGRID PARAMETERS -----%  
  
%
```

Appendix A (continued)

```
% Multi-grid levels (0 = no multi-grid)

MGLEVEL= 0

%

% Multi-grid cycle (V_CYCLE, W_CYCLE, FULLMG_CYCLE)

MGCYCLE= V_CYCLE

%

% Multi-grid pre-smoothing level

MG_PRE_SMOOTH= ( 1, 2, 3, 3 )

%

% Multi-grid post-smoothing level

MG_POST_SMOOTH= ( 0, 0, 0, 0 )

%

% Jacobi implicit smoothing of the correction

MG_CORRECTION_SMOOTH= ( 0, 0, 0, 0 )

%

% Damping factor for the residual restriction

MG_DAMP_RESTRICTION= 0.75

%

% Damping factor for the correction prolongation

MG_DAMP_PROLONGATION= 0.75
```

Appendix A (continued)

```
% ----- FLOW NUMERICAL METHOD DEFINITION -----%
%
% Convective numerical method (JST, LAX-FRIEDRICH, CUSP, ROE, AUSM, HLLC,
%
%           TURKEL_PREC, MSW)
CONV_NUM_METHOD_FLOW= ROE
%
% Roe Low Dissipation function for
% Hybrid RANS/LES simulations (FD, NTS, NTS_DUCROS)
ROE_LOW DISSIPATION= FD
%
LOW_MACH_CORR= NO
LOW_MACH_PREC= NO
MAX_ROE_TURKEL_PREC= 5.0
%
% Entropy fix coefficient (0.0 implies no entropy fixing, 1.0 implies scalar
%           artificial dissipation)
ENTROPY_FIX_COEFF= 0.001
%
% Time discretization (RUNGE-KUTTA_EXPLICIT, EULER_IMPLICIT, EULER_EXPLICIT)
TIME_DISCRE_FLOW= EULER_IMPLICIT
%
```

Appendix A (continued)

```
% Relaxation coefficient
RELAXATION_FACTOR_FLOW= 0.95

% ----- TURBULENT NUMERICAL METHOD DEFINITION -----%
%
% Convective numerical method (SCALAR_UPWIND)
CONV_NUM_METHOD_TURB= SCALAR_UPWIND
%
% Time discretization (EULER_IMPLICIT)
TIME_DISCRE_TURB= EULER_IMPLICIT
%
% Reduction factor of the CFL coefficient in the turbulence problem
CFL_REDUCTION_TURB= 1.0
%
% Relaxation coefficient
RELAXATION_FACTOR_TURB= 0.95

% ----- CONVERGENCE PARAMETERS -----%
%
% Number of total iterations
EXT_ITER= 10000
```

Appendix A (continued)

```
%  
% Convergence criteria (CAUCHY, RESIDUAL)  
%  
CONV_CRITERIA= RESIDUAL  
%  
% Residual reduction (order of magnitude with respect to the initial value)  
RESIDUAL_REDUCTION= 8  
%  
% Min value of the residual (log10 of the residual)  
RESIDUAL_MINVAL= -8  
%  
% Start convergence criteria at iteration number  
STARTCONV_ITER= 10  
  
% ----- INPUT/OUTPUT INFORMATION -----%  
%  
% Mesh input file  
MESH_FILENAME=ARN3D_fine_solved.su2  
%  
% Mesh input file format (SU2, CGNS)  
MESH_FORMAT= SU2
```

Appendix A (continued)

```
%  
  
% Mesh output file  
  
MESH_OUT_FILENAME= mesh_out.su2  
  
%  
  
% Restart flow input file  
  
SOLUTION_FLOW_FILENAME= solution_flow.dat  
  
%  
  
% Restart adjoint input file  
  
SOLUTION_ADJ_FILENAME= solution_adj.dat  
  
%  
  
% Output file format (TECPLOT, TECPLOT_BINARY, PARAVIEW,  
%  
% FIELDVIEW, FIELDVIEW_BINARY)  
  
OUTPUT_FORMAT= PARAVIEW  
  
%  
  
% Output file convergence history (w/o extension)  
  
CONV_FILENAME= history  
  
%  
  
% Output file with the forces breakdown  
  
BREAKDOWN_FILENAME= forces_breakdown.dat  
  
%  
  
% Output file restart flow
```

Appendix A (continued)

```
RESTART_FLOW_FILENAME= restart_flow.dat
%
% Output file restart adjoint
RESTART_ADJ_FILENAME= restart_adj.dat
%
% Output file flow (w/o extension) variables
VOLUME_FLOW_FILENAME= flow
%
% Output file adjoint (w/o extension) variables
VOLUME_ADJ_FILENAME= adjoint
%
% Output Objective function
VALUE_OBJFUNC_FILENAME= of_eval.dat
%
% Output objective function gradient (using continuous adjoint)
GRAD_OBJFUNC_FILENAME= of_grad.dat
%
% Output file surface flow coefficient (w/o extension)
SURFACE_FLOW_FILENAME= surface_flow
%
% Output file surface adjoint coefficient (w/o extension)
```

Appendix A (continued)

```
SURFACE_ADJ_FILENAME= surface_adjoint
%
% Writing solution file frequency
WRT_SOL_FREQ= 1000
%
% Writing solution file frequency for physical time steps (dual time)
WRT_SOL_FREQ_DUALTIME= 1
%
% Writing convergence history frequency
WRT_CON_FREQ= 1
%
% Writing convergence history frequency (dual time, only written to screen)
WRT_CON_FREQ_DUALTIME= 10
%
% Output residual values in the solution files
WRT_RESIDUALS= NO
%
% Output limiters values in the solution files
WRT_LIMITERS= NO
%
% Output the sharp edges detector
```

Appendix A (continued)

WRT_SHARPEDGES= NO

%

% Output the solution at each surface in the history file

WRT_SURFACE= NO

%

% Minimize the required output memory

LOW_MEMORY_OUTPUT= NO

%

% Verbosity of console output: NONE removes minor MPI overhead (NONE, HIGH)

CONSOLE_OUTPUT_VERBOSITY= HIGH

%

% Write binary restart files (YES, NO)

WRT_BINARY_RESTART= YES

%

% Read binary restart files (YES, NO)

READ_BINARY_RESTART= YES

%

% Reorient elements based on potential negative volumes (YES/NO)

REORIENT_ELEMENTS= YES

CITED LITERATURE

1. Pope, S. B.: Turbulent Flows. Cambridge, United Kingdom, Cambridge University Press, 2000. Reprinted 2017.
2. Spalart, P. R. and Allmaras, S. R.: A one-equation turbulence model for aerodynamic flows. Recherche Aerospatiale, (1):5–21, 1994.
3. Spalart, P. R.: Trends in turbulence treatments. AIAA 2000-2306, June 2000.
4. Spalart, P. R. and Rumsey, C. L.: Effective inflow conditions for turbulence models in aerodynamic calculations. AIAA Journal, 45(10):2544–2553, 2000.
5. Rumsey, C.: The spalart-allmaras turbulence model. Technical report, NASA, <https://turbmodels.larc.nasa.gov/spalart.html>, 2017.
6. Menter, F. R.: Two-equation eddy-viscosity turbulence models for engineering applications. AIAA Journal, 32(8):1598–1605, August 1994.
7. Rumsey, C.: The menter shear stress transport turbulence model. Technical report, NASA, <https://turbmodels.larc.nasa.gov/sst.html>, 2013.
8. Rumsey, C.: Ahsj: Axisymmetric hot subsonic jet. Technical report, NASA, https://turbmodels.larc.nasa.gov/jetsubsonichot_val.html, 2015.
9. Rumsey, C.: Ansj: Axisymmetric near-sonic jet. Technical report, NASA, https://turbmodels.larc.nasa.gov/jetnearsonic_val.html, 2015.
10. Francois Josephca. Garnier, Cdric Baudoin, P. W. N. L.: Engine emission alteration in the near field of an aircraft. Atmospheric Environment, 31(12):1767–1781, June 1997.
11. International standard atmosphere. Technical report, Engineering ToolBox, https://www.engineeringtoolbox.com/international-standard-atmosphere-d_985.html, 2005.